Numerical Simulation on Self-heating Behavior of Coal Piles Considering Aging Effect in Exothermic Oxidation

張, 河猛

Numerical Simulation on Self-heating Behavior of Coal Piles Considering Aging Effect in Exothermic Oxidation

Zhang Hemeng

2020

Numerical Simulation on Self-heating Behavior of Coal Piles Considering Aging Effect in Exothermic Oxidation

A dissertation submitted to Kyushu University

For the degree of Doctor of Engineering

By

Zhang Hemeng

Supervised by

Prof. Sasaki Kyuro

KYUSHU UNIVERSITY

Department of Earth Resources Engineering

Graduate School of Engineering

Kyushu University

Fukuoka, Japan

July 2020

Abstract

The usage of low-rank coals in steel makings is increasing with decreasing high rank coals in the world. Spontaneous combustion of coal piles and seams leads to environmental hazards and economic losses, and it has been recognized as one of sources of greenhouse gases (GHG) emission contributing to global warming and climate changes. It is required to reduce CO_2 emissions by controlling and extinguishing coal spontaneous combustions by clearing the process of exothermic oxidation and self-ignition of coals under various coal pile and environmental conditions. The Arrhenius equation has been widely used as a typical and traditional model to simulate the spontaneous combustion process leading to self-ignition of coals, while it does not be able to express the aging effect on the coal exothermic oxidation leading to a status without any reaction. To develop preventing and extinguish operations for spontaneous combustions in coal piles, a reasonable exothermic oxidation model including the aging effect for spontaneous combustion of coals has been required especially in low temperature range.

This study has investigated a new heat generation model considering the aging effect using the equivalent oxidation exposure time (EOE-time) theory and decay constant to carry out numerical simulations on spontaneous combustion process of coal stockpiles. Moreover, it has been presented that a complex chemical water solution wetting the low rank coal is able to inhibit the oxidation with shifting the critical self-ignition temperature to higher temperature side compared with ones wetted by water based on the wire-mesh basket test (WMB test).

This dissertation consists of 5 chapters as follows;

Chapter 1: This chapter introduces the hazards and troubles induced by coal spontaneous combustions in the world, mechanism and major factors leading to self-ignition of coals. Furthermore, the total amount of GHG emissions from spontaneous combustions and uncontrolled coal-fires is estimated to be 0.69 to 1.2 % of annual

global GHG emissions from all industrial sectors in the world. The previous laboratory and field-scale measurement results and some potential indexes on the spontaneous combustion of coals are discussed and compared. Besides, previous numerical simulation approaches are introduced, and the reason why the numerical simulations using by the Arrhenius equation has failed to simulate the subcritical temperature-time process without self-ignition is discussed and explained.

Chapter 2: This chapter focuses on the measurement results by WMB test using the low rank coal (lignite) excavated in Inner Mongolia, China. The coal particles crushed into particles of 8 to 12 mm in size (average d =10 mm) were packed in the baskets in four sizes (L= 5, 10, 15 and 25 cm) to form cubic coal-piles for WMB tests. The thermal behaviors of the coal piles in the rising temperature process were measured against the ambient air temperature, T_e that is kept as a constant temperature during the WMB test. The critical self-ignition temperature (CSIT), critical lead time (CLT), and activation energy were evaluated based on WMB tests. With increasing the basket size, L, CSIT was dropped from 132.5 to 87.5 °C, while CLT became longer from 4.3 to 150 h, respectively. The CSIT of dried lignite coal particles was at least 10 °C lower than that of raw one.

Furthermore, effects of wetting the coal particles with the complex chemical solution of Na_2SiO_3 (2 to 20 wt%) and polyvinyl alcohol (PVA) (0.1 to 0.5 wt%) were investigated using the WMB tests. The complex chemical solutions wetting the coal particle surface generate a cross-linked gel (named SC/PVA gel) by the chemical reaction with CO_2 gas in air and emitted from heated coal particles. For the case of the cubic coal stockpiles wetted by the complex chemical solution of 16 wt% Na_2SiO_3 and 0.2 wt% PVA, its CSIT is 12.5 °C higher than that packing with raw coal particles. It shows that the developed complex chemical solution has a potential to inhibit oxidation and spontaneous combustion of coals by forming strong and stable gel on the coal particle surface.

Chapter 3: This chapter presents the numerical simulation model on spontaneous combustion of coals considering the aging effect of exothermic oxidation expressed

by the equivalent oxidation exposure time (EOE-time) theory and decay constant γ. The aging model has been applied to 3-D numerical simulations of cubic coal piles in the WMB baskets using ANSYS FLUENT. The practical range of $\gamma = 10^{-6}$ to 10^{-5} s^{-1} has been determined based on the matching simulations for the temperature-time curves obtained by WMB tests with 4 sizes of baskets. The larger value of γ results in lower CSIT and higher CLT. It is concluded that the developed heat generation model using the EOE-time theory and the decay constant can simulate both of the supercritical and subcritical temperature-time curves, CSIT and CLT measured by WMB tests using the cubic coal-piles with different volumes. In addition, the relationship between increase of CSIT by wetting with the complex chemical solution as described in Chapter 2 and increasing of γ was derived, and it shows that a safe operation on a field scale coal stockpile by wetting coal particles with the complex chemical solution can be evaluated by the numerical simulation model presented.

Chapter 4: This chapter presents the numerical simulation results by applying the developed heat generation of coal considering the aging effect for coal spontaneous-combustion behaviors in typical coal stockpiles set on the surface under wind. The 2-D trapezoid coal-stockpiles with bottom width w = 5 to 30 m and height $h = 0.33w$ were simulated to investigate the effects of wind velocity υ = 0 to 14 m/s, coal particle size d = 0.3 to 10 mm and porosity n = 0.1 to 0.6 on the self-heating behavior in the stockpiles. The critical decay constant, γ_c for a typical condition of the pile (w = 15 m, h = 5 m, d = 3 mm, υ = 2 m/s and n = 0.33) was estimated to be $\gamma_c = 1.25\times10^{-6}$ s^{-1}. The value of γ_c is increasing with the stockpile volume that has larger effects on the self-heating behavior than other parameters. Furthermore, the sensitivity studies of each physical parameters on the value of γ_c decides CSIT. It can be summarized that the coal stockpile can keep safety on coal self-ignitions when the measured γ of the coal particles consists a stockpile is larger than γ_c that can be estimated from the numerical simulation results. The wetting operation on the stockpile using the complex chemical solution can be expected to increase γ than γ_c with shifting into a safety coal stock.

Chapter 5: This chapter summarizes the conclusions and discusses future work on

spontaneous combustion of low rank coals.

Table of Contents

List of Tables

List of Figures

Acknowledgments

Firstly, I would like to give my deepest gratitude to my supervisor, Dr. Sasaki Kyuro, for the guidance and encouragement during my study at Kyushu University. This dissertation is the result of his consistent and kind instruction. I am deeply grateful for him teaching me the abilities of independent and expanded thinking.

High tribute shall be paid to Dr. Zhang Xiaoming. I would like to express my appreciation for his careful instruction and kind support for my research and life.

I would like to show my deep gratitude and appreciation to Dr. Yuichi Sugai and Dr. Ronald Nguele for their kind supports and valuable suggestions throughout this research work.

I would like to express my deep gratitude and appreciation to Dr. Tajima Hiroshi for his critical reviews and comments on my dissertation.

Furthermore, I thank Dr. Wang and Ms. Li from Liaoning Technical University for their useful discussion on my research.

I gratefully acknowledge the financial support received from the Japanese Government (MEXT) to pursue my study at Kyushu University. I thank the Baiyinhua coal mine in Inner Mongolia for providing the coal samples.

My sincere thanks should also go to Mrs. Zhao for her care and help in my life. Special thanks should go to all members of the Resources Production and Safety Engineering Laboratory for their assistance and kind supports.

Finally, my deep acknowledge to my parents and my older brother for their support and understanding.

Chapter 1: Introduction

1.1 Global energy and coal resource

Global energy consumption grew rapidly driven by a robust economy and higher needs of heating and cooling in some parts of the world. The global energy consumption in 2018 reached 13,864.9 Mtoe (million tonnes oil equivalent), i.e. 19,807 Mtce (million tonnes coal equivalent), which was increased at a rate of 2.9% last year and the fastest since 2010 (OCDE, 2019). China, the USA, India and Russia together occupied more than half of global energy consumption in 2018.

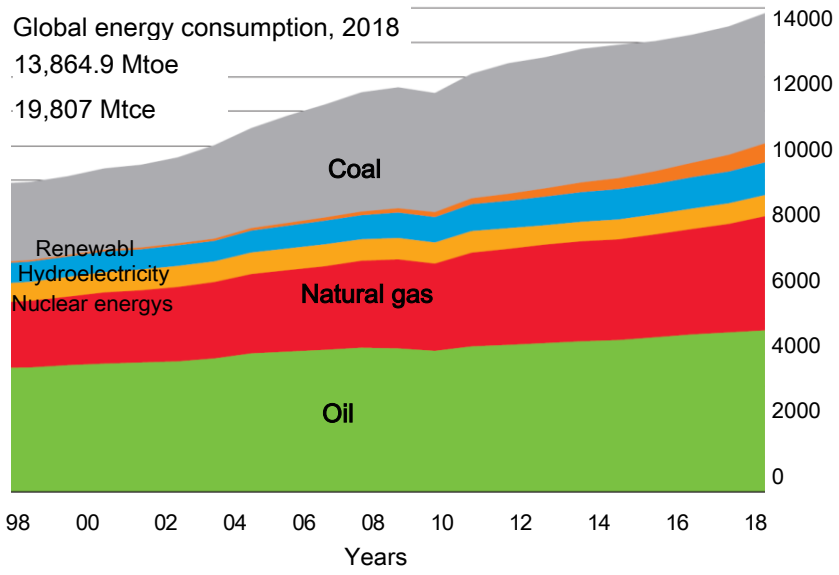

Figure 1- 1. Global energy consumption before 2019. Energy share in 2018: coal 27.2%, renewables 4.0%, hydroelectricity 6.8%, natural gas 23.9% and oil 33.6% (British Petroleum Company, 2019).

As shown in Figure 1-1, fossil resources including coal, oil and natural gas accounted for about 87.2% of the global energy consumption. The world demanded all fossil fuels increased faster than their 10-year averages, 2.4%, 5.3% and 1.4% for oil, natural gas and coal, which resulted in that carbon emissions grew by 2.0%, the fastest growth for seven years. Although the ration of clean energy resources has a fast-increased rate in

recent 10 years, fossil resources support world economic development as a pillar, even in the next 30 years.

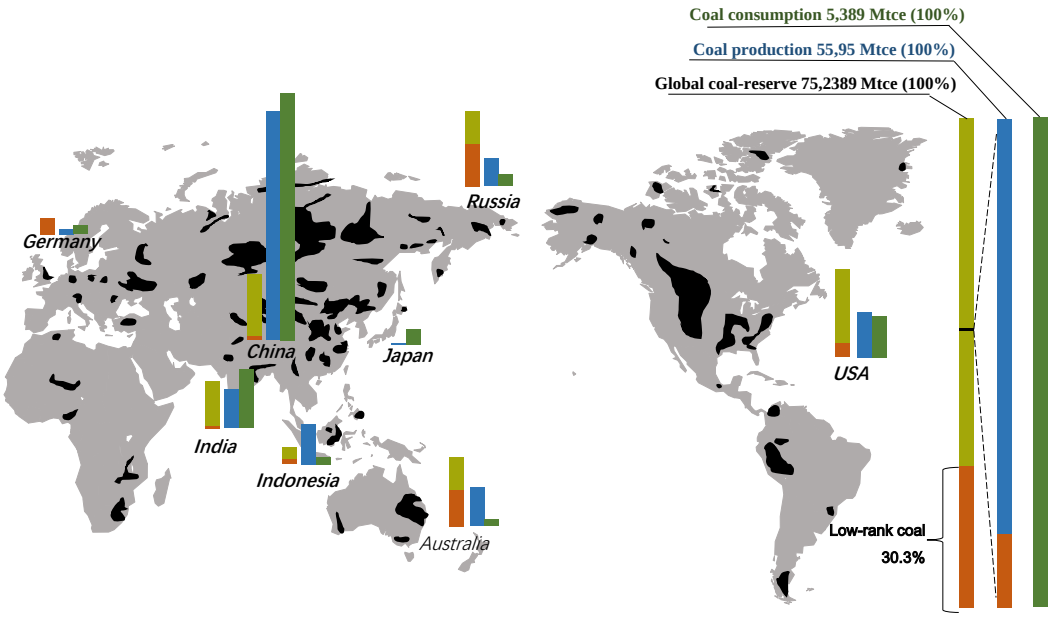

Figure 1- 2. Coal of proven reserve, production and consumption in the relative countries in the world, 2018. (British Petroleum Company, 2019).

Coal resources always accounted for a high proportion of global fossil consumption for a century due to the low-price, large-reserves and wide-distribution. Up to 2018, the global proven reserve of coal was 1,054.78 billion tonnes (=752,389 Mtce) and accounted for around 55.7% of the total proven fossil reserves. This means that there is enough coal to last us around 200 years at the current production rate of 5,595 Mtce in 2018. As shown in Figure 1-2, the coal reserve is mainly distributed in the northern hemisphere, including the Asia-European coal belt and North American coal belt, which accounted for 96% world's total. There are more than 80 countries, such as the USA, China, Russia and India, have been found the coal reserve. Coal production and consumption in 2018 were 5,595 and 5,389 Mtce, respectively. China is the biggest producer and consumer of coal (48% in global coal production and 50.7% in global coal consumption). Besides, the USA (9.3%), India, Australia (7.7%), India (7.9%), Indonesia (8.3%) and Russia (5.6%) are the major coal-produced countries. The US

(8.4%), India (12%) and Japan (3.1%) are the main coal consuming countries.

The share of global low-rank coal, including sub-bituminous coal and lignite, was surveyed to be 319.9 billion tonnes, 30.3% of all-rank coal. However, only15% of coal production in 2018 was low-rank coal. Therefore, It is expected that low-rank coal will play an increasing role in the future energy industry.

1.2 Overview of worldwide coal fires

Spontaneous combustion in coal and carbonaceous material has long been a problem for the coal industry (Stracher et al., 2014). It always breaks out at the underground and surface coal deposits in the active or abandoned coal mines. Coal fires are normally divided into natural coal fires and human-induced coal fires based on the conditions of spontaneous combustion (Lesley, 2013). Natural coal fires are normally ignited by forest fires, lightning strikes and spontaneous combustion. Heffern and Coates (2004) investigated the paleomagnetic ages of clinker and proposed that the coal seams have burned naturally during at least 4 million years in Wyoming and Montana coal fields.

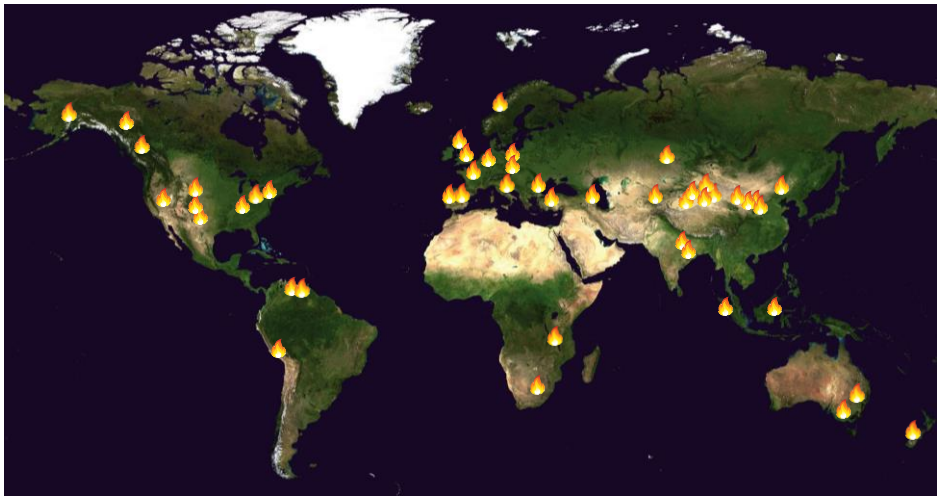

Figure 1- 3. Global distribution of undesired coal mine fires (Stracher et al., 2014).

However, In recent centuries, most coal fires are human-induced from illegal or unprofessional mining activities. Surface areas of coal deposits exposed to air by human activities are enlarged dramatically, especially for underground gobs and open-

pit mines. As given in Figure 1-3, the undesired coal fires have been reported in more than 20 countries throughout the world, especially in China, the USA and India (Gervet, 2007; Melody & Johnston, 2015; Song & Kuenzer, 2014; Stracher et al., 2014).

The present summarized situations of coal fires in main countries suffering from coal fires are as follows:

(a) China

China is the biggest coal producer and consumer in the world and faced an exceedingly severe coal-fire problem. Coal fires were firstly recorded in the historic document of "Notes on the Words in Notation on Waterways" (i.e. "Shuijingzhu") compiled by Li Daoyuan (-527). He mentioned the mountains of "lighting in the night and smoking in the day" in Xinjiang. In the last decade, over ten provinces in China have recorded coal fires. Xinjiang, Ningxia and Inner Mongolia are being undergone the most serve coal fires (Stracher & Taylor, 2004). Currently, more than 50 coal fields, about 720 km^2 of coverage area, are affected by coal fires and distributed in the 5,000 km coal mining belt (Kuenzer & Stracher, 2012; Kus, 2017). It is estimated that around 20 Mt coal (0.36% of annual national production) is lost due to direct burning and about 200 Mt coal becomes economically inaccessible (Lesley, 2013; van Dijk et al., 2011; Voigt et al., 2004). Wuda open-pit coal mine, located in Inner Mongolia, loses a coal resource of 0.2 Mt/year due to fire (Kuenzer et al., 2007). About 10% area of the three mines in the Wuda are affected by coal fires, which equals 4 km^2 (Kuenzer et al., 2007). Besides, The rapid increase of unscientific small-scale coal mining activities during the last 30-40 years is expected to have contributed to the serious problem of uncontrolled coal fires in China (Voigt et al., 2004).

(b) India

In India, around 40% of the total mining disasters and about 50% of the total fatalities of miners were due to the coal fire and explosion in coal mines during 1947–2010 (Jitendra et al., 2016). Approximate 70% of 25 major mine disasters of fire and explosion in the last 10 years were because of coal spontaneous combustions(Mohalik et al., 2017). the regions of coal self-ignition mainly concentrate on Singareni, Jharia,

Singrauli and Ranigans coalfields, in which the Jharia coalfield has adsorbed special concern worldwide due to the most intensive of surface-subsurface coal fires. Jaharia Mine has burned since 1916 and the total fire area was 8.42 km^2 in 2016 (Mishra et al., 2020). More than 37 Mt coal has been burned and 1,400 Mt coal is inaccessible due to the continuous fires.

Figure 1- 4. Coal mine fires in different countries. (a) Jharia coalfield fire, India, 2016 (Namah, 2016); (b) Centralia mine fire, USA, 2013 (Skoogfors, 2013); (c) Hazelwood open-cut mine fire, Australia, 2014 (Michael & Sawyer, 2014); (d) Wuda open-pit mine fire, China, 2006 (Wessling et al., 2006).

(c) USA

The proven reserve of coal in the USA in 2018 was 250 billion tonnes, the greatest one worldwide. Up to now, roughly an estimated 43 billion tonnes of coal in Wyoming and Montana coal fields have been naturally burned in the recent at least 4 million years (Heffern & Coates, 2004). The greatest and most famous coal fire disaster in the USA is Centralia mine fire, which starts from 1962 and enlarges to almost 15 km^2, by an average rate of 20 m/year of fire fronts, can continually burn for over 100 years (Nolter & Vice, 2004; Pennsylvania Department of Environmental Protection, 2019; Stracher et al., 2006). 35 coal fires are distributed in Pennsylvania (Protection, 2008).

According to a review by the Department of Interior's Office of Surface Mining Enforcement and Reclamation (2017). There are 98 underground fires in nine states, most of them in Colorado, Kentucky, Pennsylvania, Utah and West Virginia. However, many coal fires underground are not reported (Coates et al., 2005; Heffern & Coates, 2004).

(d) Australia

In Australia, the occurrence of spontaneous combustion in open-cut coal mines is very variable (Carras et al., 2009). Coal fires are concentrated in the open-pit mines of New South Wales, Queensland and Victoria states (Carras et al., 2009; Day et al., 2010). Australia's Burning Mountain, located in New South Wales, is the oldest coal fire worldwide and is estimated to burn at least 6,000 years (Ellyett & Fleming, 1974). In 2014, the Australian Institute for Disaster Resilience (2014) reported a coal fire in Hazelwood open-cut mine in Morwell, Victoria. The fire burned lasted for 4 weeks and the total damages were estimated to exceed $100 million.

(e) Indonesia

There is no accurate count of coal fires in Indonesia. However, coal reserves in Indonesia are mainly low-rank coal, such as lignite and peat, which has a high tendency of self-combustion. Hamilton et al. (2000) mapped the total number of 125 fire points that were observed within a 2 km strip. Extrapolating this data to areas on Kalimantan underlain by low-rank coal deposits, the number of fires was conservatively estimated to be tens of thousands, perhaps exceeding 160,000. Anther data is from Whitehouse and Mulyana (2004), in the 1997–1998 forest fires, 136 coal fires were ignited in Pusrehut and Sungai Wain. There could be between 76,000 and 300,000 coal fires were existed in East Kalimantan. Moreover, Coal fires are always ignited by the burning of the forest to clear land for plantation crops.

(f) South Africa

Witbank coalfield has the largest coal reserve and production in South Africa. The bord and pillar mining methods were applied in most coal mines of the Witbank region, resulting in the low coal recovery rate and strong airflow. Coal fire due to spontaneous

combustion has been estimated for over 50 years. Its burning area was estimated to be 1.5-2 km^2 (Bell et al., 2001). However, coal fires are continued (Pone et al., 2008). No. 3 coal seam at Arthur Taylor Colliery cannot be commercially excavated due to the high tendency of spontaneous combustion (Onifade & Genc, 2019).

Moreover, as shown in Figure 1-5, except the coal fires in subsurface coal gob, abandoned coal mines, open-pit mine and coal outcrop, spontaneous combustion of coal also breaks out in coal storage and transportation. It is not exaggerated that a certain volume of packed coal in the natural environment has the risk of spontaneous combustion (Wang et al., 2019).

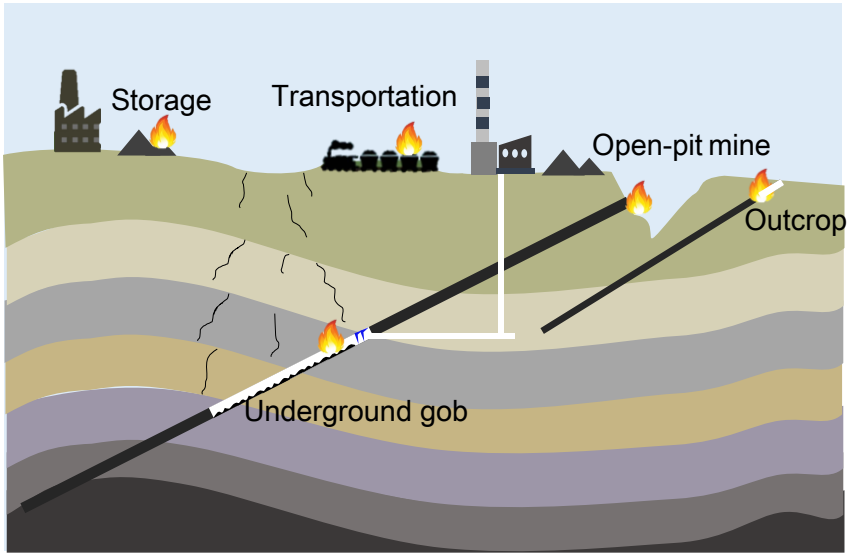

Figure 1- 5. The possible places of coal spontaneous combustion.

1.3 coal fire and greenhouse gas (GHG)

At present, there are uncertainties methodologies available for estimating the GHG from the field with coal spontaneous combustion. One important reason is that the positions and areas of underground coal fires are difficult to be detected and measured using the present technologies. On the other hand, many field coal fires are still not found. Typical GHG emitted from coal combustion includes CO_2 and CH_4 (Wang & Chen, 2015). However, coal wildfire produces all kinds of GHG, including CO, CO_2, CH_4, NO_x, SO_x, etc.. It is due to the incomplete burning (Gielisch & Kropp, 2018).

Around 36,810 Mt of CO_2 were emitted from fossil fuel and industry in 2019, and in which GHG emission by coal is 14,550 Mt, accounting to 39.5% in the fuel emission (Hausfather, 2019).

(a) China

Numerous studies have concentrated that the Chinese GHG emission from coal spontaneous combustion is larger than most other countries. The ratio of annual GHG emission of China, due to spontaneous coal ignition, to the global human-induced GHG emissions has been studied by published are 2% to 3% (van Genderen & Haiyan, 1997), 0.3% (Voigt et al., 2004), 0.1% to 0.2% (Kuenzer et al., 2007), 0.25% (Josh, 2020) and lower than 0.22% (van Dijk et al., 2011). Considering that the uncompleted combustion of coal can liberate CH_4 (1 t of CH_4 = 21 t of CO_2), 1 t of coal (75% carbon content) will lead to the emission of 2.7 t (complete combustion) to 5.1 t (Incomplete combustion) CO_2 equivalents (CO_2-eq) (Gielisch & Kropp, 2018). It has been generally accepted that around 20 Mt of coal is annually burned due to spontaneous combustion in China (Lesley, 2013; van Dijk et al., 2011; Voigt et al., 2004). Thus, approximately 57 Mt to 102 Mt CO_2-eq released by coal fires, which adds up to 0.15% to 0.28% of global human-induced GHG emissions in 2019. This result is closed to that proposed by most researchers.

(b) India

The Jharia coalfield has the largest coal fire in India. Mohalik et al. (2016) predicted the GHG emission of Jharia coalfield fire, caused by spontaneous combustion, vary from 16.86 to 20.19 Mt CO_2-eq per year. This emission rate presents the burnt coal amount of 3.3-7.47 Mt every year, which is much larger than other investigations (van Dijk et al., 2011). Therefore, the value may be overestimated. In this study,1 Mt/year of coal is consumed in Jharia fire is reasonable due to that around 37 Mt coal burned in almost 80 years (Pandey et al., 2013; Praveen & Gupta, 2017; Stracher & Taylor, 2004; van Dijk et al., 2011). Therefore, the annual GHG emission from spontaneous combustion in India is predicted to be 4.05-7.65 Mt CO_2-eq (equivalent to 1.5 Mt coal) after considering other coal fires in India.

(c) USA

In the area of 4,100 km^2 in the Powder River basin, 80-1,000 billion tonnes of CO_2 were released in the last 2 million years (Heffern & Coates, 2004). Recently, some researchers directly measured the emitted gas from the vents and solid surface above the abandoned coal mines (Engle et al., 2011, 2012; Ide & Orr, 2011; O'Keefe et al., 2010, 2011). As illustrated in Table 1-1.

Table 1- 1. Summary of CO_2 fluxes for coal fires in the United States.

Fire position	CO_2 emission (kt/year)	Source
Hotchkiss, Wyoming	1.33-1.63	(Engle et al., 2012)
Welch Ranch, Wyoming	1.02-3.22	(Engle et al., 2011)
Ankney, Wyoming	4.57-142.67	(Engle et al., 2012)
North, Colorado	0.47-0.85	(Engle et al., 2012)
Mulga, Alabama	77.48-137.75	(Engle et al., 2011)
Ruth Mullins, Kentucky	0.73-2.00	(O'Keefe et al., 2010)
Truman Shepherd, Kentucky	1.40	(O'Keefe et al., 2010)
Old Smokey, Kentucky	1.00	(O'Keefe et al., 2011)
San Juan Basin Durango, Colorado	3.57	(Ide & Orr, 2011)

There is no clear data to explain the CO_2 emission in the famous Centralia mine fire. However, based on the present data of initial coal reserve (25 Mt), recovery rate (50%-70%), and predicted burning time (160-200 years), the coal combustion amount of coal is estimated to be 37.5 kt to 78.1 kt/year. Therefore, the annual GHG emission amount is 135 kt to 398 kt. However, referring to Table 1-1, the annual CO_2 emission rate in the normal fire points is lower than that of Centralia mine fire. Hence, the total CO_2 emission rate in the USA is predicted to be lower than 9.82-38.6 Mt/year, after counting the present 97 coal fires in the whole country. In this study, 30-80% of 9.82-38.6 Mt CO_2-eq /year, i.e. 2.95-30.9 Mt CO_2-eq/year, is estimated as the annual GHG emission rate of the USA. This predicted range of 14-290 Mt/year lies in the lower limit of that presented by O'Keefe et al. (2010).

(d) Australia

In 2017, the GHG emission rate from the coal mining industry was around 27 Mt CO_2-eq，which contributes 6.1% of the nation's total emissions (439.2Mt) (Department of the Environment and Energy, 2019). Carras et al. (2009) measured the GHG emission from six open-cut coal mines and estimated the annual emission rate due to spontaneous combustion was 0.365 Mt CO_2-eq. He also proposed that spontaneous combustion accounted for almost 1/3 of all emissions in some mines. Here, supposing that a total of 10-30% GHG from the coal mining industry sourced from the spontaneous coal combustion, an estimation of 2.7-8.1 Mt CO_2-eq/year was released. Moreover, Williams et al. (1998) estimated the GHG emission of spontaneous combustion from open-pit coal mine was 1.87 Mt CO_2-eq. Based on the production ratio of underground and surface coal mines (2.56:1) (Department of the Environment and Energy, 2019), the GHG emission by spontaneous combustion from the underground coal mine is 4.79 Mt CO_2-eq. Therefore, the total annual GHG emission rate from coal self-ignition is 6.66 Mt CO_2-eq. This estimated value is in the range of GHG emissions of the above estimation. In this study, the GHG emission rate deduced from the investigation from Carras et al. (2009) is applied, i.e. 2.7-8.1 Mt CO_2-eq/year.

(e) Indonesia

Uncontrolled peat fire in Indonesia is mainly due to climate change, land reclamation and forest fires. In the 1997 Indonesian fires, Page et al. (2002) investigated the 7,300 km^2 of the burned peatland area, in Central Kalimantan, Borneo. Around 190-230 Mt of CO_2 was emitted to the atmosphere by peat combustion. In the 2013 Sumatran fires, Gaveau et al. (2014) estimated about 154.83 Mt CO_2-eq was emitted due to the peatland burning. Kurata et al. (2016) predicted that the peatlands fire (comprise above and below-ground biomass) in 2015 resulted in around 653.2 Mt CO_2 emitted based on satellite data. Austin et al. (2018) applied the reference approach to analyze six national inventories of Indonesia, and estimated the average annual GHG emissions (2000-2012) due to peat fire was 160Mt/year. This value is relatively comprehensive and reliable.

(f) South Africa

Cook and Lloyd (2012) measured the CO_2 emission rate of six surface mines and on a large discard dump on a seventh mine. He proposed that CO_2 is the largest contributor to GHG from the surface and abandoned coal mines of South Africa at around 1.95 ± 0.35 Mt/year.

(g) Global GHG emission

Table 1-2 shows the estimation of worldwide GHG emission from the uncontrolled coal spontaneous combustion. Around 229.3-320.95 Mt CO_2-eq/year in total is due to the direct coal combustion.

Table 1- 2. Worldwide GHG emission estimation from uncontrolled coal burning

Country	GHG emission (Mt CO_2-eq/year)	Source
China	57-102	(Lesley, 2013; van Dijk et al., 2011; Voigt et al., 2004)
India	4.05-7.65	Present study
USA	2.95-30.9	Present study
Australia	2.7-8.1	Present study
Indonesia	160	(Austin et al., 2018)
South Africa	1.6-2.3	(Cook & Lloyd, 2012)
Other countries	1-10	Present study
Total	229.3-320.95	

However, the amount of methane form abandoned mine was expected to be 22 Mt (462 Mt CO_2-eq) in 2020 (International Energy Agency, 2019; Josh, 2020; Kholod et al., 2020). Coal-burning underground decreases the surrounding rock pressure, increases the paths linking underground and ambient, as well as strengthens the chimney effect, which accelerates the methane emission rate. Therefore, the underground methane emission from abandoned mine is inevitably affected by the coal fire. Supposing that 5-30% of global methane from abandoned mine is emitted due to coal fire, the GHG emission rate of 23.1-138.6 Mt CO_2-eq/year contributes to the global greenhouse effect. Therefore, the global annual GHG emission due to uncontrol coal fire is predicted as

252.4-459.55 Mt CO_2-eq/year, accounting for 0.69-1.2% of global GHG emission. The estimation value is higher 1-3 times than that predicted by van Dijk et al. (0.38%) (van Dijk et al., 2011).

1.4 Other impacts of coal fire

Spontaneous combustion of coal is a significant worldwide issue. Coal spontaneous combustion threatens the mining, transportation and storage of coal industry. It not only endangers miners'life but also causes huge coal resource losses and great ecological damage (Zhang et al., 2016). Except for the GHG emission, the other impacts generated by coal fire are listed as follows.

Figure 1-6. Impacts of coal spontaneous combustion. Coal fire results in (a) Environmental damage, India, 2019 (Rahi, 2019); (b) Severe smog, Indonesia, 2019 (Adam, 2019); (c) Subsidence of road, USA, 2016 (Calderone & Insider, 2016); (d) Sulphur minerals near a vent, China, 2003 (Kuenzer et al., 2007).

1.4.1 Methane explosions

the coal mines or gangue dump with a high content of methane always has a high tendency of spontaneous combustion and methane explosion (Pan et al., 2009). In

China, 32.3% of 229 coal mines have the potential with a combined occurrence of flammable gas evolution and coal spontaneous combustion (Qin et al., 2016). More than 70% of major accidents in coal mines was because of methane explosion, in which some accidents were ignited by coal self-ignition (Ministry of Emergency and Management, 2010). During the 2001–2010 period, the gas explosion and fire in the coal mine resulted in 6,607 deaths (Chen et al., 2012). In 2004, 166 persons were died due to a methane explosion because of coal spontaneous combustion in Datong, China (Yongchen et al., 2016). Moreover, from 1947 to 2010, around 50% of the total fatalities of miners were due to the coal mine fire and explosion in Indian coal mines (Jitendra et al., 2016).

1.4.2 Economic lost

Coal fires directly cause danger to mining equipment and activities. The substantial coal reverses are burned, leading to economic losses. However, normally much more coal reserves than burned coal are locked and unable be mined. In India, About 1,900 Mt coal is difficult to be excavated due to coal fires (Jitendra et al., 2016). Massive funds need to be invested in coal fires disasters. The estimated cost of extinguishing the spontaneous coal fires in Xinjiang regions, China, is more than $10 million. In the USA, Percy mine fire, burned over 30 years, need around $30-40 million costs for extinguishing. Besides, the state government has to offer large funds for relocating the town's residents (Stracher & Taylor, 2004).

1.4.3 Subsidence and landslide

Plenty of surface displacements generate due to the underground volume loss of coal burning. Coal fires cause the thermal effects on the adjacent rock mass, resulting in cracks and fissures. Subsidence caused by coal mine fire extensively damages surface structures, roadway and farmland, and thus affects social activities and human safety, as illustrated in Figure 1-6(c). Zhou et al. (2013) applied ALOS PALSAR data for

monitoring long-term ground displacement due to underground coal fires. The mean deformation rates were in the range of 3.92-8.93 cm/year. In 1996, 219 houses were influenced as a consequence of coal fire in Jharia coalfield. Moreover, coal spontaneous combustion in open-pit mines results in rock loose, fracture and subsidence, companying with a landslide on the slope. It seriously threatens the mining work and mine-environmental restoration.

1.4.4 Toxic gas and trace elements

Coal-fire exhaust is enriched in toxic gases: CO, SO_2, H_2S, N_2O, NO_X and NH_3 (Kuenzer et al., 2007; Zhang et al., 2008). Cook and Lloyd (2012) estimated that around 2,040 t/year of SO_x, 306 t/year of NOx and 31 t/year of NH_3 were emitted from all surface mines in South Africa. Hazardous trace elements, including As, F, Hg, Tl, Pb, Cd, Sn, Ge and Se, are released to the atmosphere and earth during coal spontaneous combustion (Liang et al., 2014; O'Keefe et al., 2010; Song & Kuenzer, 2014; Zhao et al., 2008). In 2013, approximately 1.13 Mt of S, 246 t of As, 45 t of Hg and 63,298 t of F were emitted from coal gangue spontaneous combustion in China (Wang et al., 2016). Those toxic elements are adsorbed by crops and taken by animals and humans. Final concentration and absorption in humans serve damage to the nervous system, critical organs and skin.

1.4.5 Soil and water pollutant

Wang et al. (2016) investigated the organic contaminants from the backfilled region in the Wuda coalfield in China and proposed that polycyclic aromatic hydrocarbons in the earth due to coal spontaneous combustion deserves urgent attention. Zhang et al. (2013) investigated the bacterial and archaeal diversity near three coal-fire vents and found that underground coal fires significantly affect soil pH, moisture and NO_3^- content. Toxic metals can be washed by rainwater to the surface rivers and groundwater. Acid gases and drainage due to coal self-ignition can reduced pH in the water and have

a detrimental impact on the streams of aquatic environments.

1.4.6 Air pollution and ecological pollution

SO_2, NO_2 and particulate matter generated by coal fires can dramatically reduce the air quality near the coal fireplace. Pandey et al. (2014) assessed the air pollution around the Jharia Coalfield and proposed that coal mining and active mine fires are the main contributors, accounting for around 57.71%. Coal fires threaten Indonesia's shrinking ecological resources in Kutai National Park and Sungai Wain Nature Reserve. A third of the world's wild orangutans are threatening by forest fires partly ignited by coal fires. Coal fire near the surface destroyed the farmland and houses. It also generated smoke to disrupt air travel and increase hospital admissions (Whitehouse & Mulyana, 2004). After the Avondale catastrophe in the USA, coal fires burning across Pennsylvania have destroyed floral and faunal habitats and made Pennsylvania the most serve of acid-rain producing state (Stracher & Taylor, 2004).

1.5 Coal spontaneous combustion and the influence factors

1.5.1 Oxygen adsorption at low temperatures

Coal is a complex-organic macromolecule with amounts of functional groups and chemical bonds. Coal is mostly carbon with various elements, including O, H, N, S, etc.. In the 17th century, Plolt and Berzelius put forward the mechanism of pyrite Factors (Wang et al., 2008). In the following hundreds of years, considerable investigators have been proposed some different mechanisms on coal self-ignition, including bacteria effect, absorption of water vapor, heat conduction by crustal movement, action theory of phenolic group, free radical reactions and coal-oxygen compound theory (Bowes, 1984; Li et al., 2009; Niu & Zhang, 2007). At present, the coal-oxygen compound theory has been widely recognized (Calderone & Insider, 2016). According to this theory, after the fresh coal exposing to air at low temperatures,

coal-oxygen adsorption starts and liberates heat to ambient. The coal-oxygen reaction includes three stages: physical adsorption, chemical adsorption and chemical reaction. physical adsorption and chemical adsorption play distinct roles in the heat generation process at low temperatures (Hayward & Trapnell, 1964; Kong et al., 2018; Parsa et al., 2017).

Physical adsorption is reversible and can rapidly achieve saturation. The adsorption amount is proportional to ambient pressure and inverse-proportional to temperature. Sevenster (1961) proposed that physical adsorption plays a major role below 273 ºC and becomes negligible above 50 ºC. Oxygen molecules enter the inner coal porous media and result in single or multiple layers of adsorbed molecules by valence forces (Allardice, 1966; Wang et al., 2003). The heat generation by physical adsorption is low, around 6.7 to 20.9 kJ/mol, due to the week inter-molecular force (Hayward & Trapnell, 1964).

With the coal temperature increasing, chemical adsorption begins to dominate the oxygen adsorption. However, some researchers also found that simultaneous physical and chemical adsorption of oxygen on coals (Allardice, 1966; Karsner & Perlmutter, 1982). The chemical adsorption is irreversible. Active groups on the coal surface can react with oxygen and form coal-oxygen compounds. It is limited to a monolayer of molecules on the pore surfaces. The bond energy in chemical absorbed molecules is 83.6-418.0 kJ /mol (Hayward & Trapnell, 1964; Jones et al., 1996; Sondreal & Ellman, 1974), which is much larger than that of physical adsorption. Michael and Sawyer (2014) studied the infrared spectra differences between oxygen and nitrogen desorption in coal and proposed that the site of oxygen chemisorption is located on the hydroxy and carboxyl groups on the coal surface. Anderson and Johns (1986) put forward that both aromatic and aliphatic hydrocarbon moieties in coal can be oxidized at low temperatures. Generally, non-aromatic structures and groups in coal are oxidized at low temperatures. It contributes to the major heat generation source of coal to spontaneous combustion.

As shown in Figure 1-7, the structures of coals with different ranks and the basic

structures of low-rank coal are benzene ring, naphthalene ring and phenanthrene rings. With the coal rank increasing, the aromatic ring dramatically increases (Ghani et al., 2015). Therefore, the amount of fixed carbon decrease from anthracite coal to lignite. However, the no-aromatic groups, including Alkyl, hydroxy, carboxyl and methoxy, increase with reducing the coal rank. That is why low-rank coal always has a higher tendency of spontaneous combustion.

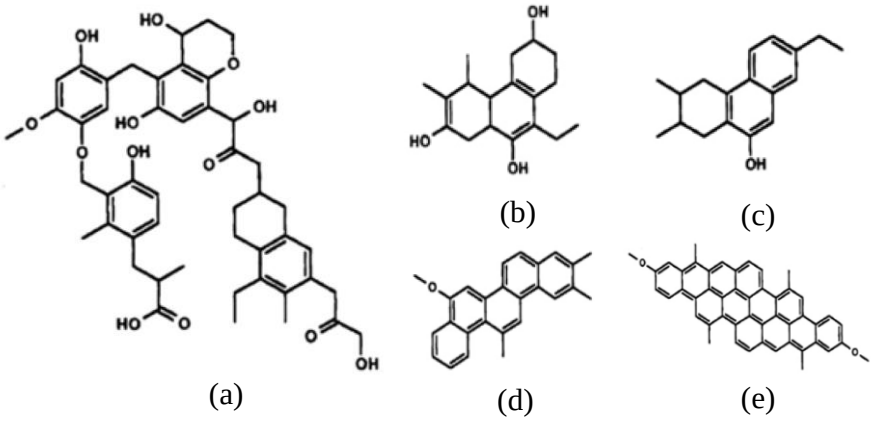

Figure 1- 7. The structural model for coals of different ranks. (a) Low-rank brown coal, (b) Subbituminous coal, (c) High volatile bituminous coal, (d) Low volatile bituminous coal and (e) Anthracite coal (Ghani et al., 2015).

1.5.2 Influence factors on coal spontaneous combustion

Coal spontaneous combustion is a slow, complex and dynamic process with heat generation. When the fresh coal pile is exposed to air, oxygen adsorption starts. Weak heat of coal liberates to the outside and thus accumulates in the coal pile. When the heat generation of coal pile is larger than heat dissipation from pile to ambient, coal temperature gradually increases.

This self-acceleration heat of coal results in the ignition breaking out. The self-ignition process of coal is complex, involving heat generation of coal, oxygen supply and consumption, heat transfer in the pile, as well as water phase-change and transfer. Therefore, the process is affected by many factors. Three elements are basic: coal, oxygen and heat (accumulation), for coal spontaneous combustion. Based on the three

elements, more specific and detail are listed in Figure 1-8.

Coal properties are the key inducing spontaneous combustion. McManus et al. (1999) discussed the influence of mineral matter on the spontaneous combustion of coal. The mineral matter could affect the heat dissipation and inhibition of oxygen adsorption. Kuchta et al. (1980) certificated that the low-rank coals, such as lignite and sub-bituminous coals, were more prone to spontaneous ignition than high-rank coals. Deng et al. (2015) studied the effect of pyrite on spontaneous combustion. The effect of moisture on the self-heating process of coal has been widely investigated by many researchers (Arisoy et al., 2017; Chandralal et al., 2014; Kaji et al., 1986; Miura, 2016; Xuyao et al., 2011). The effects of coal moisture include that (a) evaporation of coal moisture could consume the generated heat from coal oxidation and (b) the high moisture content in the ambient would promote coal spontaneous combustion due to moisture adsorption. Therefore, Nelson and Chen (2007) suggested that dry coal piles should be separated from a damp place. The absorption amount of oxygen in coal is limited at low temperatures. It results in that the heat generation of coal is inevitably affected by the aging effect (Beamish et al., 2000; Lacey & Wake, 1983; Schmal, 1987; Song et al., 2015; Zhang et al., 2013). Akgün and Arisoy (1994) analyzed the effect of coal particle size on the oxidation rate.

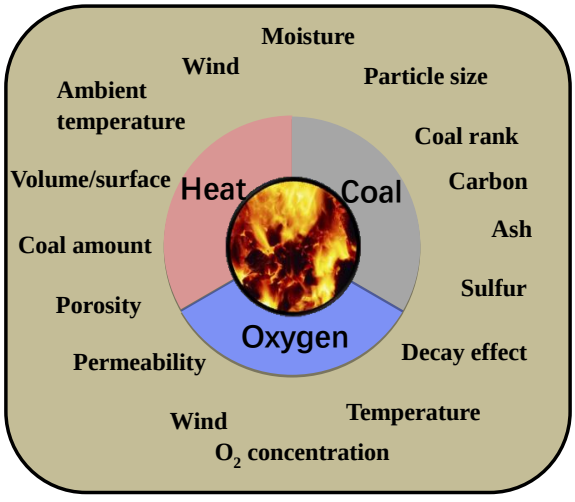

Figure 1- 8. Influence factors of coal spontaneous combustion (Liu & Zhou, 2010; Sloss, 2015; Zhang et al., 2016).

Junice et al. (2014) applied the Wire-mesh basket to study the effect of ambient temperature on coal temperature evolution. Wang et al. (2003) measured the heat generation rate with elapsed time under different constant temperatures. Chu et al. (2017) presented a decrease in permeability and porosity by reducing fragmentation degree could prevent coal self-heating. Ozdeniz (2010) conducted field experiments and studied the effects of ambient conditions, including air temperature, air humidity, atmospheric pressure and velocity, on the temperature of coal pile. Fierro et al. (1999) investigated the oxidation and spontaneous combustion of coal piles and took different measures on suppressing coal self-heating, including periodic compaction (reducing porosity and permeability), low angle slope (decreasing ratio of surface/volume), artificial barrier and ash-water slurry cover (decreasing wind velocity).

More researchers applied numerical simulations to study the effect of external factors on coal spontaneous combustion. The effects of pile height (Zhang et al., 2016; Zhang et al., 2016; Zhu et al., 2013), porosity (Brooks & Glasser, 1986; Ejlali et al., 2011; Krajčiová et al., 2004; Schmal et al., 1985; Zhang et al., 2016; Zhang et al., 2016; Zhu et al., 2013), particle size (Zhang et al., 2016), wind velocity (Krishnaswamy et al., 1996; Schmal et al., 1985; Taraba et al., 2014; Zhang et al., 2016; Zhu et al., 2013), slope angle (Krishnaswamy et al., 1996; Zhang et al., 2016; Zhu et al., 2013), particle size(Brooks & Glasser, 1986; Krishnaswamy et al., 1996; Zhang et al., 2016), bottom characteristic (Zhang et al., 2016), permeability (Ejlali et al., 2011), oxygen concentration (Zhu et al., 2013), sun radiation (Krajčiová et al., 2004), ambient temperature (Zhang et al., 2016), thermal conductivity of coal (Schmal et al., 1985), ratio of surface to volume (Zambra et al., 2012) on spontaneous combustion of coal have been studied in detail.

The effects of particle size (Yuan & Smith, 2008), methane (Zong et al., 2008), air leakage or ventilation flux (Liu & Qin, 2017; Xia et al., 2016; Xia et al., 2015; Yang et al., 2009; Zong et al., 2008), advancing rate of the coalface (Liu & Qin, 2017; Liu et al., 2017; Taraba & Michalec, 2011; Xia et al., 2016; Xia et al., 2015), gas extraction (Hongqing & Xingkui, 2012; Xia et al., 2017), porosity (Wang et al., 2015; Zhang et

al., 2006), ventilation resistance (Xia et al., 2015), the thickness of crushed coal (Liu & Qin, 2017), coalface width (Xia et al., 2016), were investigated on spontaneous heat process of coal mine gob.

The effects of pillar length (Nordon, 1979), airflow (Nordon, 1979), permeability (Xia et al., 2014), porosity (Xia et al., 2014; Xia et al., 2015), differential pressure (Xia et al., 2014; Xia et al., 2015) were studied on self-heating of underground coal pillar.

1.6 Experiments on coal spontaneous combustion

Experiments are the best and direct method for the researchers to find better assess, prevent, and deal with the risk of coal spontaneous combustion. The self-heating behaviors and the criteria for the self-ignition tendency of coal are normally obtained from the lab-scale experiments. In the recent 100 years, some researchers have been carried out various experiments of large-scale (coal amount of 10^2-10^5 kg) and lab-scale (coal amount of 10^{-4}-10^2 kg) to investigate the spontaneous combustion properties of coal.

1.6.1 Large-scale experiments

In the 1920s and 1930s, Mason and Tideswell (1939) built a test apparatus within 10 t of coal. A warm airflow of 35-65.5 ºC was injected into the coal pile for 9 months without a detectable reaction. However, heating development was recorded when airflow temperature is increased from 65.5 to 76.7 ºC.

Scott (1980) carried out a large-scale experiment with 1 t of coal in a one-dimensional cylinder (0.6 m in diameter and 5 m in length). However, the maximum coal temperature was unable to exceed 41 ºC due to radial heat losses. Then in 1986, they built a new full-scale laboratory apparatus (2 m long and 0.3 m in diameter). The similar column-apparatus were wildly applied in the study of coal self-ignition (Akgün & Arisoy, 1994; Arisoy et al., 2006; Beamish et al., 2002; Onifade et al., 2018; Stott & Dong, 1992).

Chauvin et al. (1985) carried out the test involving around 1 to 5 t of dry coal in insulated containers. Oxygen entered the coal pile by natural diffusion and self-heating occurred in the area of sufficient O_2 concentration.

Smith et al. (1991) built a large chamber, containing 13 short tonnes of bituminous coals, to simulate the self-heating behavior of coal mine gob. The experiment results showed that the self-heating of a large coal pile depends on coal reactivity, particle size, the freshness of coal surfaces, heat-of-wetting effect and ventilation rates.

Cliff et al. (1998) carried out a large-scale experiment, similar to the adiabatic method, with approximately 15 t coal. The hotspot appeared in the coal pile within 1 m of the inlet after 5 months.

From the 1980s, Xi'an University of S&T (Deng et al., 2015; Jingcai et al., 1989) has investigated the characteristics of coal spontaneous combustion at low temperature by carrying out the large-scale experimental furnace. The coal amounts were from 0.4 to 15 t.

Wang et al. (2017) conducted the large-scale wire-mesh basket test (0.71 t of lignite) to investigate the heating character and critical self-ignition temperature of the cubic coal pile.

1.6.2 Small-scale experiments

Despite the large-scale experiments have the benefit to apply the results to coal piles or seams, it is not easy due to the high-cost, long-term and unpredictable risks. Therefore, small-scale experiments ($< 10^2$ kg) are the fundamental approaches to research the behaviors of coal spontaneous combustion. The small-scale methods have the advantages of high repeatability and operability. As shown in Table 1-3, the main small-scale methods include chemical constituents analysis, oxidation oven methods and thermokinetic methods (Mohalik et al., 2017). With technological development, more and more new methods will be developed to further investigate the exothermic coal-oxygen reaction.

Table 1- 3. The main small-scale experiments for coal spontaneous combustion.

Chemical constituents analysis	Oxidation oven methods	Thermokinetic methods	Other methods
Proximate and ultimate analysis	Crossing point temperature (CPT) method	Differential thermal Analysis (DTA)	Russian U25 index
Mineral matter study	Adiabatic method	Differential scanning calorimetry (DSC)	Amount of O_2 adsorption
Petrography analysis	Wire-mesh basket (WMB) test	Thermo-gravimetric analysis (TGA)	Olpinski index method
X-ray diffraction (XRD) techniques	Hot plat method		Pulse calorimetry method
Fourier transform infrared spectroscopy (FTIR)			Flammability temperature
Gas chromatography (GC)			Wet oxidation potential analysis
Nuclear magnetic resonance spectroscopy (NMR)			Comprehensive systematic data analysis

(a) Chemical constituents analysis

Chemical constituents analyses mainly scan and examine the elements, structures, or surface of coal at low temperatures. Moreover, the reaction products of coal oxidation are captured and detected.

Beamish and Arisoy (2008) applied X-ray powder diffraction analysis to study the effect of mineral matter on the coal self-heating rate.

Petrography studies could be utilized to identify the mineral contents and the textural relationships within coal samples. Geologists found that vitrinite was useful to determine the potential of coals at self-ignition (Mohalik et al., 2017).

Nuclear magnetic resonance spectroscopy (NMR) is used to observe local magnetic fields around atomic nuclei. It can be used to measure the concentration of free radical concentrations in coal. With the oxidized degree of coal increasing, the free radical concentration was increased and then decreased (Xu et al., 2018; Yokono et al., 1981).

Fourier transform infrared spectroscopy (FTIR) technique was widely applied to analyze the distribution and structural characteristics of functional groups (Clemens et al., 1991; Xin et al., 2014; Zhang et al., 2015). X-ray diffraction (XRD) technique can be used to examine the mineral transformation and catalytic action of minerals of oxidizing coal (Henao et al., 2010; Kök, 2008). However, this technique cannot provide a classification system for coal self-ignition (Mohalik et al., 2017).

GC technique is applied to measure the reacted gas and oxygen consumption in the process of coal-oxygen reaction. This method is always co-used with other techniques (Jo et al., 2013; Lu et al., 2004; Wang et al., 2009). Some indexes, for evaluating the tendency of spontaneous combustion, include O_2/sum (CO, CO_2, CH_4, H_2, C_2H_4) (Wang et al., 2018), CO (Xu et al., 2018), CO/CO_2 (Kuchta et al., 1982), C/H (Ghosh & Banerjee, 1967), Willet's ratio (Willet, 1952), O_2 adsorption amount (Qi & Qian, 1996), Graham's ratio (Graham, 1920), CO/O_2 (Singh et al., 2007), CO_2/CO (Singh et al., 2007), were tested and determined by GC or other gas detecting techniques.

(b) Oxidation oven methods

The mainstream oxidation oven method is classified into crossing-point temperature

(CPT) method, adiabatic method and wire-mesh basket (WMB) test. Different methods demand the corresponding thermal boundary conditions.

The crossing point temperature (CPT) method, namely the programmed temperature method, was developed at CANMET Coal Research Laboratory in Alberta, Canada (Chakravorty & Kar, 1986). Oven temperature is increased with a constant heating rate and coal sample in the vessel is thus heated, accompanied with heat generation. In case that the heat generation rate is increased, the coal temperature will exceed the oven temperature with achieving self-acceleration heating.

The traditional CPT method is as follows (Choi et al., 2014; Küçük et al., 2003; Ogunsola & Mikula, 1991): Two vessels, each containing the same mass of coal sample (35-60 g), are installed in an oven, and then are injected nitrogen and air under programmed increased temperature. When coal temperature meets the increasing oven temperature, the coal temperature is CPT. Some researchers (Saffari et al., 2019; Xuyao et al., 2011) analyzed the possibility of using CPT for judging the tendency of coal self-ignition. This method was developed to a new system by combining with the CG method (Li et al., 2019; Xu et al., 2017; Zhong et al., 2010). The developed system is generally used to measure the generation of reaction gas or consumption of oxygen in the process of coal oxidation.

The information about the adiabatic method for studying spontaneous heating of coal was particularly published by Davis and Byrne (1924). In the recent 40 years, this method has been widely applied in the field of coal oxidation behaviors at low temperatures (Hill, 1986; Luo & Wang, 2012; Springenschmid, 1997; Wang et al., 2018). The temperature of injection gas should be kept consistent with the transient temperature of coal. Theoretically, this process is an exothermic reaction in which the generated heat is absorbed by coal and used for moisture evaporation. Therefore, the sensitivity of gas temperature and heat-insulating of the oven are important to carry the experiment. Based on the Adiabatic method, some institutions and researchers have presented the different evaluation indexes for identifying the potential of thermal run-aways of coal, such as R70 (Beamish et al., 2000; Humphreys, 1979), activity energy

(Lu et al., 2006), SHT (Smith et al., 1988), average temperature rise (Zubíček, 2008) and T180 (Le, 2018).

Wire-mesh basket (WMB) test has been widely used to study coal self-heating characteristics. The oven with constant temperature supports the stable thermal boundary for heating coal samples. A coal pile in the oven is initially heated by absorbing energy from the hot ambient. Then, the coal pile liberates heat to the outside environment once its temperature higher than the oven temperature. whether self-ignition breaks up or not is a critical result in the WMB test. In the 1970s, WMB tests were carried out largely at the Fire Research Station in the UK and a formulation of a test for predicting the self-heating tendency of coal or carbon material (Bowes & Cameron, 2007; Jones, 2006). Based on the WMB test, some industry standards for predicting and evaluating the self-heating substances were developed, such as EN standard of EN15188:2007 (European committee for standardization, 2007), German standard of VDI 2263 (Guideline, 1992) and UN standard (Committee of Experts on the Transport of Dangerous, United Nations, 2009). Moreover, a new CPT index has been developed by Chen and Chong (1999, 1998). The CPT value was the coal temperature when the center temperature meets the temperature of a certain point, which was located between the center point and surface. The theory of Frank-Kamenetskii (Frank-Kamenetskii, 2015) was used to measure and analyze the activation energy of WMB tests (Jones, 1999, 2000; Jones & Cook, 2000; Jones & Vais, 1991; Zhong et al., 2006).

Besides, a semi-isothermal method, similar to the WMB test, is hot plat test. A ring is filled with the coal dust sample and heated by a hot plate with constant temperature (Janès et al., 2019; Li et al., 2020; Yuan et al., 2019). In the standard ASTM E2021 (Astm, 2001), the hot plat test is defined to measure relevant thermal and kinetic parameters such as thermal conductivity, activation energy, the heat of reaction, and pre-exponential factor. These parameters can be utilized to determine the spontaneous combustion of a dust material deposited on the plates.

(c) Thermokinetic method

Thermokinetic methods are primarily Differential thermal analysis (DTA), Differential scanning calorimetry (DSC) and Thermo-gravimetric analysis (TGA). In 1967, Banerjee and Chakravorty (1967) used the DTA technique to explain the self-heating phenomenon of coal. Afterward, TG/DTA/DSC techniques were widely applied to the fields of coal spontaneous combustion and burn off. Li et al. (2014) put forward that the TGA–DSC method is a cost-effective technique for deriving the kinetics of coal oxidation at low-temperature oxidation. Avila et al. (2014) used the TG analysis to develop the TG phi-index, a relationship between the mass-loss rate and temperature, to estimate the potential of coal spontaneous combustion. The thermokinetic methods are popular to estimate the self-ignition potential of coal by applying the activation energy (Liu et al., 2005), ignition activation energy (Wang et al., 2008), pyrolysis activation energy (Long & Hanxu, 2016) and activation energy of DSC-sub (Li et al., 2016). Muangthong-On et al. (2017) investigated the adsorption/desorption of water in coal using TG-DSC techniques.

(d) Other methods

The following small-scale methods are mainly applied to predict the tendency of coal spontaneous combustion.

Russian U25 index was developed by a research group, the Russian Research Institute of Mine Rescue (Panigrahi et al., 1997; Russian Technical Standard Association, 1997). It is based on an idea of isothermal absorption of oxygen by coal sample, which is confined into a flask with a temperature of 25 °C. A similar criterion, using O_2 adsorption to predict the tendency of spontaneous coal heating, has been published by the Standardization Administration of China as a national standard (Qi & Qian, 1996).

Olpinski index method was proposed by Olpinski and Struminki (Adamus, 1998; Zubíček, 2008). The activation energy was calculated based on the temperature increase ratio due to coal oxidation at 237 and 190 °C. This method has been applied in the National standard of PN-93 G-04558 (Le, 2018; Sáowik, 2008).

Method of pulse calorimetry is the assessment of heat quantity released from coal oxidation in the calorimeter. Václav (Zubíček, 2008) presented the index of q30,

namely the cumulative heat generated by coal oxidation in the first 30 minutes using the isothermal calorimeter. Three degrees on spontaneous combustion were divided into the classification of susceptibility according to this method.

Flammability temperature is defined as the minimum temperature at which the coal starts to ignite (Adamus, 1998; Nimaje & Tripathy, 2016). An intimate coal dust/air mixture was injected to furnace and the temperature of coal catching fire was measured by repeating tests.

Wet oxidation potential analysis (Ray et al., 2016; Tarafdar & Guha, 1989) was carried out with potassium permanganate ($KMnO_4$) as an oxidizer in potassium hydroxide (KOH) solution. The difference between the potential difference of the mixture before and after complete oxidization of the coal sample was considered as a parameter for the susceptibility of coal to spontaneous combustion.

In the recent 20 years, a comprehensive systematic data analysis method using PC has risen the more and more attention of researchers, for instance, the analytic hierarchy process (AHP) and artificial neural networks (ANN). The method normally involves massive influencing variables, such as intrinsic, geological and mining characteristics. Eventually, comprehensive indexes are calculated by evaluating the thermal run-away propensity of coal. Saffari et al. (2017) proposed CSCPI classification based on the Fuzzy Analytic Hierarchy Process (FAHP) approach. Panigrahi and Sahu (2004) applied the ANN technique to classify the coal seams into four different categories of spontaneous combustion.

1.7 Numerical simulation on coal spontaneous combustion

A numerical simulation is a calculation to obtain the desired parameters and results by implementing a mathematical model to a certain physical model. Compared to real experiments, mathematical calculation is safe, economic for studying coal spontaneous combustion. During the half a century, considerable researches with the numerical simulation of coal self-ignition have been investigated in different types, such as small-scale lab experiments (Choi et al., 2011; Wu et al., 2017; Yuan et al., 2019; Zhang et

al., 2018), large-scale experiments (Wen et al., 2017; Yuan & Smith, 2009), coal piles (Krishnaswamy, et al., 1996; Schmal et al., 1985; Taraba et al., 2014; Zhang et al., 2016; Zhu et al., 2013), mine gob (Liu & Qin, 2017; Liu et al., 2017; Taraba & Michalec, 2011; Xia et al., 2016; Xia et al., 2015), underground coal pillar (Nordon, 1979; Xia et al., 2014; Xia et al., 2015) and coal seam outcrop (Tang et al., 2019; Wessling et al., 2006, 2008).

The development of numerical models on heat generation of coal at low temperatures is an important aspect of performing numerical simulations of self-heating or spontaneous combustion. These models have taken into account that the chemical adsorption or reaction of O_2 with coal at low temperatures with the physical properties of the coal and the environmental conditions (Wang et al., 2003). The conventional Arrhenius equation has been used to assess the simple exothermic reaction of coal at low temperatures (Hooman & Maas, 2014; Kim & Sohn, 2016; Song et al., 2014; Xiaodong, 2014). This equation is written as

$$q_h = CA_0 \exp\left(-\frac{E}{RT}\right) \tag{1- 1}$$

where q_h (W/kg) is the heat generation rate in the coal, C (-) is the O_2 concentration, T (K) is the coal temperature at a specific position in the coal pile, A_0 (W/kg) is the pre-exponential factor, E (J/mol) is the activation energy, and R (J/(mol·K)) is the gas constant. According to this equation, oxidative heat generation increases exponentially with the coal temperature, T. An obvious defect in modeling by Equation (1-1) is that the heat generation rate of the coal is assumed to maintain a constant value versus time under a constant temperature. It does not coincide with actual experimental observations (Fierro et al., 2001; Miura et al., 2017; Wang et al., 2003; Wang et al., 2017; Wu et al., 2016).

As shown in Figure 1-9, when a coal mass is exposed to air or oxidizing atmosphere at low temperatures, heat generation is primarily determined by the rates at which O_2 molecules can be physically and chemically adsorbed on the internal surfaces of micro-

pores in coal matrix (Zhang et al., 2016). The oxidation rate of the chemisorption decreases with the increasing number of blocked sites in the micro-pores by the adsorption. This deactivation of reactive sites leads to the so-called aging effect. This decay of oxidative exothermic reaction at low temperatures is similar to Elovich kinetics. Generally, a high rate of O_2 chemical adsorption will be observed in the initial stage after exposure to air, because fresh coal has significant quantities of reactive sites. However, the oxidation rate decays with an elapsed time (after several hours), which has been reported by several studies (Arisoy & Beamish, 2015; Kaji et al., 1987; Nordon et al., 1979; Sasaki et al., 1987).

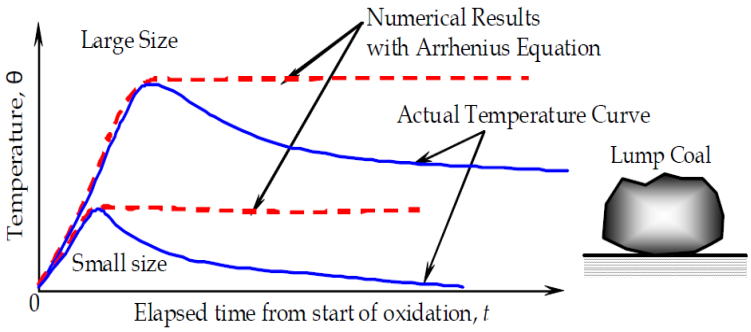

Figure 1- 9. Temperature change between the Arrhenius equation and the actual process for small lump coal (Sasaki & Sugai, 2011).

Wang et al. (2003) conducted isothermal tests and reported that the O_2 consumption rate of coal is decreased over elapsed time. Miura et al. (2017) measured the heat generation rate of coal under constant temperature by using TG-DSC analyzer and discovered reducing trends with time. Wang et al. (2017) measured the temperature of the wire-mesh basket (WMB) test and proposed coal temperature was decreased after reaching the maximum temperature with non-ignition. Moreover, Arisoy and Beamish (2015) and Zarrouk et al. (2006) suggested that the plotting of $\ln(dT/dt)$ vs. T^{-1} does not follow the Arrhenius equation after implementing the adiabatic test, due to the aging effect of coal oxidation. Thus, this aging effect is the intrinsic characteristic of coal heat generation and plays a significant role in the process of self-ignition.

Kaji et al. (1987) conducted measurements of coal heat generation at constant temperature and O_2 concentration and found an exponential decay in the heat generation rate over time following the initial exposure to hot air. Sasaki and Sugai (2011) developed a heat generation model incorporating aging by combining the Arrhenius equation including an aging effect is expressed as

$$q_h(T,C,t) = CA_0 \exp\left(-\frac{E}{RT}\right)\exp(-\gamma t) \quad (1\text{-}2)$$

γ (s^{-1}) is the decay-power factor that is a kinetic parameter and reflects the reduced degree of coal oxidation at low temperatures. When the aging effect is removed by setting $\gamma = 0$, Equation (1-2) becomes Equation (1-1) (Arrhenius equation). The value of γ is mainly determined by coal rank, particle size, as well as has a pronounced effect on the heat generation potential of the coal.

1.8 Objectives of the present research

As mentioned above, the traditional Arrhenius model has been widely applied in the numerical simulation on coal spontaneous combustion. However, aged coal shows low reactivity due to the removal of active sites by precious oxidation. Few researchers considered the aging effect on the heat process of coal, especially for field-scale coal. Therefore, the potential of coal self-ignition using the Arrhenius equation is inaccurate prediction for a coal operation. In the aging effect model, the decay-power factor, γ, is the key parameter, which reflects the coal reactivity.

The gel has advantages in decreasing coal temperature and isolating the air leakage, and it is expected to suppress the exothermic coal-oxygen reaction. Therefore, It is an effective material in preventing coal spontaneous combustion. In the case of a silicate-gel formation on coal particle or lump surface to prevent coal file, sufficient chemical concentration and conditions are prepared before wetting the coal surface to induce fast gelation time and large polymer size, because the gelation time is an important factor to control effectiveness of gel preventing coal fire (Adewunmi et al., 2015).

Therefore, it is a relatively severe challenge for operators conducting fire-prevention work to determine the amount of coagulation accelerator due to its cost.

Therefore, in this study, the WMB tests with different basket sizes were carried out for investigating the self-ignition behaviors and critical parameters. A novel sodium metasilicate nonahydrate-polyvinyl alcohol (SMN/PVA) gel was developed to prevent and extinguish coal fire. We attempt to apply the EOE-time model with an aging effect in the self-ignition process of the WMB tests to certify that the more superior of this model than the Arrhenius model. Besides, the EOE-time model is applied in the spontaneous combustion in the field-scale coal, such as stockpile. The sensitivities of influencing factors of field coal are analyzed using the EOE-time model. Moreover, the effect of gel covering the coal surface on CSIT of coal in WMB tests was evaluated in this study.

1.9 Outline of chapters

Chapter 1 illustrates an overview of the global energy status and the hazard of coal self-ignition in the world. Global GHG emissions from the uncontrolled coal fire are estimated. Moreover, the mechanism, influence factors and developed techniques related coal spontaneous combustion are discussed. Besides, it is concluded that considering the depleting or aging effect on coal oxidation is necessary, because the Arrhenius model does not to simulate the practical process of coal spontaneous combustion.

Chapter 2 addresses the WMB tests for wet and dried coal. Four cubic basket sizes (L = 5, 10, 15, 25 cm) for wet coal and three sizes (L = 5, 10, 15 cm) for dried coal were applied to do the tests. Two key parameters of critical self-ignition temperature, CSIT, and critical lead time, CLT, were estimated. A novel complex water solution (C-WS) of SMN and PVA, which formed cross-linked gel (SMN/PVA gel) with CO_2 gases, for preventing spontaneous combustion of coal piles/stocks is developed based on wire-mesh basket (WMB) tests. The effects between SMN/PVA gel and conventional gel on coal spontaneous combustion were compared.

Chapter 3 presents a mathematical 3-D model on the WMB tests. The theory of equivalent oxidation exposure (EOE) time is used to simulate the heating process of the coal sample. Numerical simulations with various decay-power factors, γ, are conducted for determining the optimal one. Further, the heating process of L = 25 cm including airflow velocity, temperature and O_2 concentration are investigated.

Chapter 4 focuses on the coal spontaneous combustion of a field-scale coal stockpile at low temperatures at low temperature range. The effect of γ on the spontaneous combustion of the coal pile is firstly investigated and the critical value of decay-power factor, γ_c is discussed. Relationship between γ_c and stockpile size is investigated. Effects of various parameters (pile length, porosity, particle size and wind velocity) on the self-ignition of the coal pile are investigated from a viewpoint of safe coal-stockpile operation.

Chapter 5 concludes the thesis and presents the outlook.

Chapter 2: Critical self-ignition temperature of coal measured by WMB test

2.1 Introduction

The Wire-mesh basket (WMB) tests have been used to investigate the critical self-ignition temperature (CSIT) of coal due to its excellence to find the effect of coal volume on coal spontaneous combustion. Researchers have carried out different scales WMB tests, in which coal mass ranges from 10 g to 1000 kg, to satisfy various purposes. In this study, the laboratory WMB tests were carried out using WMB sizes ranged from L= 5 cm to 25 cm and the average particle size of d = 10 mm.

Furthermore, the WMB tests (L = 2.5 to 10 cm and d = 0.7 to 7.5 mm) were carried out to evaluate the effect of an inhibitor, which was a cross-linked gel (named SMN/PVA gel) and formed from the complex water-solution (C-WS) of sodium metasilicate nonahydrate (SMN) and polyvinyl alcohol (PVA) and CO_2 gas, on the coal spontaneous combustion.

2.2 Wire-mesh basket (WMB) tests

2.2.1 Coal sample, measurement apparatus and tests procedure

The coal sample used for the WMB tests was low-rank coal excavated from the Baiyinhua coalfield in Inner Mongolia, China. The proximate analysis and ultimate analysis of lignite coal are provided in Table 2-1. The fresh coal was crushed and sieved to particle sizes, d, in the range from 8 to 12 mm (average 10 mm). Figure 2-1 presents a schematic diagram of the apparatus used for WMB tests. Two types of hot ovens (AS ONE Corporation, DOV-300A and Shanghai Jing Hong Laboratory Instrument Co., Ltd., DHG-9203A) were used in the WMB tests.

Table 2- 1. Proximate analysis and ultimate analysis of lignite coal.

		Wet coal	Dry coal
Proximate analysis (wt%)	Moisture	27.2	0
	Fixed carbon	24.7	37.4
	Ash	8.3	11.4
	Volatiles	39.8	54.6
		Dry ash-free basis	
Ultimate analysis (wt%)	C	70.44	
	H	4.91	
	O	21.39	
	N	1.35	

Four cubic WMBs in length L = 5, 10, 15 and 25 cm were used to investigate the effect of volume size on wet coal self-heating. The coal particles were naturally packed in the basket that had a mass uncertainty of ± 0.0005 kg. The baskets were made from copper wire-mesh (16 mesh). The WMB covered with a rectangular copper screen so that the bottom and top faces were exposed to air, to prevent the coal samples from the forced convective airflow in the oven. Three thermocouples were inserted at vertical positions from the basket bottom y_t/L = 0.2, 0.5 and 0.8 along the vertical center axis of each coal pile to monitor the internal temperature. The ambient temperature in the oven, T_e (ºC), was held constant with a thermal stability of ± 0.5 °C and monitored by an additional thermocouple. The temperatures were recorded at 10s intervals using a data logger (Graphtec Corporation, midi LOGGER GL 220).

Once the coal temperature in the pile center, T_c, reached a value of 60 °C higher than T_e, the self-ignition of the coal was expected. The WMB tests were repeated by increasing T_e with 5 °C increments to determine the super-critical and sub-critical temperatures of coal. Considering the thermal stability of the hot oven, thus the uncertainty of critical self-ignition temperature was estimated up to ± 3.5 °C. The decreased mass of coal particles before and after each test was measured.

The wet coal particles (d = 10 mm) were dried in the vacuum at 40 °C for 10 h (Wang et al., 2018), then placed in three different WMBs (L = 5, 10 and 15 cm) and tested following the steps described above.

(a) physical photo

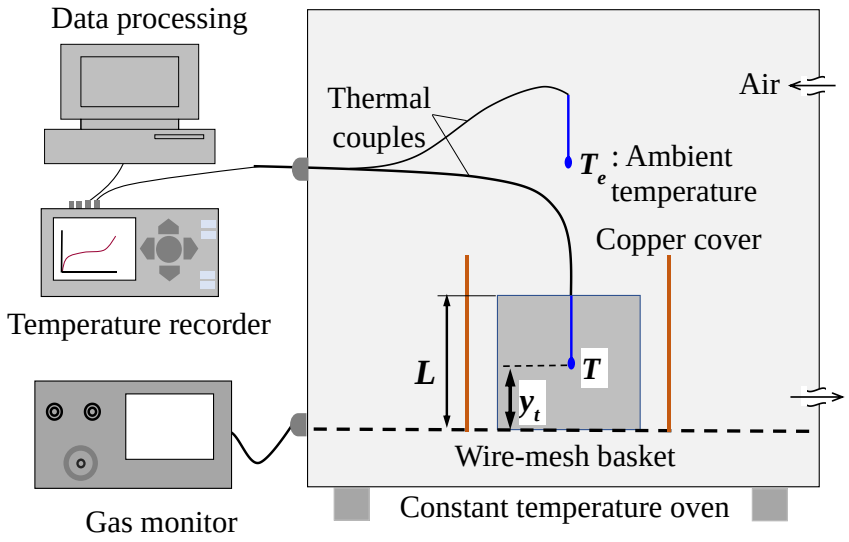

(b) Schematic diagram

Figure 2- 1. Laboratory wire-mesh basket test apparatus.

2.2.2 Parameters definition

As shown in Figure 2-2, the WMB tests were performed by heating coal piles (basket) in an oven at a constant ambient temperature, T_e (ºC) and constant O_2 concentration, C_e (= 23% in mass fraction). The temperature at the center position in the basket, T_c, was monitored to determine the critical self-ignition temperature (CSIT), T_{CSIT}, defined as the lowest ambient temperature, $T_{e\text{-}super}$, leading to ignition of the coal pile (super-critical). This CSIT was estimated according to finding a value intermediate between

the supercritical and subcritical temperatures ($T_{e\text{-}sub}$ and $T_{e\text{-}super}$) measured by WMB tests (García-Torrent et al., 2012). The CSIT is an important and effective index for the evaluation of the self-ignition tendency of coal piles (Wang et al., 2017).

The lead time to self-ignition, t_{lt}, is the induction time from the initial exposure of the coal pile to hot air (T_e) up to the time which the coal temperature, T_c, equals T_e. In the case that $T_e = T_{CSIT}$, the critical lead time (CLT), t_{CLT}, is defined as the induction time reaching T_{CSIT}. Therefore, t_{CLT} can be used as the time in which coal can be stored safely before an ignition hazard. Both T_{CSIT} and t_{CLT} are important factors to evaluate and compare the self-heating and spontaneous combustion of coal piles for managing coal piles.

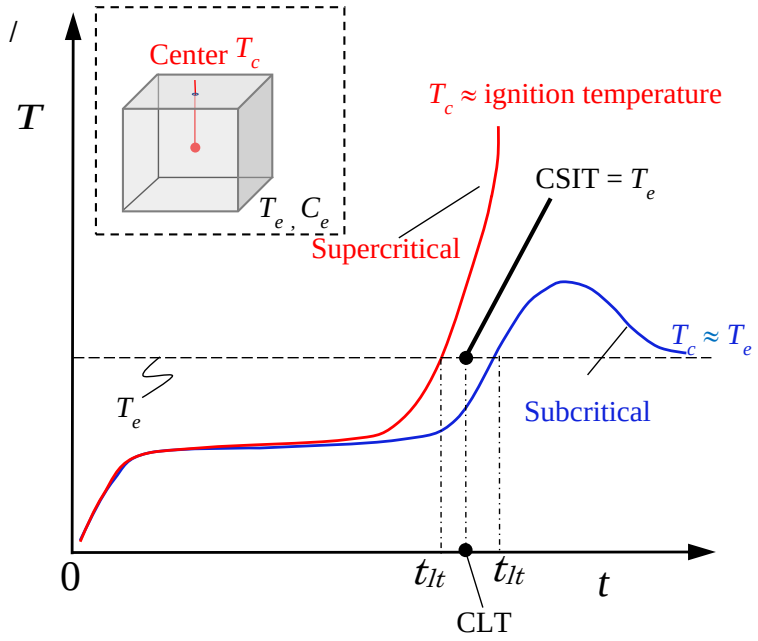

Figure 2- 2. A schematic showing definition of the critical self-ignition temperature (CSIT) and critical lead time (CLT) in WMB tests.

The evaluation methods by the WMB tests were used to investigate the characteristic parameters, such as Pseudo-Arrhenius method (Li et al., 2009), Semenov method (Bowes, 1984), Frank-Kamenetskii method (Jones, 1999, 2000; Jones & Cook, 2000; Jones & Vais, 1991) and Heat-release method (Wang et al., 2019). Those methods are mainly based on the theory of approximate thermal balance. Jones and his co-authors

(1999, 2000, 1991, 2000) used Frank-Kamenetskii method and measured the critical self-ignition temperature (T_{CSIT}) of different pile sizes ($L = 2r$, where r is the equivalent radius of the coal pile), as given in Equation (2-1). Zhong et al. (2006) proposed the heating rate ($\partial T_c/\partial t$) in the pile center, when T_c arrives T_e, as expressed in Equation (2-2) in the Heat-release method.

$$\ln\left(\frac{\delta T_{CSIT}^{\ 2}}{r^2}\right) = \ln\left(\frac{A_0}{\lambda}\frac{E}{R}\right) - \frac{E}{RT_{CSIT}} \tag{2-1}$$

$$\ln\left(\frac{\partial T_c}{\partial t}\right)_{T_c=T_e} = \ln\left(\frac{A_0}{C}\right) - \frac{E}{RT_e} \tag{2-2}$$

By plotting $\ln(\delta T_{CSIT}^2/r^2)$ against $1/T_{CSIT}$ or $\ln(\partial T_c/\partial t)_{Tc=Te}$ against $1/T_e$ as shown in the two equations, the activation energy, E, can be calculated from the slopes of the fitting curves, respectively. The difference between the two methods is whether considering the effect of basket size. Moreover, based on the graph, the CSIT value of the large-size coal piles can be extrapolated.

2.3 Results of Wire-mesh basket (WMB) tests

2.3.1 WMB tests with different pile volume

Figure 2-3 shows the center temperature, T_c, of wet coal piles for the temperatures ($T_e = T_{e\text{-}sub}$ and $T_{e\text{-}super}$). CSITs of the wet coal piles of L = 5, 10, 15 and 25cm were evaluated to be 132.5, 112.5, 97.5 and 87.5 °C, respectively. The CLTs of which were estimated as 4.32, 22.8, 39 and 109 h, respectively.

With increasing WMB size, CSITs show a decreased trend versus L. It was due to reducing the ratio of pile surface over pile volume. The coal pile with larger volume has a larger potential accumulating oxidized heat in the pile with a higher spontaneous combustion tendency, while, CLTs show increasing trend versus L.

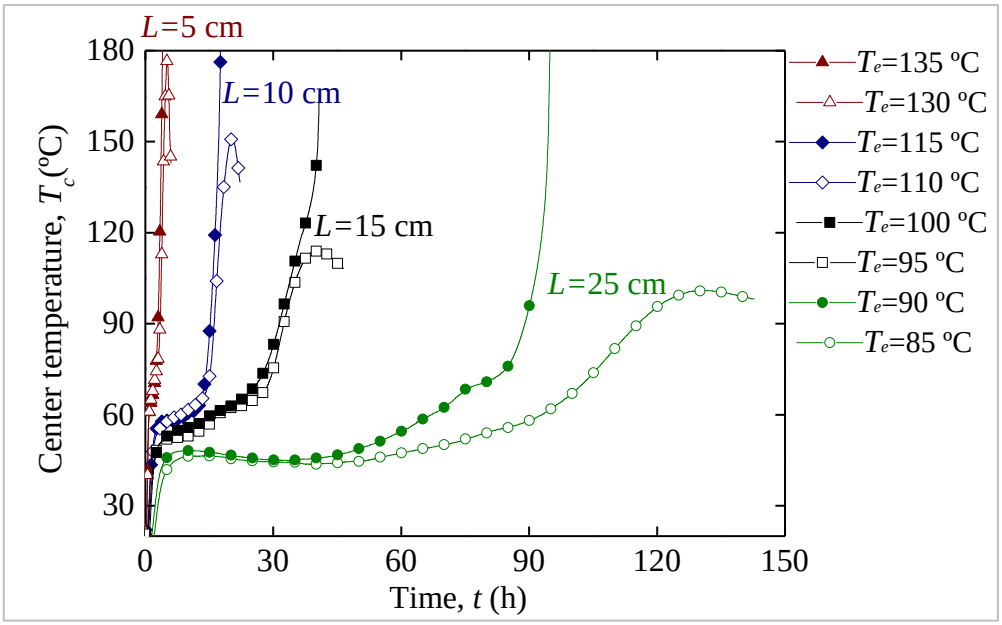

Figure 2- 3. Center temperature profiles of different sizes of WMB tests for super- and sub-critical temperatures (wet coal).

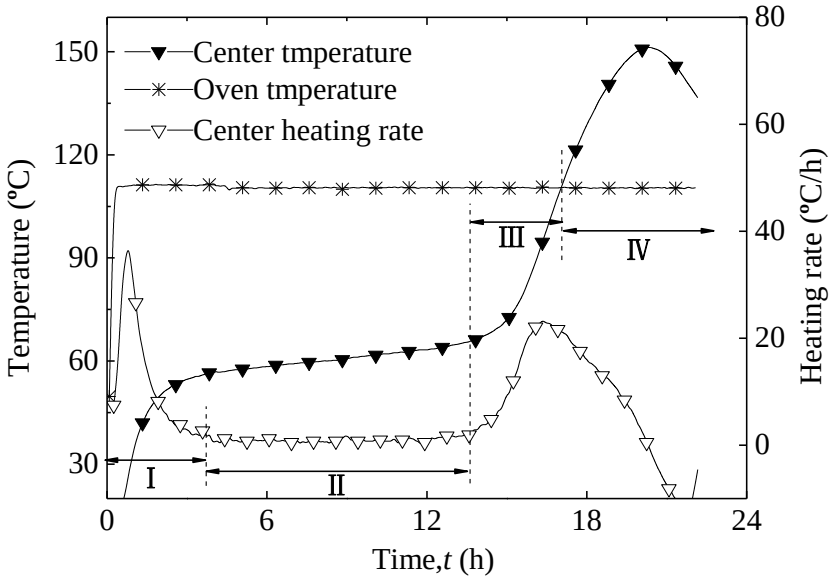

Figure 2- 4. Division of heating stages in the WMB tests (L = 10 cm, T_e = 110 °C).

The results of WMB tests under different conditions showed a similar trend. Taking L = 10 cm, T_e = 110 °C for example, A four-stage heating process was observed in the temperature heating rate curves, as shown in Figure 2-4: fast temperature-rise (t = 0-3.7 h, stage I), slow temperature-rise (t = 3.7-14.1 h, stage II), rebound temperature-

rise (t = 14.1-17.9 h, stage III) and ignition/decline stage (t = 17.9-22.3 h, stage IV). As illustrated in Figure 2-3, it is obvious that temperature curves in stages I and II of the same pile size for different T_e had almost coincident trends.

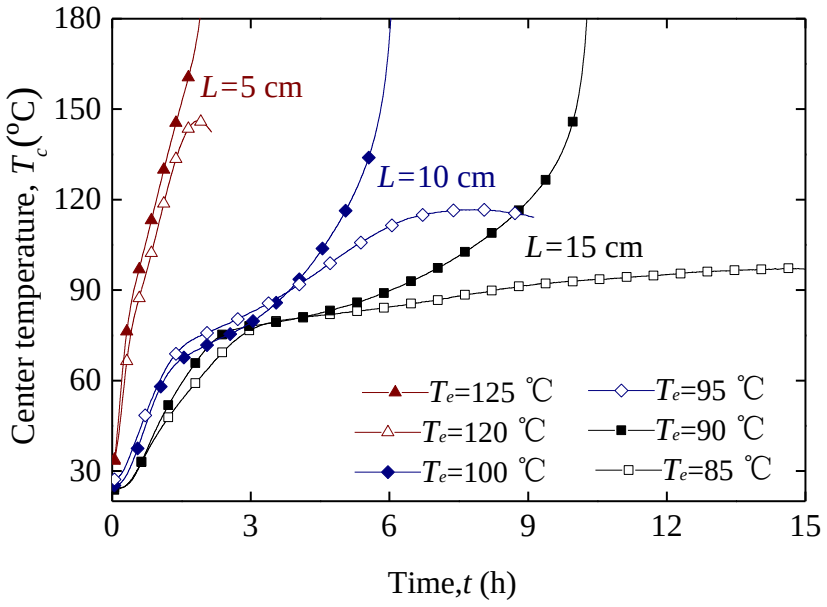

Figure 2- 5. Center temperature profiles of different sizes of laboratory WMB tests at each super- and sub-critical temperatures (dried coal).

Figure 2-5 shows the center temperature, T_c, of different dried-coal sizes at the critical temperatures ($T_e = T_{e\text{-}sub}$ and $T_{e\text{-}super}$) versus time. The CSITs of dried coal piles of L = 5, 10 and 15 cm were evaluated to be 122.5, 97.5 and 87.5 °C, as well as the corresponding CLTs were estimated as 1.2, 4.2 and 6.1 h, respectively. Compared with wet coal, CSITs of dried coal were dropped dramatically, around 10 °C, while, CLTs of wet coal were longer 2-5 times than those of dried coal. It was no doubt that water evaporation played an important effect on the self-heating process of coal. However, turning points at around 80 °C to 100 °C were observed in the WMB test using the baskets of L = 10 and 15 cm (Figure 2-5). The possible reason was the influence of inherent water, which is difficult to be moved in the drying process.

To eliminate the effect of water evaporation from coal, the activation energy is estimated following the Frank-Kamenetskii method (Equation (2-1)) and Heat-release method (Equation (2-2)). As illustrated in Figure 2-6, the activation energy, E, by

fitting $\ln(\delta T_{CSIT}^2/r^2)$ vs. $1/T_{CSIT}$ is estimated to be 78.9 kJ/mol. However, the activation energy by fitting the curves of $\ln(\partial T_c/\partial t)_{Tc=Te}$ vs. $1/T_e$ is respectively 79.26, 81.27 and 114.81 kJ/mol for L = 5, 10, 15 cm. According to Equation (2-2), with increasing pile size, the approximate thermal balance at $T_e = T_c$ becomes no-precious. Furthermore, the activation energy of the smallest basket size, L = 5 cm is estimated as 79.26 kJ/mol from Equation (2-2), which is most close to that evaluated from Equation (2-1). Besides, the Frank-Kamenetskii method considers the effect of the coal pile sizes. Therefore, the Frank-Kamenetskii method has higher accuracy than the Heat-release method.

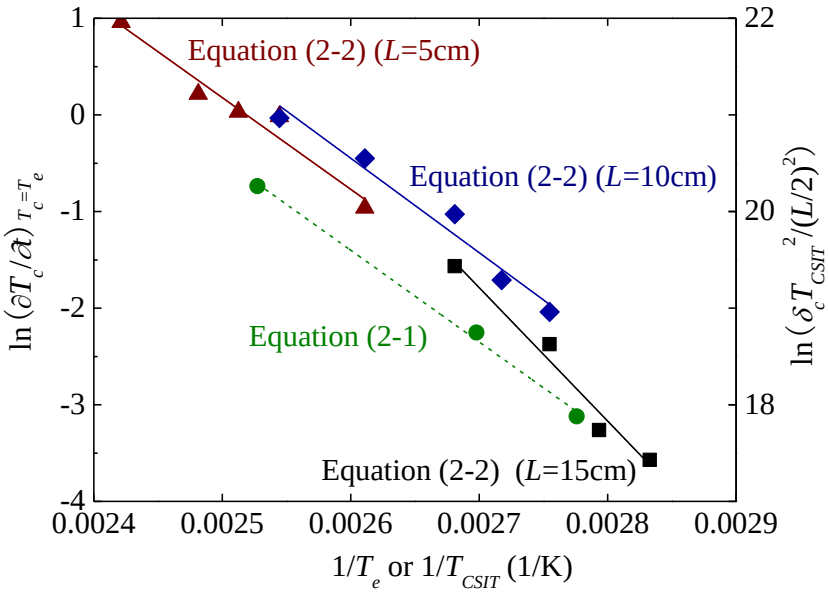

Figure 2- 6. Plot and fit of self-heating curves by Equation (2-1) and (2-2).

2.3.2 WMB tests with different particle sizes

Wang et al. (2017) conducted the upscale WMB tests using Baiyinhua lignite with an average particle size of 46 mm in three pile volumes, L = 25, 50 and 100 cm. The CSITs and CLTs of their WMB tests with L = 25, 50 and 100 cm (d = 46 mm) were measured to be 104, 92 and 81 °C as well as 28, 65 and 308 h, respectively. The relationship between CSIT and CLT versus coal pile volume, V (= L^3) are illustrated in Figures 2-7 and 2-8. CSITs of d = 46 mm are higher than those of small d = 10 mm

(16.5 °C in CSIT difference of L = 25 cm) and the CSIT difference become larger with increasing pile volume.

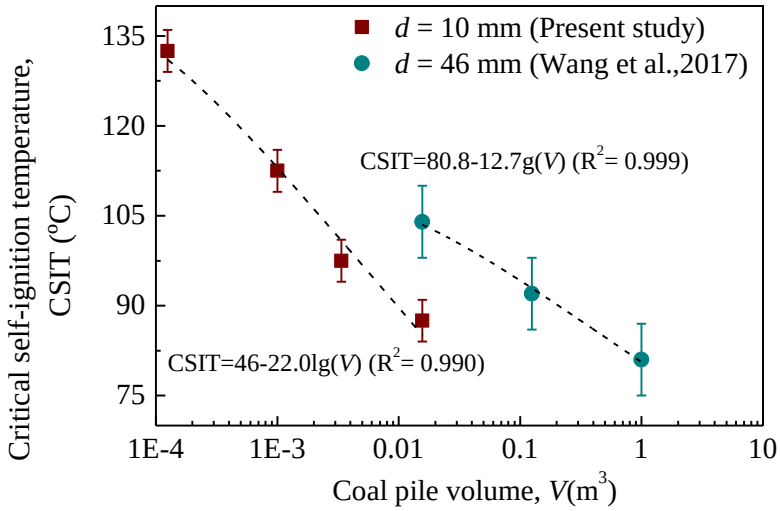

Figure 2- 7. Relationship between CSIT and coal pile volume.

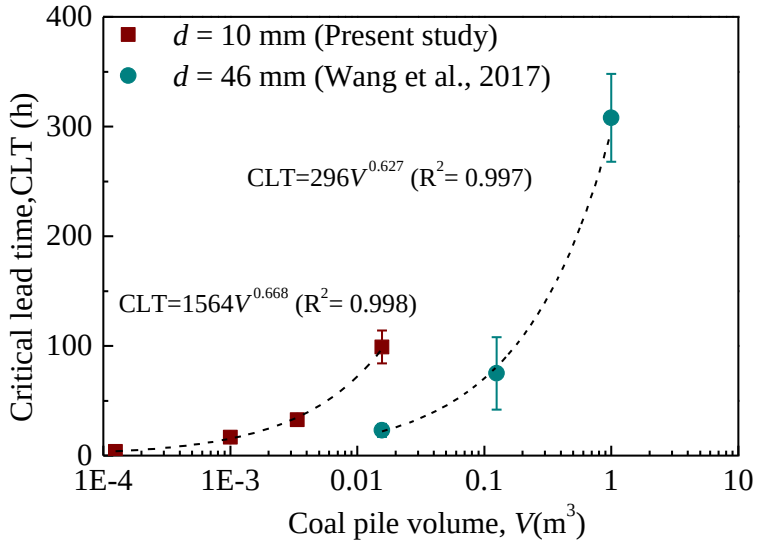

Figure 2- 8. Relationship between CLT and coal pile volume.

In Figure 2-7, the fitting logarithm equations are applied to match the measured CSIT versus V, as shown in the following two equations.

For d = 46 mm and L = 25, 50 and 100 cm (Wang et al., 2017):

$$\mathrm{CSIT}=80.8-12.7\log_{10}(V) \qquad (2\text{-}3)$$

For d = 10 mm and L = 5, 10, 15 and 25 cm (Present study)

$$\mathrm{CSIT} = 46 - 22.01\log_{10}(V) \quad (2\text{-}4)$$

However, CLT versus V is only matched by power fitting equations as follows,

For d = 46 mm and L = 25, 50 and 100 cm (Wang et al., 2017):

$$\mathrm{CLT} = 296V^{0.627} \quad (2\text{-}5)$$

For d = 10 mm and L = 5, 10, 15 and 25 cm (Present study)

$$\mathrm{CLT} = 1564V^{0.668} \quad (2\text{-}6)$$

It indicates that the coal pile with smaller particle size has a higher potential and longer period to spontaneous combustion state.

For further analyzing the effect of particles size in the process to coal spontaneous combustion state, the comparison of the WMB test result of L = 25 cm at T_e = 90 °C between d = 10 mm (Present study) and d = 46 mm (Wang et al., 2017) is shown in Figure 2-9.

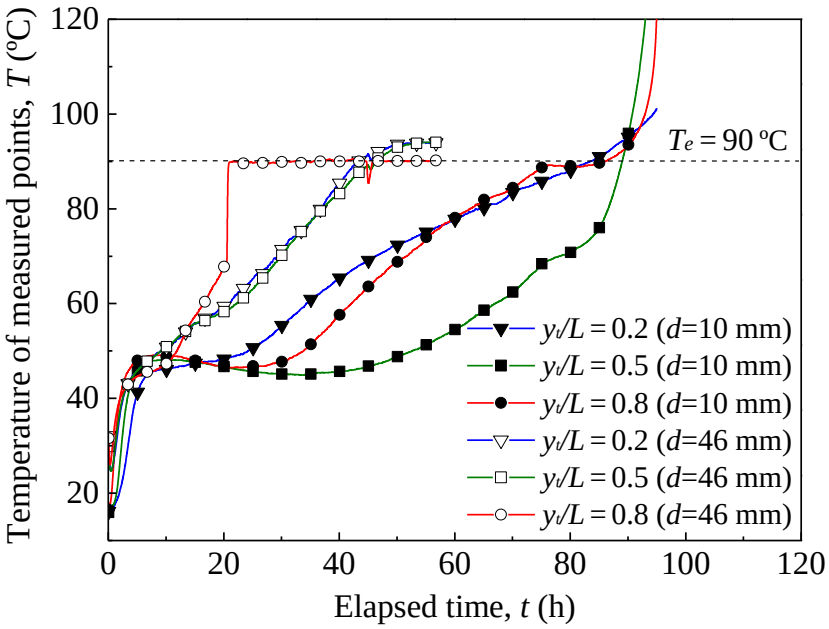

Figure 2- 9. Temperature profiles in the coal pile of L = 25 cm for different particle sizes, d = 10 and 46 mm.

The coal pile with larger *d* showed a shorter heating period (56.8 h) than that of smaller *d* (95 h). While the coal pile with smaller *d* indicated a higher tendency of self-ignition. It was due to the following reasons:

(a) Smaller coal particles possess the larger exposed surface to air than larger particles and thus more active groups could react with O_2. Therefore, it infers that the decay-power factor of heat generation for small coal particles is smaller than that of large coal particles, indicating that the heat generation rate of large coal particles is vulnerable to the aging effect.

(b) Permeability of coal pile with larger *d* is higher and the seepage airflow resistance is smaller. Thus, more heat from the oven entered into the coal pile by convection airflow, and thus the evaporated water vapor was easier to liberate to the hot oven. When the coal temperature rises over than T_e, oxidated heat from coal pile with smaller *d* is not dissipated to the ambient air than that of a larger one.

Some researches have been conducted the WMB tests using Baiyinhua raw lignite with different *V* and *d*. Wang et al. (2017) carried out laboratory WMB tests (L = 2.5, 5 and 10 cm, d = 0.48 mm) and upscale WMB tests (L = 25, 50 and 100, d = 46 mm). Wang et al. (2019) implemented the laboratory WMB tests for the piles of L = 2.5, 5, 10 and 15 cm, d = 0.5, 1, 3, 5, 7.5, 10 mm to investigate the effect of particle sizes of coal on spontaneous combustion. Besides, the supplied WMB tests using the Baiyinhua raw coal with L= 2.5 cm and d = 0.7, 1.3 and 3 mm (Run#0 tests in Section 2.4.2) were considered. Wang et al. (2019) compiled the above results and proposed the formula on the relationship between CSIT and pile volume ($V = L^3$) as well as particle size (d) as follows,

$$\mathrm{CSIT}_{\mathrm{raw}}(V, d) = 93\text{-}12.7\log_{10}(V)+10.9\log_{10}(d / L) \qquad (2\text{-}7)$$

This modified equation is based on Equation (2-3) by adding the effect of particle size. In this study, the CSITs vs. *V* of the raw coal described in Section 2.3.1 were considered. The estimated CSITs based on Equation (2-7) vs. the measured CSITs are shown in Figure 2-10. The fitting linear curve ($y = x$) possesses an R^2 of 0.873.

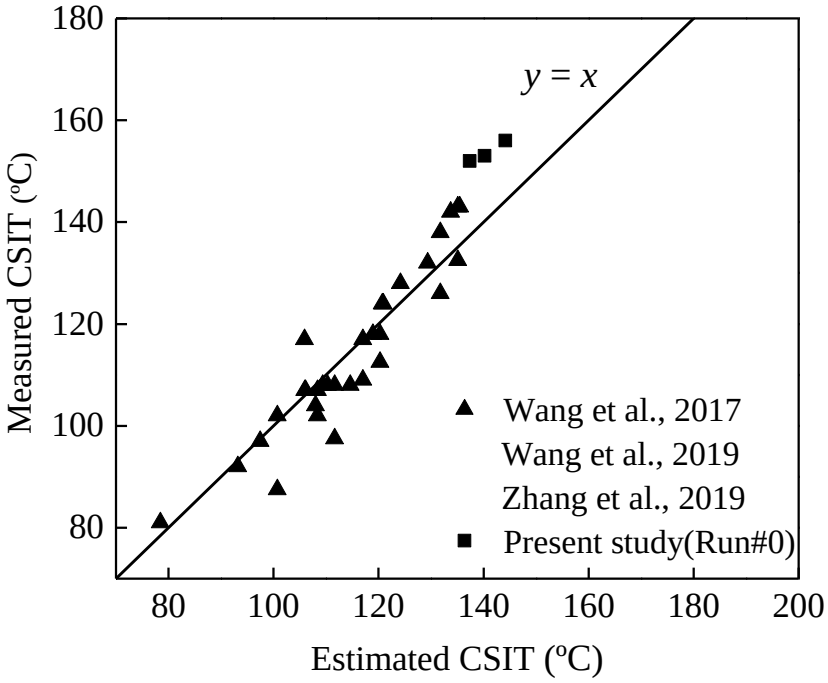

Figure 2- 10. Relationship between measured CSITs and estimated CSITs by Equation (2-7) for Baiyinhua raw coal.

2.4 WMB tests using coal coated by SMN/PVA gel

In the recent thirty years, a considerable amount of experimental and practical studies on inhibitors of coal spontaneous combustions have been conducted on pressure balance, grouting, inert gas, physical inhibitor, chemical inhibitor, gels, foam and form-gel (Colaizzi, 2004; Deng et al., 2018; Fan et al., 2020; Qin et al., 2017; Ren et al., 2019; Ren et al., 2015; Smith et al., 1988; Taraba et al., 2011; Vinogradov et al., 2016; Xi et al., 2019; Zhang et al., 2016; Zhou et al., 2015; Zhu et al., 2012). The gel is an effective material in inhibiting coal self-ignition and can decrease coal temperature and isolate air leakage. It is generally formulated with water, base material, coagulation accelerator and auxiliary additive (Huang et al., 2018; Ren et al., 2019; Yu & Jia, 2012). Sodium silicate has been widely used as the base material due to its excellent performance in fire prevention, low-price and harmless. The coagulation accelerator promotes the generation of orthosilicic acid. The conventional silicate-gel has the disadvantages of fast gelation time and large polymer size. Also, a great

demand amount of coagulation accelerator inevitably improves the cost of traditional gel.

2.4.1 Preparation of the complex water-solution (C-WS)

The chemicals used in present laboratory WMB tests were sodium-metasilicate nonahydrate (SMN), $Na_2SiO_3 \cdot 9H_2O$ (Junsei Chemical Co., Ltd.), polyvinyl alcohol (PVA) (Mitsubishi Chemical Co., Ltd., alcoholysis degree: 85.5-88.0 mol%) and sodium bicarbonate ($NaHCO_3$, Wako Pure Chemical Industries, Ltd.). Initially, a certain amount of SMN (Table 2-2) was slowly added into 100 g deionized water and stirred at 800 rpm until it dissolved completely (without suspended crystals). Then, a certain amount of PVA powder (Table 2-2) was added with stirring at 400 rpm to the SMN water-solution to form the complex water solution, C-WS. Moreover, the conventional silicate-gel was formed by adding sodium bicarbonate, which molar ratio to SMN was 2:1, in the C-WS, and stirred at 800 rpm until forming high-viscosity gel.

2.4.2 WMB tests of C-WS wetting coal

Properties of the coal sample are listed in Table 2-1. As listed in Table 2-2, five series of WMB tests (Run#1 to Run#5) were carried out to study the effeteness of SMN, PVA, and C-WS on fire-prevention of the lignite coal (L = 2.5 to 10 cm and d = 0.7 to 7.5 mm). The experimental details of WMB tests have been introduced in Section 2.2.1. The center temperature, T_c measured at y_t/L = 0.5 in the basket was recorded by a data logger. The five series of WMB tests were planned as follows:

Run#1: Study the inhibitory property of coal particles wetted by water, PVA water-solution, SMN water-solution, and C-WS.

Run#2: Compare the fire-prevention property of coating coal particles by SMN/PVA gel and conventional silicate-gel.

Run#3: Study the fire-prevention property of coal particles wetted by C-WSs with different SMN concentration.

Table 2- 2. C-WS components, basket size and coal particle size used in WMB tests.

Raw coal					
Run#	SMN(wt%)	PVA(wt%)	$NaHCO_3$(wt%)	*L* (cm)	*d* (mm)
0	-	-	-	2.5	0.7
				2.5	1.3
				2.5	3
Coal wetted by complex water-solutions (C-WSs)					
Run#	SMN(wt%)	PVA(wt%)	$NaHCO_3$(wt%)	*L* (cm)	*d* (mm)
1	0	0/0.2	0	2.5	3
	7	0/0.2			
2	0	0	0	2.5	3
	7	0.2	4.1		
	7	0.2	0		
	12	0.2	7.1		
	12	0.2	0		
3	2	0/0.2	0	2.5	3
	7				
	12				
	16				
	20				
4	7/12/16	0	0	2.5	3
		0.1			
		0.2			
		0.5			
5	16	0.2	0	2.5	0.7
				2.5	1.3
				2.5	3
				4	0.7
				4	1.3
				4	3
				4	7.5
				5	0.7
				5	1.3
				5	3
				5	7.5
				10	3

Run#4: Study the fire-prevention property of coal particles wetted by C-WSs with different PVA concentration.

Run#5: Investigate the effects of C-WSs on coal fire-prevention with different pile volume and particle size.

The process of applying the water-solutions on coal particles was as follows: a) Prepare coal particles by crushing coal lumps and sieving in the range from 2.5 to 3.5 mm, b) Dip the coal particles slowly in the solution and then stir the solution for 10 minutes at 100 rpm to insure the solutions on the coal particles surface. c) Drain solution drops from the samples and then disperse them on a flat sieve. d) Dry the coal particles for 3 h (24 h for Run#2 tests) in a constant temperature oven (30 °C, 35-40 %Rh). e) Keep the dried particles in the sealed plastic-bags before conducting WMB tests to prevent oxidation.

2.4.3 Amount of wetting C-WS by coal particles

The C-WSs used in Run#3 tests (PVA-0.2 wt%) were prepared by mixing different SMN concentrations. Firstly, around 2 to 3 g of the coal particles of d = 3 mm in size were set in a WMB and weighed. Secondly, the WMB was dipped in the C-WS and stirred at 100 rpm for 10 minutes in a beaker. Thirdly, extra-solution was removed from coal particle surface by a centrifugal separator to keep the minimum wetting solution on the coal particles surface. Finally, the wetted coal particles were moved to a dried WMB container and weighed. The tests using different SMN concentrations (0 to 20 wt%) were repeated three times respectively.

2.4.4 Gelation mechanism of SMN/PVA gel

As shown in Figure 2-11, SMN powders are dissolved in the water and few silicate anions (SiO_3^{2-}) are hydrolyzed with forming metasilicate (H_2SiO_3), as expressed in Equation (2-8). After pouring PVA is the solution, the hydroxyl ions (-OH) in H_2SiO_3 react with hydroxyl groups in PVA and dehydrate to the C-O-Si bands. However,

hydrogen bonds (-OH…O-) between hydroxyl groups in PVA and SiO_3^{2-} are more common in the C-WS, even though the bond energy is low (Zhang et al., 2015). A small number of hydrogen ions (H^+) are formed by the reaction between molecules of H_2O and CO_2 dissolved in water (Equation (2-9)).

$$SiO_3^{2-} + 2H_2O = H_2SiO_3 + 2OH^- \quad (2\text{-}8)$$

$$2CO_2 + 2H_2O = H^+ + HCO_3^- + H_2CO_3 \quad (2\text{-}9)$$

The weakened hydrogen bonds capture H^+ to become the strong-bonds (-O-) of SMN/PVA. On the other hand, the reaction between H^+ and free SiO_3^{2-} forms $Si(OH)_4$ as Equation (2-10).

$$2H^+ + SiO_3^{2-} + H_2O = Si(OH)_4 \quad (2\text{-}10)$$

$$nSi(OH)_4 = [Si_nO_{2n-m}(OH)_{2m}] + (2n-m)H_2O \quad (2\text{-}11)$$

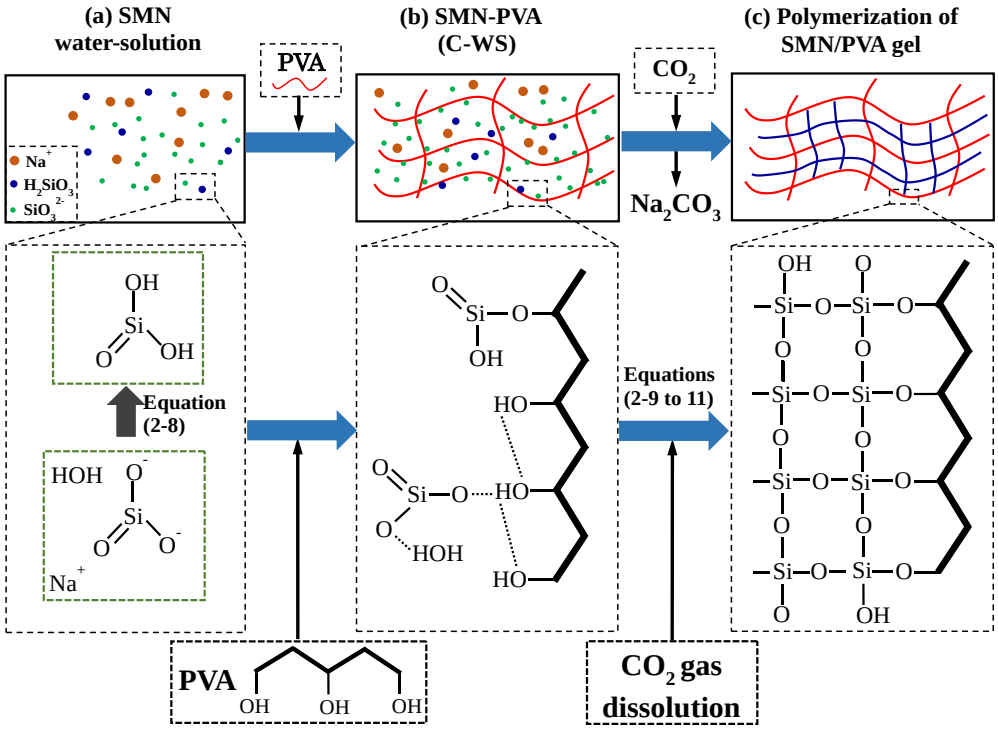

Figure 2- 11. Schematic diagram of the forming process of cross-linked SMN/PVA gel.

Large quantities of $Si(OH)_4$ polycondensate and dehydrate form SiO_2 oligomer with silanol groups on the surface (Equation (2-11)) (Marfin et al., 2013). The interaction between abundantly exposed –OH (including hydroxyl groups in PVA and silanol groups on SiO_2 oligomer and $Si(OH)_4$) generates the cross-linked chemical SMN/PVA gels (Pingan et al., 2017). The cross-linked gels are expected to have higher stability and compatibility than other silicate gels.

Run#1 tests were used to investigate the inhibitory property of coal particles coated by water, PVA water solution, SMN water solution and C-WS. CSITs of Run#1 tests are plotted in Figure 2-12. The PVA water solution included high-molecular polymers which were reported as the oxygen-insulating barrier (Meng et al., 2010). However, the PVA concentration used in this study was low to find an efficient property, because the CSIT of PVA-0.2 wt% water solution shows only 1 °C higher than that of pure water. On the other hand, the CSIT of SMN-7 wt% solution was 158 °C which exhibited much better inhibition effect than PVA-0.2 wt% solution and water, but slightly weaker effect than SMN/PVA gel. Accordingly, to some extent, the cross-linked SMN/PVA gel showed isolate coal particles from oxygen molecules and retard the exothermal coal-oxidation reaction.

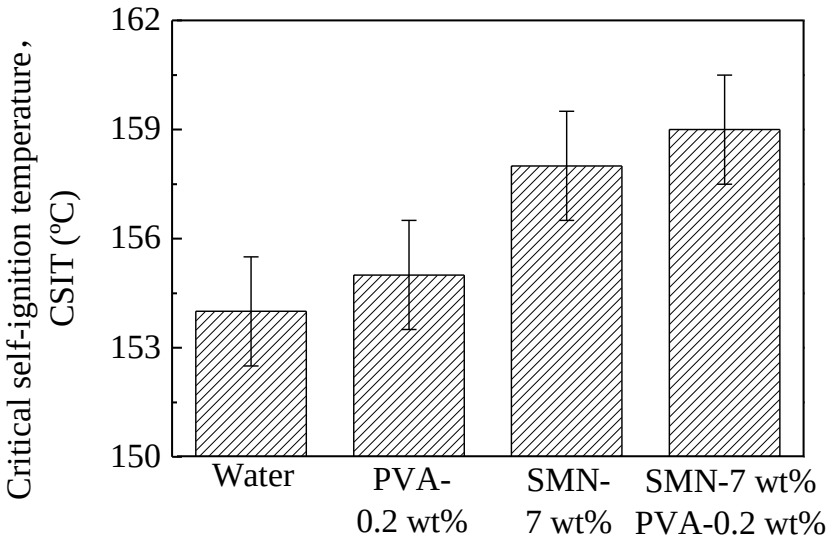

Figure 2- 12. Critical self-ignition temperatures of lignite coal wetted by different situations in Run#1 test.

2.4.5. Comparison between SMN/PVA gel with conventional silicate-gel

Run#2 WMB tests were conducted to compare the fire-prevention property of naturally formed SMN/PVA and conventional silica-gels. The usual silica-gel was formed with SMN, PVA, and sodium bicarbonate before being applied to the coal particles, while the SMN/PVA gel was formed after wetting the coal with C-WS. The results of CSIT obtained from Run#2 tests are shown in Figure 2-13. The CSIT values of SMN/PVA gel formed from SMN-7 wt% and 12 wt% were 10 and 15 °C higher than that of the silica-gel, respectively. This indicated that naturally formed SMN/PVA gel from C-WS on the particle surfaces exhibited more efficient fire inhibitory ability than the usual silica-gel. Liu et al. (2018) reported that lignite pores with the size range of 10–100 nm accounted for 70.7–97.5% of the total volume. Furthermore, Lu et al. (2019) reported the average pore sizes of raw and dewatered lignite to be 10.34–15.89 nm. As shown in Figure 2-14, the size of silica-gel ranged from 5 to 50 μm, which was significantly larger than lignite pore-size range. Therefore, silica-gel could only just cover the outer surface of lignite pores with a large size polymer. Nevertheless, the C-WS used in this study consisted of nanometer-size ions, which were easily adsorbed on the coal surface and enter the inlets of micropores in the coal matrix. Subsequently, the cross-linked SMN/PVA gel was formed by reacting with CO_2 gases present in atmosphere air and that emitting from coal oxidation in the pores. This gel prevented oxidation on the coal active sites by filling the pore inlets. Therefore, the area contacted with SMN/PVA gel on the coal particle surfaces was expected to be larger than that of silica-gel. Thus, SMN/PVA gel exhibited a better potential to suppress spontaneous coal combustion than silica-gel. Moreover, the free-natural coagulation accelerator of CO_2, instead of conventional coagulants, could reduce the commercial cost for field preventing fires in coal seams or piles.

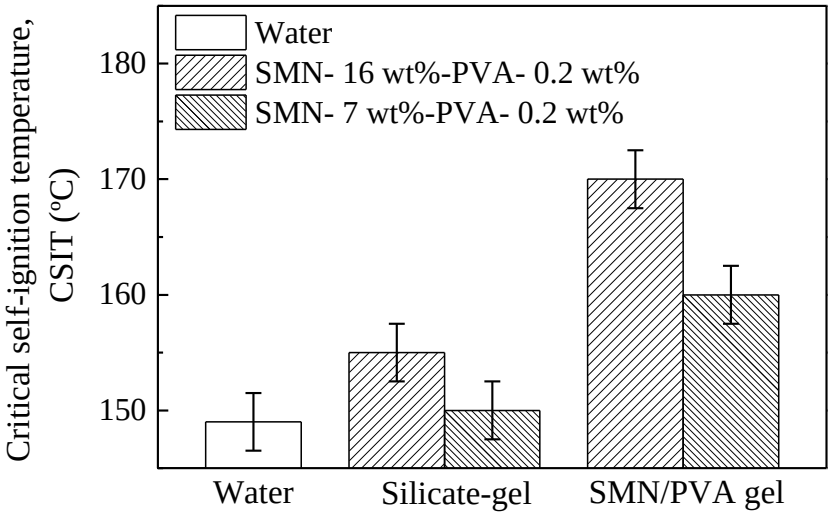

Figure 2- 13. Critical self-ignition temperatures, CSIT, of lignite coal treated by water, conventional silicate-gel and C-WS (SMN/PVA gel) in Run#2 tests.

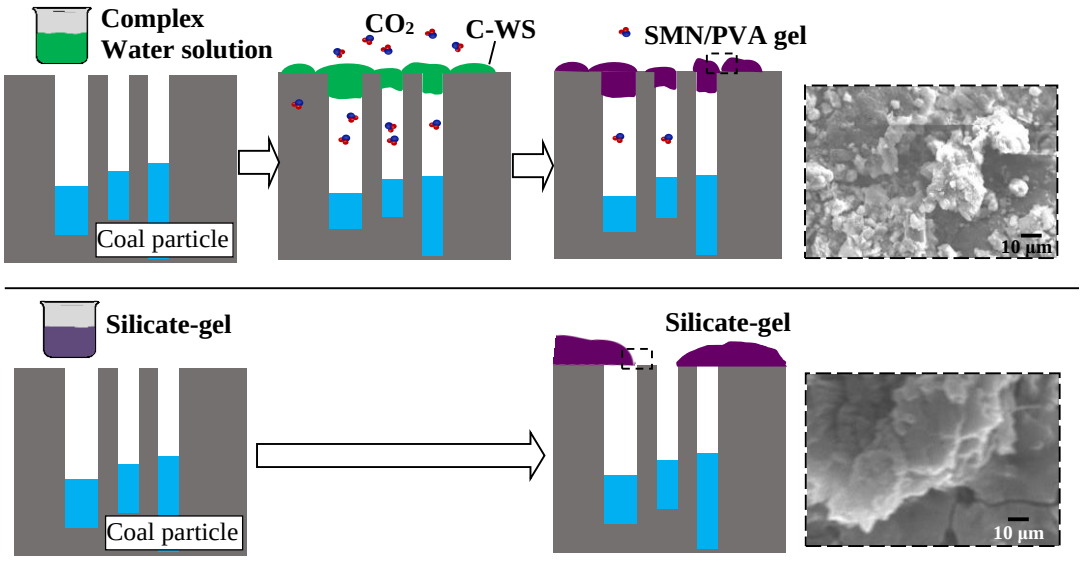

Figure 2- 14. Schematic of SMN/PVA gel formation with comparison to silicate-gel.

2.4.6. Effect of SMN concentration on fire-prevention property

Figure 2-15 shows the CSITs for different SMN concentrations in C-WS. For PVA-0.2 wt%, the coal particles wetted with C-WS, including higher SMN-concentrations, exhibited higher CSITs, especially for over 7 wt% of SMN. The effect of SMN (wt%) on increasing the CSIT (ΔCSIT) shows the relation expressed by ΔCSIT =

$0.080 \cdot SMN^2$. The higher concentration of silicate anions generated more SMN/PVA gels covering the micropore inlets on the particle surfaces. While preparing C-WS (SMN-20 wt% and PVA-0.2 wt%), some suspended off-white flocs were formed once PVA was added to the SMN water-solution. This indicated that the high concentration of SMN in C-WS decreased the hydrophilicity of PVA by reacting with hydroxyl group (Mitsumata et al., 2007). This showed the maximum limit of SMN concentration in C-WS to be lower than 20 wt%. The relationship between CSIT and SMN concentration in the SMN water-solutions (PVA-0 wt%) showed same trend as that of PVA-0.2 wt%. However, C-WS solution (PVA-0.2 wt%) exhibited a better inhibitory property than PVA-0 wt% when SMN concentration was higher than 7 wt%.

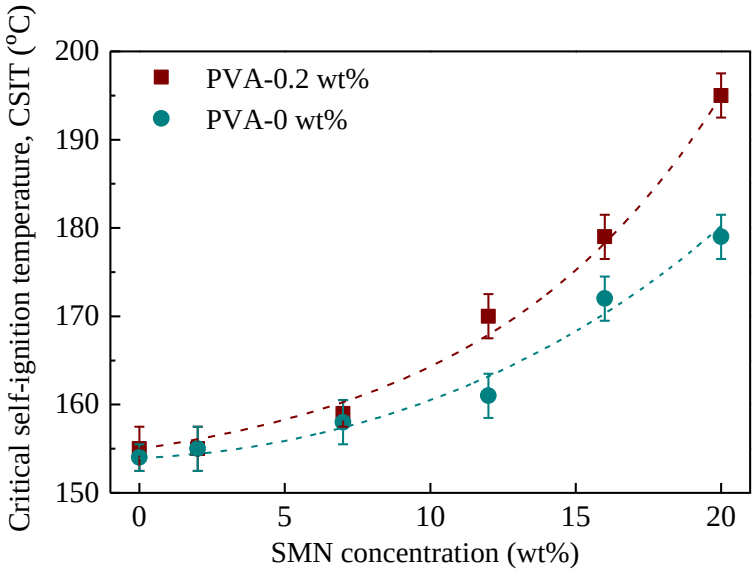

Figure 2- 15. Critical self-ignition temperatures of lignite coal wetted by C-WSs with different SMN concentrations in Run#3 tests (PVA-0 and 0.2 wt%).

2.4.7. Effect of PVA concentration on fire-prevention property

Run#4 tests were conducted to examine the effect of PVA concentration on CSITs. Figure 2-16 shows the CSIT values for lignite coal wetted by C-WS with SMN as 7, 12, and 16 wt% and different PVA (wt%) concentrations. When PVA concentration was lower than 0.2 wt%, CSIT (ΔCSIT) exhibited a seemingly increasing trend, as

expressed by ΔCSIT = 25·PVA. The increase in CSIT was more apparent because of the increase in the source of hydroxyl groups reacting with SiO_2 polymer to prevent contact with oxygen. However, the fire-prevention ability of PVA-0.5 wt% was reduced compared to PVA-0.2 wt% (SMN-12 wt% and 16 wt%). We estimated that the fast synthesis rate of the cross-linked SMN/PVA gel due to higher SMN and PVA concentrations resulted in the formation of larger sized non-uniform gel, with performance similar to silica-gel.

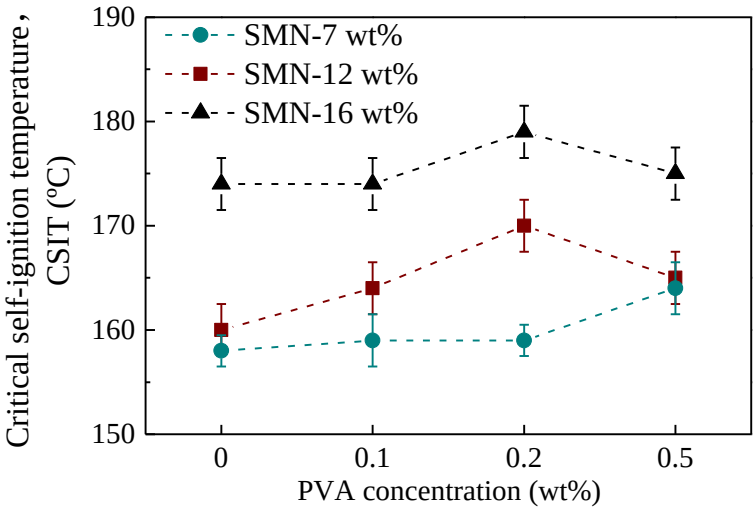

Figure 2- 16. Critical self-ignition temperatures of lignite coal wetted by C-WSs with different PVA concentrations in Run#4 tests (SMN-7, 12 and 16 wt%).

2.4.8. Determination of the optimal C-WS

Figure 2-17 shows the comparison between the amount of C-WS with different SMN concentrations (PVA-0 and 0.2 wt%) wetting the coal particles. For PVA-0.2 wt%, the amount of C-WS wetting the coal surface increased linearly with increasing SMN concentration. However, it slightly decreased for SMN-16 to 20 wt%. Thus, PVA-0.2 wt% could promote the wetting of coal surfaces with C-WS, thus, increasing the CSIT values compared to that of PVA-0 wt%. Generally, the analyses of the effects of SMN and PVA concentrations on CSIT suggested that SMN-16 wt%-PVA-0.2 wt% in C-WS is one of the optimal combinations due to the excellent fire-prevention property and

low material cost.

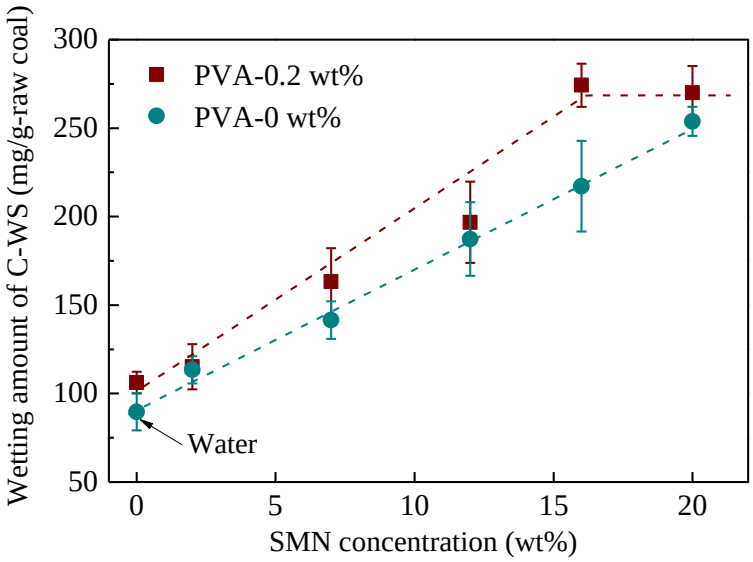

Figure 2- 17. Wetting amount of C-WS with different SMN concentrations by coal particles (PVA-0 and 0.2 wt%).

2.4.9. CSITs estimation of coal pile with different pile volume and particle size

Figure 2-18 shows the effects of pile size (1.56×10^{-5} m^3 $\leq V \leq$ 1 m^3, i.e. WMB size: 2.5 cm $\leq L \leq$ 100 cm) and particle size (0.48 mm $\leq d \leq$ 46 mm) on CSITs of raw coal (Run#0 tests, (Wang et al., 2017, 2019; Zhang et al., 2019)) and coal wetted by C-WS from Baiyinhua open-pit coal mine (Runs#3-5 WMB tests).

Figure 2-19 shows measured CSITs and estimated CSITs by Equation (2-7) of Baiyinhua lignite coal, which can be seen to be concentrated around the line of $y = x$ (prediction precious of 100%). Baiyinhua coal wetted by the optimal C-WS (SMN-16 wt%, PVA-0.2 wt%) was tested in Run#5 tests and which measured CSITs were higher around 26 °C (line of $y = x$+26 °C in Figure 2-19) than raw coal.

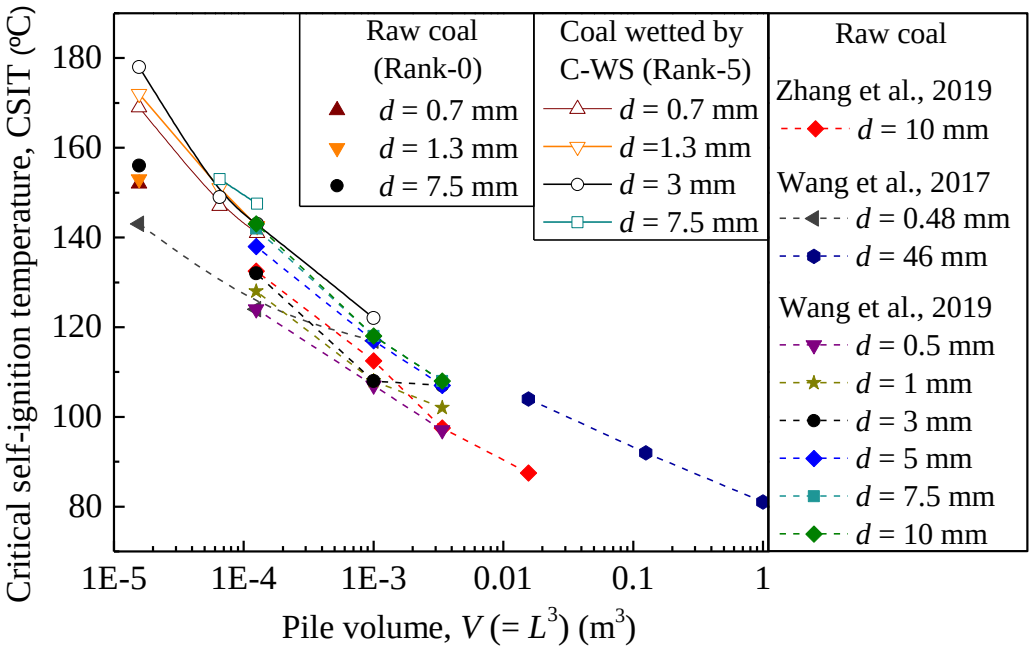

Figure 2- 18. CSITs of Baiyinhua raw coal and coal wetted by C-WS (SMN-16 wt%, PVA-0.2 wt%) coal in WMB tests with different pile volume and particle size.

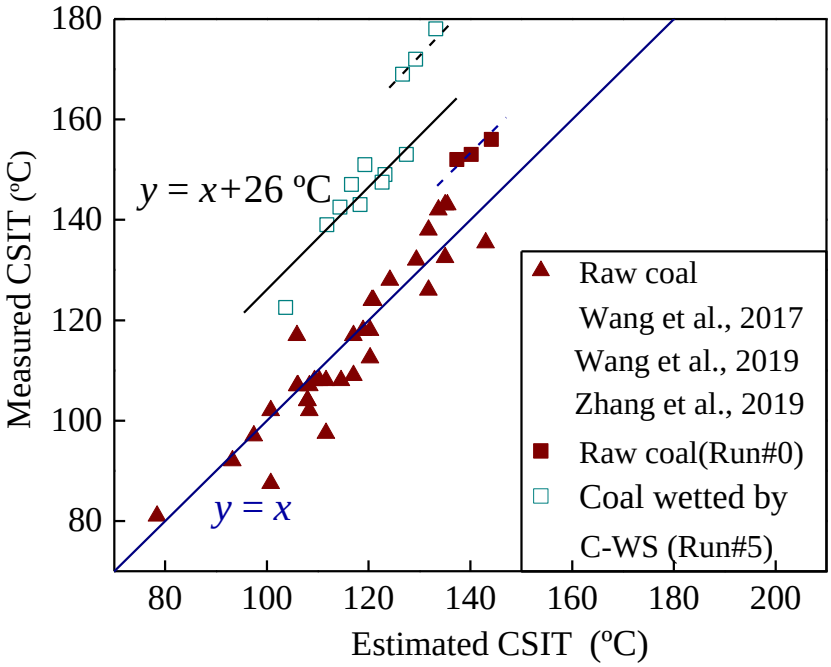

Figure 2- 19. Estimated CSITs (raw coal) and measured CSITs (raw coal and coal wetted by optimal C-WS (SMN-16 wt%, PVA-0.2 wt%)) in WMB tests using Baiyinhua lignite coal.

Furthermore, an improved-empirical equation could be applied to estimate the measured CSITs of coal wetted by C-WS with different V and d, as follows,

$$\begin{aligned} &CSIT_{C\text{-}WS} = CSIT_{raw}(V, d) + 0.08\ SMN^2 + 25\ PVA\ ; \\ &0 \le SMN\ (wt\%) \le 20\ wt\%,\ 0 \le PVA(wt\%) \le 0.5\ wt\% \end{aligned} \quad (2\text{-}12)$$

The estimated CSITs of coal wetted by C-WS (Runs#3-5 tests) are plotted against measured ones in Figure 2-20, which has a correlation factor $R^2 = 0.9214$, combined with the fitting between estimated and measured CSITs of raw coal (Run#0 tests, (Wang et al., 2017, 2019; Zhang et al., 2019)). Therefore, for preventing the spontaneous combustion of field coal pile or gob, the C-WS with reasonable concentrations of SMN and PVA should be considered by measuring the field coal pile volume and particle size and referring Equation (2-12).

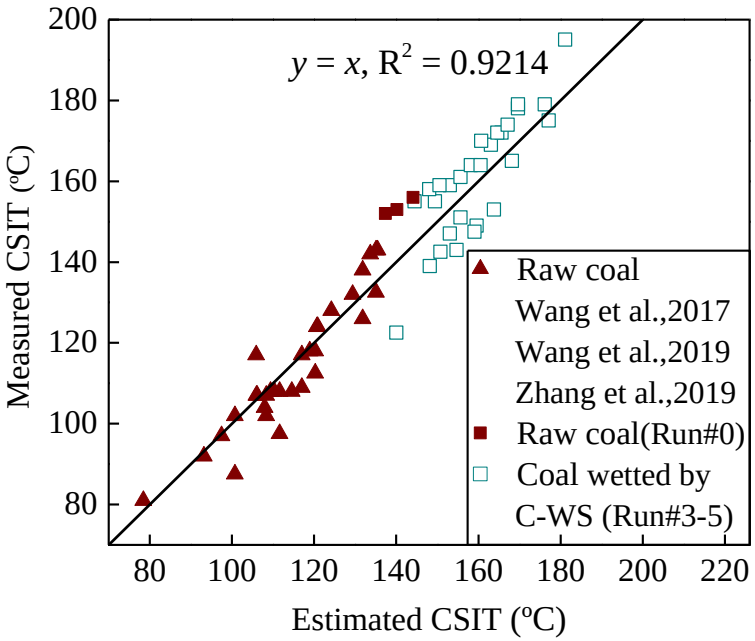

Figure 2- 20. Estimated and measured CSITs in WMB tests of raw coal and coal wetted by C-WS.

2.5 Conclusions

In this study, WMB tests were applied to investigate the exothermic process and characteristic behaviors, which mainly include critical self-ignition temperature (CSIT) and critical lead time (CLT). The complex water solution (C-WS) was developed to shift CSIT to a higher value than raw coal. The C-WS includes water, SMN and PVA for preventing coal from spontaneous combustion. Natural CO_2 substituted the traditional coagulation accelerator and reacted with the inhibitory solution to form a novel cross-linked SMN/PVA gel, that naturally seals the coal pores.

(a) The effects of pile volume and particle size on the characteristic parameters were analyzed. CSITs of wetted coal (d = 10 m) with L = 5, 10, 15 and 25 cm were 132.5, 112.5, 97.5 and 87.5 °C, respectively. CLTs of which was 4.32, 22.8, 39 and 109 h. With the size of the coal pile increasing, a decreased trend in CSITs and an increasing trend in CLTs are observed respectively. However, CSITs of dried coal samples were lower at least 10 °C than those of wet samples. CLTs of wet coal were higher 3-5 times than that of dried coal. The coal pile with larger coal particle size had a higher CSIT and shorter CLT.

(c) The C-WS on the coal surface and in the inlets of coal micropores could react with CO_2 emitted from coal oxidation and air atmosphere to form the crosslinked polymeric gel. The SMN/PVA gel possessed a more efficient property of coal fire-prevention than single-component solutions and conventional silicate-gel. Effects of SMN and PVA concentrations in C-WS on the coal fire-prevention property were investigated and the optimal combinations of SMN and PVA concentrations have been suggested as 16 wt% and 0.2 wt% that the CSITs showed higher around 26 ºC than those of raw coal. CSITs of coal wetted by C-WS were measured by the WMB tests, and the empirical equation to estimate the CSIT has been presented by adding the effects of SMN and PVA concentrations to the previous equation between CSIT and pile volume for the raw coal.

Chapter 3: Numerical simulations on WMB tests by considering the aging effect

3.1 Introduction

The WMB tests with different basket sizes were carried out for measurement results of CSIT and CLT. However, it is usually difficult to implement large-scale WMB tests due to time-consuming and economic disadvantages. For an example of conducting the 1m-size WMB tests (Wang et al., 2017), it used almost 1 t of coal and needed more than 700 h. It is required to develop a reliable simulation model and method on investigating the coal self-ignition. In this study, by comparing the results of WMB tests and numerical simulations, the simulation model on the exothermic process of coal oxidation was developed. It also can be applied for predicting the heating processes of coal piles in large-scale tests and field conditions using the model presented in this research.

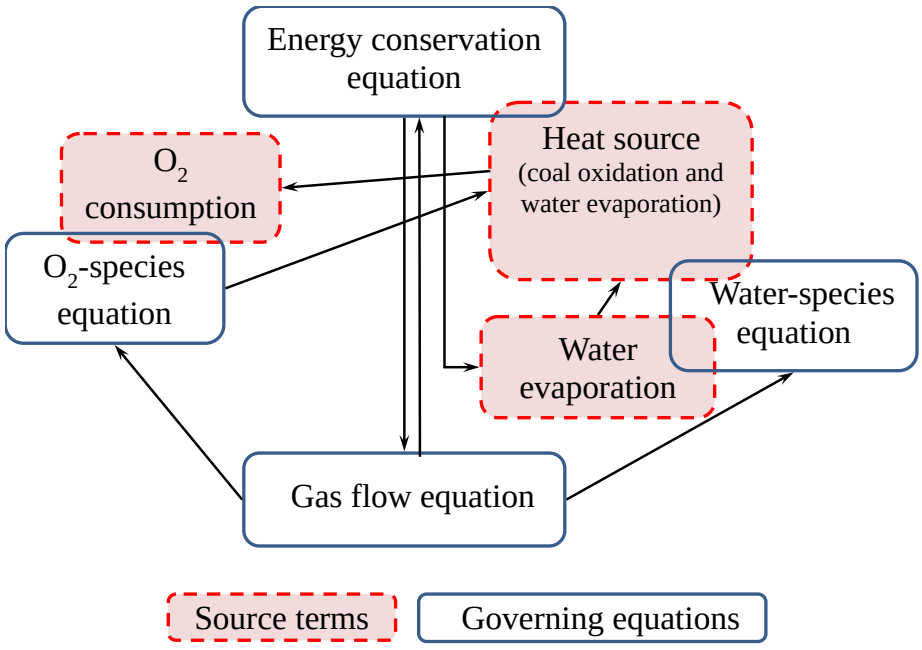

Figure 3- 1. Coupled interactions of coal spontaneous combustion.

The theoretical model of numerical simulation on coal self-ignition is complicated because the valuables are coupled and related to each other. As shown in Figure 3-1, the core constituents and the governing equations have been developed by referring to the reality of coal spontaneous combustion. The theoretical model has to include how the heat is generated and transferred, how the air, water vapor and O_2, diffuse in the coal porous media, and how the O_2 is adsorbed and water is evaporated.

For the details of numerical simulation on coal spontaneous combustion, Wu et al. (2016) conducted the simulation using the mathematical model without moisture evaporation on the small-basket coal ignition and proposed the numerical temperature curves does not to match experimental due to the drying process. Hooman and Maas (2014) have succeeded to apply the approximate simulation for large-moist coal stockpiles using the scale analysis and explored the expressions of the temperature and inflection point as functions of the key parameters of the stockpile. However, their "approximate" solution by omitting terms with small order magnitude in the governing equation was not fit for the WMB test due to the small coal piles under relatively high-temperature range. Sasaki and his co-authors (1987, 2011) presented simulations of the spontaneous combustion of a one-dimensional coal seam by applying the aging model according to Equation (1-2) in conjunction with the equivalent oxidation exposure time (EOE-time) theory. However, they did not compare the simulation results with any experimental and field data and did not consider the effect of moisture evaporation on the heating processes in coal seams or piles. Therefore, it has not been confirmed that Equation (1-2) can be applied to numerical simulations on actual coal temperature-time curves including supercritical and subcritical profiles, because the model assumes constant ambient temperature and O_2 concentration. Furthermore, a methodology to determine the optimal value of γ has not been presented to date.

In this chapter, the numerical simulations of three-dimensional (3-D) coal piles were run to determine the optimal value of γ by history matching with experimentally-acquired coal temperature-time curves obtained from the WMB tests using low-rank coal. This work also assessed whether or not the heat generation model incorporating

the EOE-time theory together with the moisture evaporation model could produce results that agreed with WMB test results for the low-rank coal piles in different WMB volumes. Finally, the differences between the heating processes of wet and dry coal piles were also simulated, employing a moisture evaporation model. Moreover, the temperature and O_2 concentration distribution in different volumes of coal piles are compared and analyzed.

3.2 Governing equations

3.2.1 Energy conservation equation

The temperature distribution is calculated based on oxidative heat generation rate, q_h, endothermic rate associated with moisture evaporation, q_w, and heat transfer (conduction and convection) to the ambient atmosphere in the coal pile. Therefore, in the self-heating process of coal piles, heat source, q (W/kg-coal) is expressed by

$$q = q_h - q_w \tag{3- 1}$$

The porous medium and fluid flow are assumed to be in thermal equilibrium. Considering the porosity, the species equation and the energy equation in the porous are as follows

$$\begin{aligned} \frac{\partial}{\partial t}\left\{\left[n\rho_a c_a + (1-n)\rho_c c_c\right]T\right\} + \nabla\cdot(\rho_a c_a \mathbf{v}T) = \\ \nabla\cdot\left\{\left[n\lambda_a + (1-n)\lambda_c\right]\nabla\cdot T\right\} + (1-n)q \end{aligned} \tag{3- 2}$$

where ρ_a (kg/m^3) and ρ_c (kg/m^3) are the air and coal density respectively, c_a (J/(kg·K)) and c_c (J/(kg·K)) are the specific heat capacity of air and coal respectively, n is the porosity of the pile, $\mathbf{v}$ (m/s) is the seepage air velocity vector, λ_a (W/(m·K)) and λ_c (W/(m·K)) are the thermal conductivities of air and coal particles, respectively.

3.2.2 Momentum governing equations

Assuming the porosity of coal piles examined by WMB tests was isotropic porosity, and the momentum governing equation is given by (Ansys Fluent Inc, 2012)

$$\frac{\partial(n\rho_a \mathbf{v})}{\partial t} + \nabla \cdot (n\rho_a \mathbf{v}\mathbf{v}) = -n\nabla p + \nabla \cdot (n\boldsymbol{\tau}) + n\mathbf{B} - nS_i \quad (3\text{-}3)$$

where p (Pa) is the static pressure, $\boldsymbol{\tau}$ (Pa) is the stress tensor, $\mathbf{B}$ (N/m^3) is the gravitational body force, and S_i is the momentum source term. The natural convection in the porosity was forced by the according to the Boussinesq model, and the gravitational body force, **B**, can be expressed by (Ansys Fluent Inc, 2012)

$$\mathbf{B} = -\rho_{a0}\alpha(T - T_0)\mathbf{g} \quad (3\text{-}4)$$

where ρ_{a0} (= 1.225 kg/m^3) is the operating air density, $\mathbf{g}$ (m/s^2) is the gravity acceleration, α (= T^{-1} K^{-1}) is the thermal expansion coefficient (Lienhard, 2011), T_0 (= 299.2 K) is the operating temperature.

The momentum loss, S_i, in Equation (3-3) was expressed as

$$S_i = \frac{n\mu}{k}\mathbf{v} + \frac{n^2 F_2}{2}\rho_a |\mathbf{v}|\mathbf{v} \quad (3\text{-}5)$$

where μ (Pa·s) is the air viscosity. The permeability, k (m^2), and inertial resistance coefficient, F_2 (m^{-1}), were calculated using the equations (Zhang et al., 2016)

$$k = \frac{d^2}{150}\frac{n^3}{(1-n)^2} \quad (3\text{-}6)$$

and

$$F_2 = \frac{3.5}{d}\frac{1-n}{n^3} \quad (3\text{-}7)$$

where d (m) is the average size of the coal particles.

3.2.3 Species governing equations

Heat generation of coal consumes oxygen molecules, resulting in a decrease of O_2 concentration. O_2 molecules can transfer to the parts with lower O_2 concentration by diffusion forced by differential O_2 concentration and convection forced by differential pressure. The O_2 governing equation is formed by adding source terms, as follows,

$$\frac{\partial(n\rho_f C)}{\partial t} + \nabla(n\rho_f \mathbf{v}C) = \nabla(nD\nabla(\rho_f Y)) + S_f \qquad (3\text{-}8)$$

The formation of governing equation for water vapor is similar to Equation (3-8).

3.3 Equivalent oxidation exposure (EOE) time theory

The heat generation model expressed by Equation (1-2) is used to predict the effect of aging on coal oxidation. However, because the γ values in prior research are always determined under constant temperature and O_2 concentration conditions, there was no clear means of applying Equation (1-2) to numerical simulations for a scenario in which both the coal pile temperature and O_2 concentration change over time. Sasaki and his co-authors (1987, 2011) proposed the concept of the EOE-time. This process is summarized diagrammatically in Figure 3-2.

The EOE-time value for each time interval based on cumulative heat generation or O_2 consumption of the coal mass are estimated in the model. In each simulation, a coal pile is placed in an ambient atmosphere with varying temperature, T, and O_2 concentration, C. At an elapsed time t_i (= $i\Delta t$) the temperature and O_2 concentration around the coal are defined as T_i and C_i, respectively, where i is the number of calculation intervals and Δt is the time interval. The quantity of heat generated by the coal per unit mass will be q_{hi} between times t_i and t_{i+1}, and the generation of a specific quantity of heat, $\Delta t q_{hN}$ ($i = N$ indicates the interval numbers having been taken), is required between present time t_N and subsequent time t_{N+1} (= $t_N + \Delta t$) to continue the simulations of temperature and O_2 concentration.

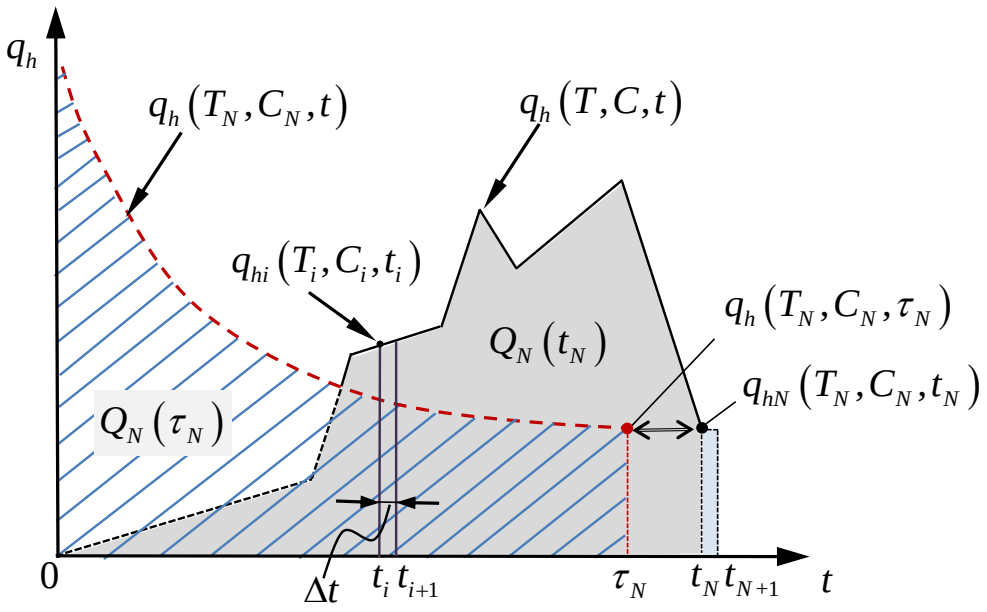

Figure 3- 2. A schematic summarizing the definition of the equivalent oxidation exposure time as used to estimate the heat generation rates of coal samples.

Assuming a unit mass of coal is placed in the virtual constant environment at temperature $T = T_N$ and O_2 concentration $C = C_N$ from $t = 0$ to τ_N, where τ_N has the same step number as t_N, the total amount of heat generated, $Q_H(\tau_N)$ (J/kg) can be expressed as

$$Q_H(\tau_N) = \int_0^{\tau_N} q_h(T_N, C_N, t)dt = \frac{C_N A_0}{\gamma} \cdot \exp\left(-\frac{E}{RT_N}\right)\left(1-\exp(-\gamma\tau_N)\right) \quad (3\text{- }9)$$

The total amount generated heat for the actual condition from $t = 0$ to t_N, is given as

$$Q_H(t_N) = \int_0^{t_N} q_h(T, C, t)dt = \sum_{i=0}^{N-1} q_{hi}\Delta t \quad (3\text{- }10)$$

If the integrated heat generation values in the actual and virtual processes are equal, meaning that

$$Q_H(t_N) = Q_H(\tau_N) \quad (3\text{- }11)$$

The EOE-time at t_N, τ_N, is expressed by

$$\tau_N = -\frac{1}{\gamma} \cdot \ln\left[1 - \frac{\gamma}{C_N A_0} \cdot \frac{\sum_{i=0}^{N-1} q_{hi} \Delta t}{\exp\left(-\frac{E}{RT_N}\right)}\right] \quad (3\text{- }12)$$

The most important characteristic of EOE-time theory is that if a part of coal releasing heat to its surrounding, the EOE-time is increased (Sasaki & Sugai, 2011). Another important parameter is the ratio of EOE-time over time (EOE-t/t), which has a positive correlation with the heat generation rate of coal (Zhang et al., 2018).

3.4 Source terms

3.4.1 Heat generation rate

Based on the above derivation, we can assume that the quantity of heat generated, q_{hN} could be calculated from Equation (1-2) by inputting $t = \tau_N$ using the same values for T_N, C_N and Q_H, even if the exothermic process and elapsed time are different. Therefore, substituting $t = \tau_N$, $T = T_N$ and $C = C_N$ into Equation (1-2), the heat generation, q_{hN}, at $t_N + \Delta t$ is given by

$$q_{hN}(T_N, C_N, t_N) = C_N A_0 \exp\left(-\frac{E}{RT_N}\right) \exp(-\gamma \tau_N) \quad (3\text{- }13)$$

As an example, consider a fully oxidized coal mass that is no longer undergoing oxidation at a specific temperature, for which the EOE-time value is becoming ∞. Upon increasing the ambient temperature and/or O_2 concentration, oxidation is reinitiated. According to the EOE-time theory, the EOE-time value will be decreased to ∞ after the temperature increase as oxidation begins again. However, in the case that the coal cannot reach its self-ignition temperature even in the presence of a sufficient O_2 concentration because heat is rapidly dissipated from the coal to its surroundings, the EOE-time becomes ∞ and Q_H approaches $Q_H(\infty)$. The latter parameter represents the maximum total heat generation amount. Therefore, the

sample does not generate any additional heat after this point, even if the higher ambient temperature is maintained. The EOE-time value can, therefore, indicate the activity level of the coal upon aging. That is, as the coal ages, its EOE-time becomes greater and heat dissipation ceases. Conversely, low EOE-time values are associated with 'younger' coal that actively undergoes oxidation.

3.4.2 O_2 consumption

Assuming that the O_2 consumption rate of coal per unit mass, Φ_{ON} (mol/(kg·s)), is proportional to the heat generated, q_{hN} (Arisoy & Beamish, 2015; Song et al., 2014; Zhang et al., 2016). Φ_{ON} can be obtained as,

$$\Phi_{ON} = \frac{q_{hN}}{\Delta H} \tag{3- 14}$$

where ΔH (= 3.8×10^5 J/mol-O_2) is the reaction heat of coal oxidation (Zhang et al., 2016).

3.4.3 Latent heat for the coal drying process

Desorption or evaporation of moisture in the coal micro-pores needs latent heat that is provided from coal particles and pore air. Therefore, the heat used for evaporating moisture induces the cooling of the coal piles and affects the self-heating process. Sasaki et al. (1992) presented the model for the moisture evaporation rate from coal particles according to the difference between the relative coal moisture ratio, φ_c, and air relative humidity, φ_a. The relative moisture ratio in the coal, φ_c, is defined as

$$\varphi_c = \frac{\omega}{\Omega} \tag{3- 15}$$

where ω (kg-H_2O/kg-coal) is the transient moisture in the coal particles and Ω is the saturated water content of the coal (0.272 kg-H_2O/kg-coal for the present coal).

The relative humidity of the air around the coal particle, φ_a, is given by

$$\varphi_a = \frac{P_v}{P_{sat}} \tag{3- 16}$$

where P_v (Pa) and P_{sat} (Pa) are the ambient vapor pressure of water and the corresponding saturated vapor pressure, respectively, and have the values reported by Oyj (2013). When $\varphi_a < \varphi_c$, the coal mass undergoes continuous drying and releases water to the air. The endothermic rate due to moisture evaporation, q_w (W/kg-coal) is provided from coal particles and air in the pile is estimated by Sasaki et al. (1992)

$$q_w = l_w \beta_c \left(\varphi_c - \varphi_a\right) / t_w \tag{3- 17}$$

where l_w (= 2.25×10^6 J/kg-H_2O) is the unit latent heat of water evaporation, β_c (= 0.078 kg-H_2O/(kg-coal)) is the coal moisture change rate for air humidity change (Sasaki et al., 1992), φ_c-φ_a is the difference between coal relative moisture ratio and air relative humidity, and t_w (= 7700 s) is the time constant (Sasaki et al., 1992).

3.5 Definition of decay-power factor

The decay-power factor, γ, in Equation (1-2) defines the exponential decay of the coal heating process over time. A low γ value indicates slow decay of the heat generation rate during oxidation as the reactive sites available for the chemical adsorption of O_2 are used up. Previous experimental studies (Kaji et al., 1987; Krishnaswamy et al., 1996; Nordon et al., 1979; Sasaki et al., 1987; Wang et al., 2003) have determined the decay curves for coal heat generation at a constant temperature, and the associated measurement conditions (such as temperature, O_2 volume fraction and coal properties) are summarized in Table 3-1.

This summary shows that the values determined for γ vary over the range of 6.7×10^{-7} to 1.0×10^{-4} s^{-1}. This value is partly affected by both the coal rank and elapsed time after exposure to air. Therefore, in this study, we applied the aging model (with $\gamma > 0$ in Equation (1-2)) in conjunction with EOE-time theory and the Arrhenius equation ($\gamma = 0$ in Equation (1-2)) in numerical simulations. On this basis, the optimal value of γ

was obtained by comparing the simulated coal temperature-time curves to the measured data acquiring during the WMB tests.

Table 3- 1. Values for the decay-power factor, γ, measured in previous studies

Source	Coal rank	Particle size (mm)	Temperature (°C)	O_2 volume fraction	Fitting γ (s^{-1})
(Wang et al., 2003)	-	< 0.5	60 70 80 90	0.21	2.81×10^{-5} 2.59×10^{-5} 4.51×10^{-5} 5.04×10^{-5}
(Nordon et al., 1979)	Lignite	3.35-9.5	85	Dried air (0.21)	1.58×10^{-6}
(Sasaki et al., 1987)	Bituminous	-	45	1	2.46×10^{-6}
(Kaji et al., 1987)	Bituminous	0.105-0.21	23.8 50 63.3	0.212	6.2×10^{-5} 8.41×10^{-5} 1.02×10^{-4}
(Krishnaswamy et al., 1996)	Sub-bituminous	1.415	27 38 49 60	Air (0.21)	3.59×10^{-6} 4.92×10^{-6} 6.67×10^{-7} 9.11×10^{-6}

3.6 Physical model

3.6.1 Mathematical model and mesh block division

The computational fluid dynamics (CFD) software package ANSYS FLUENT is used to simulate the self-heating behavior of coal piles with porosity $n = 0.34$ in WMB tests. Algebraic equations are converted from general scalar transport equations based on a control-volume-based technique. The governing equations are spatial and/or temporal discretized by second-order accurate schemes. Then, the SIMPLE-Consistent scheme is applied in the pressure-based coupled algorithm to solve the discretized equations. The absolute convergence criterion of 10^{-6} is used in the simulations. An initial 3-D grid block model is constructed according to the laboratory WMB (hereinafter WMB) test conditions (Figure 3-3).

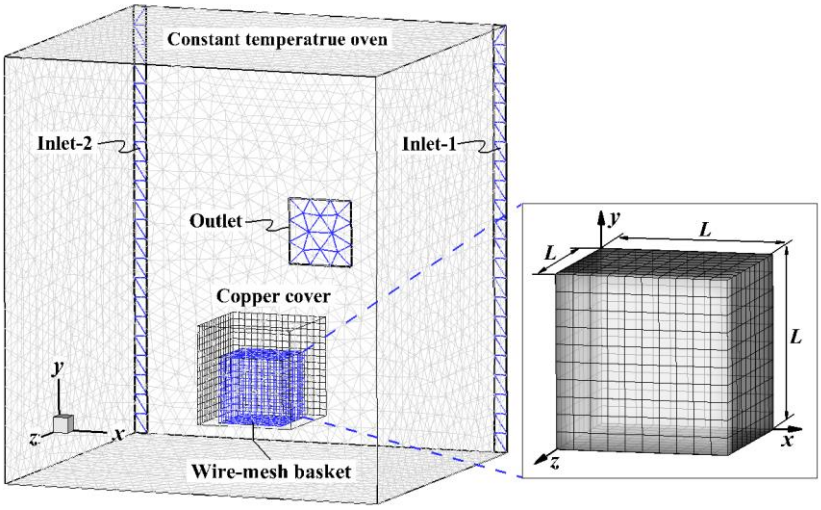

Figure 3- 3. A mathematical model to simulate the wire-mesh basket tests.

The coal pile (and cooper zone) and the rest oven zone are meshed by hexagonal structured and tetrahedral unstructured grids respectively. The grid independence for each WMB size L is checked. For an example of L = 10 cm, three grid sets are conducted and the maximum temperature at the pile center for T_e = 110 °C is focused to compare the grid independence. Considering the temperature difference and CPU-time, the grid number of 72101 is selected for the simulations. Moreover, Total grid numbers of 67245, 79250 and 82026 are used to the other three WMB sizes of L= 5, 15 and 25 cm, respectively. For each coal pile size, the simulations are repeated for different values of T_e by increasing at 0.5 °C. The T_e is set from the temperature, which is 2.5 °C lower than the measured subcritical-temperature until the supercritical temperature profile is observed. The estimated error of CSIT from the simulation results is expected to be less than ± 0.25 °C that is smaller than the experimental one of ± 3.5 °C.

3.6.2 Physical parameters

For simplicity, the following assumptions are made in the numerical simulations:

(i) The volume decrease of coal pile with the water evaporation is not considered;

(ii) Properties such as porosity, thermal conductivity, heat capacity and coal density are independent of time and temperature;

(iii) Heat radiation between coal particles, pile surface and hot oven not considered;

(iv) The coal porous media is assumed as homogeneous;

(v) The effect of water evaporation on the heat generation of coal oxidation is not considered.

The activation energy, E, and pre-exponential factor, A_0, are pivotal for the heat generation model and should be adjusted with different rank coal. Many researchers have carried out the numerical simulation on coal spontaneous combustion and their relationships between E and A_0 are plotted in Figure 3-4 (Akgün & Essenhigh, 2001; Akgün & Arisoy, 1994; Arisoy & Akgün, 1994; Ejlali et al., 2011; Fierro et al., 2001; Hull et al., 1997; Nordon et al., 1979; Saleh et al., 2017; Salinger et al., 1994; Sasaki & Sugai, 2011; Schmal, 1987; Song et al., 2014; Taraba et al., 2014; Xia et al., 2017; Yuan & Smith, 2008; Zhang et al., 2016). The unit of A_0 is unified as W/kg. It is clear that E has a positive relation with ln(A_0). The values applied in this study (E = 78.9 kJ/mol and A_0 = 2.62×10^{11} W/kg (Zhang et al., 2018)) are located in the plotted reasonable range.

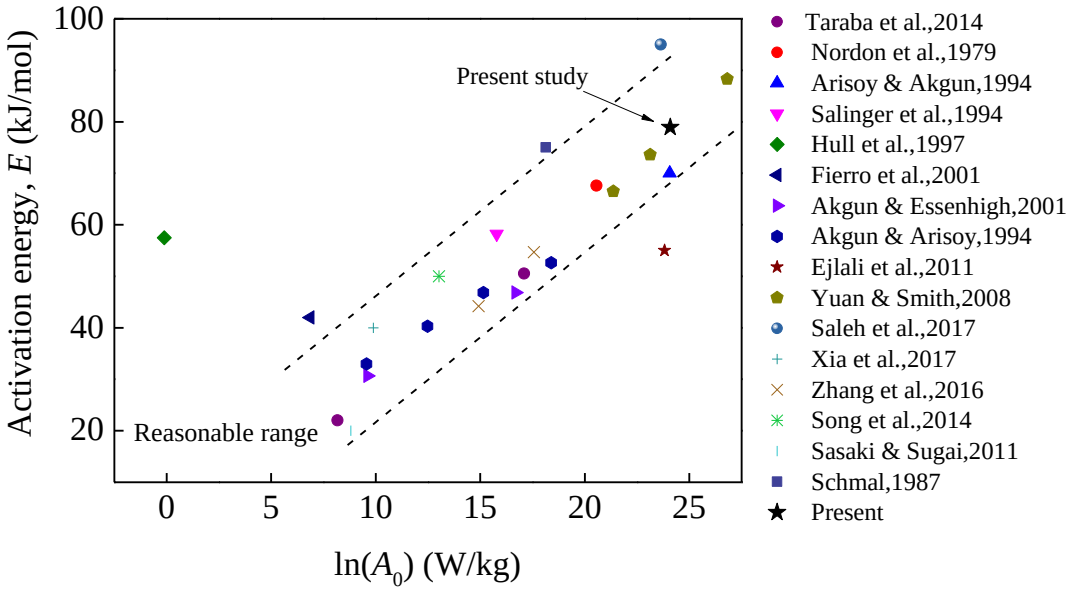

Figure 3- 4. Relationship between activation energy and pre-exponential factor.

Table 3- 2. Input parameters used for numerical simulations.

Parameters	Items	Value	Unit	Source
R	Universal gas constant	8.314	J/(mol·K)	Constant
n	Porosity	0.34	-	Meas.
ρ_a	Density of air	1.225	kg/m^3	(Lienhard, 2011)
ρ_c	Density of coal	1300	kg/m^3	Meas.
c_a	Specific heat capacity of air	1007	J/(kg·K)	(Lienhard, 2011)
c_c	Specific heat capacity of coal	1210	J/(kg·K)	Meas.
λ_a	Thermal conductivity of air	0.04	W/(m·K)	(Lienhard, 2011)
λ_c	Thermal conductivity of coal	0.21	W/(m·K)	Meas.
μ	Viscosity	1.72×10^{-5}	Pa·s	(Lienhard, 2011)
	Diffusion coefficient of O_2	1.76×10^{-5}	m^2/s	(Sasaki & Sugai, 2011)
	Diffusion coefficient of H_2O	2.82×10^{-5}	m^2/s	(Lienhard, 2011)

Table 3- 3. Boundary and initial conditions used in the simulations.

Boundary conditions	Inlet	Airspeed: 0.1 m/s Temperature: setting temperature (T_e) Air species mass fraction: O_2 (0.23) and H_2O (0.0002)
	Outlet	Free outflow
	Oven wall	Heat flux: 0
Initial conditions	Coal mass	Temperature: room temperature Moisture content: 0.272 (kg-H_2O/kg-coal)
	Air in the oven	Temperature: room temperature Air species mass fraction: O_2 (0.23) and H_2O (0.0002)

The parameters used in the simulations are provided in Table 3-2, while the boundary and initial conditions employed during the simulations are given in Table 3-3. The same points at which the thermocouples had been inserted during the WMB tests were

monitored in the simulations. Different parameters such as temperatures, oxygen concentration and seepage velocity are recorded at an intervals of 10 s.

3.7 Numerical simulation results and discussion

3.7.1 Effect of the decay-power factor on laboratory CSIT and CLT

In this study, the temperature evolution behaviors of coal piles having varying sizes are simulated by heat generation models based on either EOE-time theory with γ = (2 to 6)×10^{-5} s^{-1} in Equation (1-2) or the Arrhenius equation with γ = 0 in Equation (1-2). Figure 3-5 shows the T_c-t plots generated by the simulations and experimental work for a coal pile having L = 10 cm at the supercritical and subcritical ambient temperatures, T_e = 110 and 115 °C. In the case of the subcritical conditions, as shown in Figure 3-5(a), the T_c-t curves simulated using the Arrhenius model (γ = 0) and the aging model with the lowest γ value of 2×10^{-5} s^{-1} indicates ignition. This result demonstrates that a reduced aging effect ($\gamma \leq 2\times10^{-5}$ s^{-1}) does not properly model the heat generation rate of actual coal. In contrast, the T_c-t curve in Figure 3-5(b) obtained using the aging model with γ = 6×10^{-5} s^{-1} shows depletion that is too early relative to T_e because the heat generation rate is suppressed by applying an aging effect stronger than that which occurs in reality. The intermediate value of γ = 4×10^{-5} s^{-1} produces satisfactory heat generation rates under both subcritical and supercritical conditions that match those obtained from the WMB tests. The apparent differences between the temperature profiles of the EOE-time and Arrhenius model are observed. It indicates that the effects of various γ ($\leq$ 6×10^{-5} s^{-1}) on the heat process of coal pile are not clear discrepancies.

However, regardless of the γ value applied in the simulations, deviations between the measured and numerical T_c-t plots are found over the T_c range of 60 to 90 °C (that is, during the water evaporation stage). This discrepancy likely occurs because the coal particles fractured during drying, such that the pile volume or height is reduced and the porosity decreased. The simulation does not model the delayed drying of internal

coal particles due to volume reduction, which will be expected to reduce the permeability of the coal pile and result in less O_2 diffusing into the piles, therefore suppressing coal oxidation.

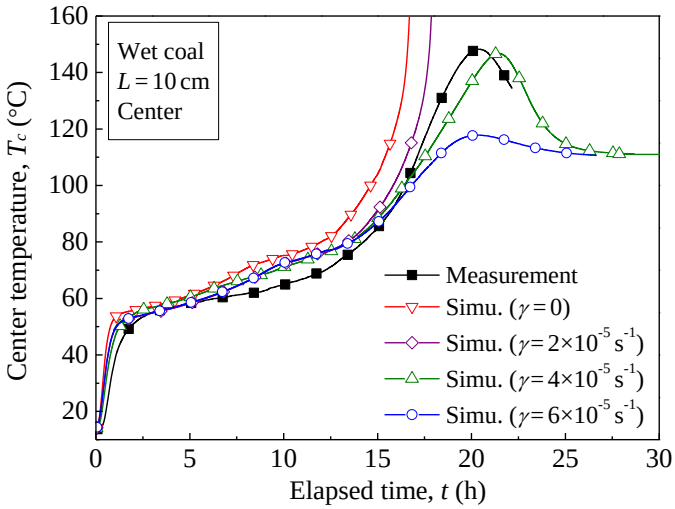

(a) T_e = 110 °C

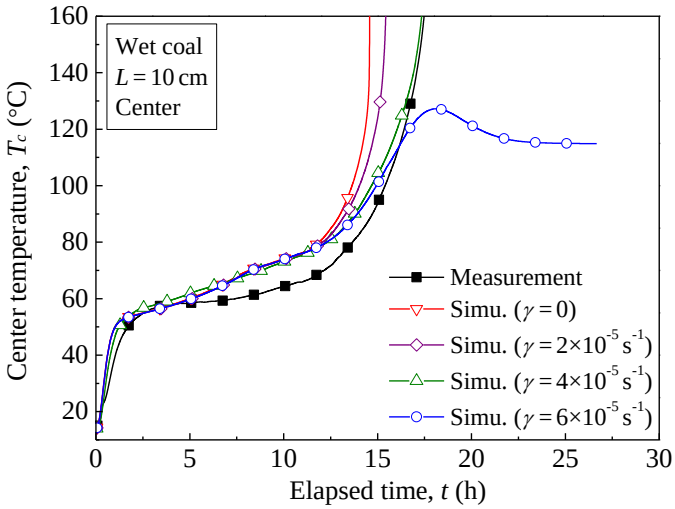

(b) T_e = 115 °C

Figure 3- 5. The measured and simulated center temperature profiles as functions of time for different decay-power factors and at two T_e values (L = 10 cm).

When T_c is close to T_e, the effects of the thermal boundary modeling without convection and radiation heat transfers directly from the airflow to the coal particles are very small due to the small temperature difference and gradient in the coal pile. The heat generation rate of coal when T_c is close to T_e is accelerated to be much larger

than that of the low-temperature range including moisture evaporation. This thermal situation at $T_c \sim T_e$ is the condition assumed to derive the Frank–Kamenetskii equation which determines the CSIT between supercritical and subcritical temperature profiles. To verify the validity of the aging model incorporating EOE-time theory, simulated heat generation-time curves, q_h vs. t, and ratios of EOE-time to elapsed time, τ_N/t_N versus t, using $\gamma = 4\times10^{-5}$ s^{-1} at T_e = 115 °C (supercritical) and 110 °C (subcritical) are plotted (Figure 3-6).

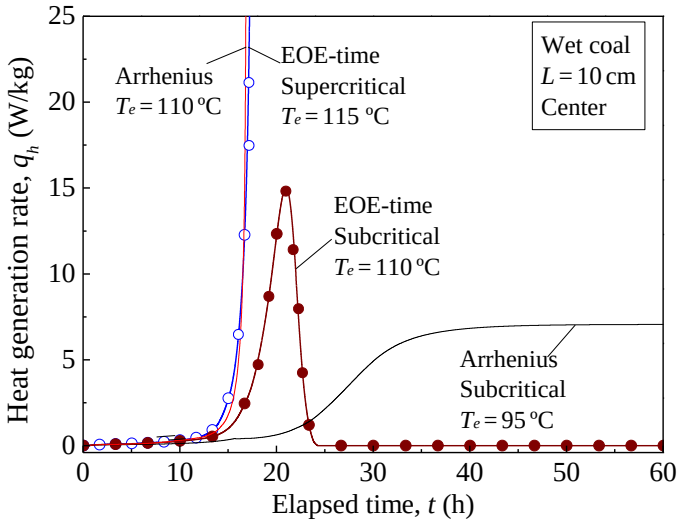

(a) Heat generation

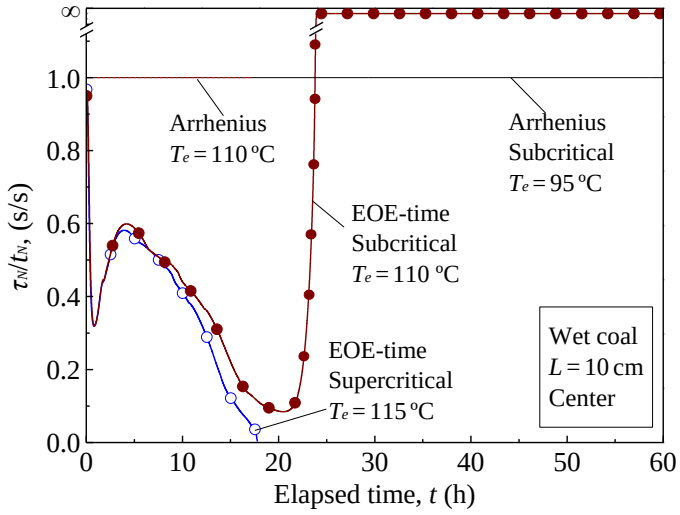

(b) τ_N/t_N

Figure 3- 6. Comparisons of simulation for heat generation and τ_N/t_N as functions of time using the EOE-time model and Arrhenius model (L = 10 cm).

These theoretical results are compared with those obtained using the Arrhenius equation ($\gamma = 0$) at T_e = 95 °C and 110 °C. The value of τ_N/t_N can be used to assess the exothermic oxidation potential of coal because a decrease of τ_N/t_N to 0 in the supercritical case indicates the potential for further oxidative heat generation. It is apparent that, at the subcritical temperature, the q_h value predicted by the aging model falls to 0 as τ_N is increased to ∞ after the peak temperature. In contrast, the simulations performed using with Arrhenius model show that q_h is either constant or infinite because the results from the Arrhenius model are determined solely by the coal temperature. At the supercritical temperature, the heat generation-time curves for self-ignition simulated with the aging model below T_e = 115 °C and the Arrhenius model below T_e = 110 °C are almost overlapped in Figure 3-6(a) which indicates the effect of aging on the heating process of coal.

As shown in Figure 3-6(b), for the supercritical case, the τ_N/t_N values at the pile center simulated using the aging model decrease as heat is received from the surroundings, while τ_N goes to ∞ and the sample becomes inactive after the peak temperature in the subcritical case. Therefore, the aging model in association with EOE-time theory generates reasonable results in both subcritical and supercritical scenarios. In contrast, the Arrhenius model does not perform well in the subcritical case.

3.7.2 Best decay-power factor for WMB tests

Figure 3-7 shows the relationship between γ and CSIT. The horizontal dotted lines indicate the experimentally determined CSIT values for the four coal piles sizes, while the solid curves are the simulated CSIT values plotted against γ. A larger γ results in more rapid decay of the exothermic reaction of coal, along with an increase in CSIT. That is, increasing γ inhibits spontaneous combustion. It is also apparent that a γ value of (3.8-4.3) $\times 10^{-5}$ s^{-1} is required to match the measured results. Therefore, in summary, Equation (1-2) with $\gamma = 4\times 10^{-5}$ s^{-1} represents the optimum heat generation model incorporating the EOE-time theory for the present low-rank coal. Figure 3-8 presents the simulated CSIT and CLT values for various coal pile volumes, V (m^3). These

results confirm that the present heat generation model according to EOE-time theory and using $\gamma = 4\times10^{-5}$ s^{-1} shows good agreement with the results of WMB tests.

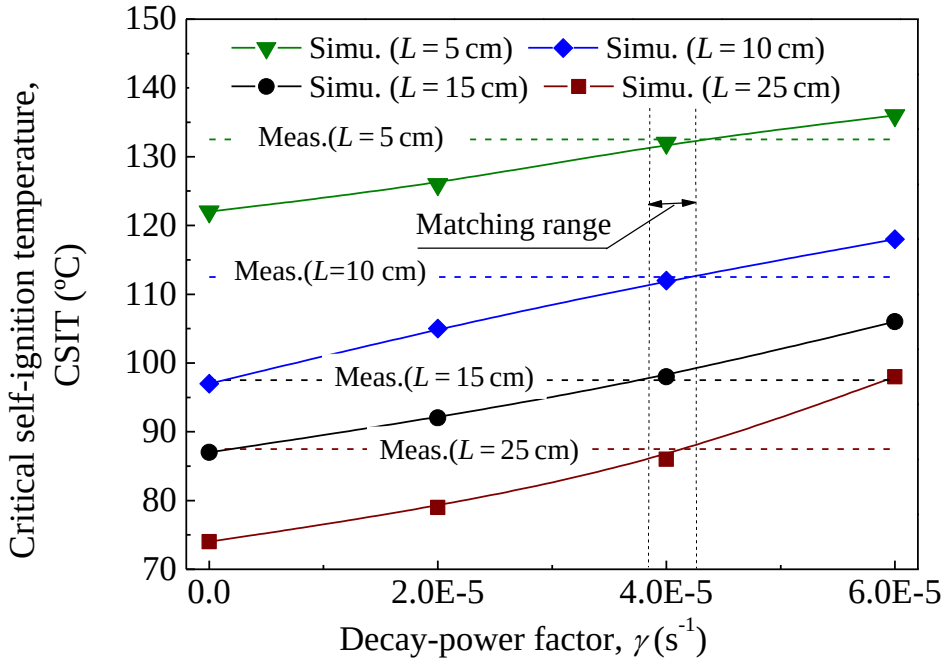

Figure 3- 7. Comparison of decay-power factors for coal piles of different volumes.

The simulated and measured CSIT values are seen to both decrease with increases in *V*. Consequently, heat dissipation to the atmosphere per unit volume (W/m^3) also becomes smaller with increasing volume, because heat dissipation is proportional to the total surface area while heat generation is approximately correlated with volume (Restuccia et al., 2017).

Therefore, a larger volume will be associated with a lower CSIT. However, the CLT values become longer with increasing volume, as shown in Figure 3-8. This effect is attributed to the greater time required for the oxidation rate in a large coal pile to reach the CSIT because the O_2 diffusion rate per unit volume is reduced.

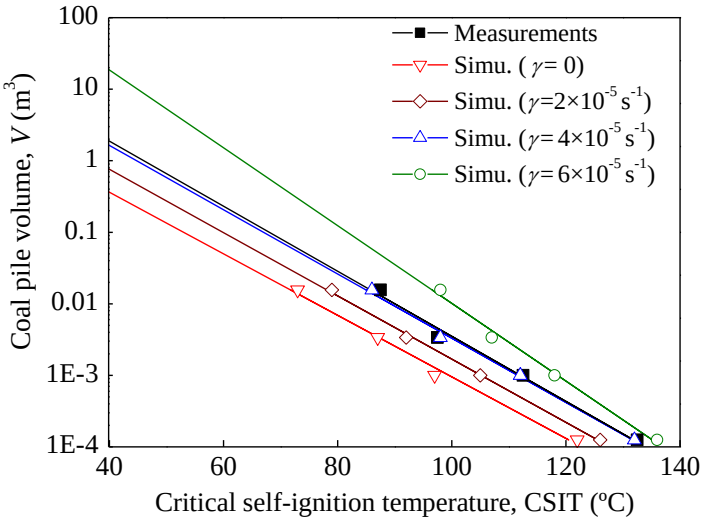

(a) CSIT

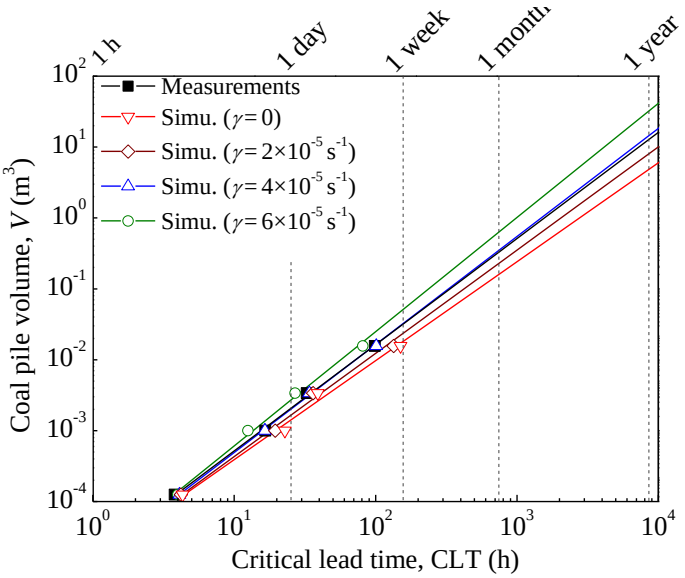

(b) CLT

Figure 3- 8. Plots of measured and simulated CSITs and CLTs versus coal pile volume, as obtained using different decay-power factor.

3.7.3 Simulated temperature and O_2 curves for different pile sizes

Figure 3-9 shows both the results of WMB tests and numerical simulations of coal temperature-time curves (heating curves) at measurement points y_t/L = 0.2, 0.5 and 0.8, for L = 25 cm and T_e = 90 °C. The simulated heating curves are in good agreement

with the measured values. The simulation results for vertical airflow velocity and O_2 concentration at various points in the coal pile are also provided in Figures 3-10.

After setting the basket in an oven with temperature T_e, naturally occurring downward convective airflow (in the negative direction along the *y*-axis) is induced owing to the temperature difference between the interior and exterior of the pile. This flow assists in heating the coal particles in the initial stage. However, the coal temperature in this period remains low and so oxidation and moisture evaporation are limited, such that the O_2 concentration in the coal pile remains relatively high (see Figure 3-10(b)).

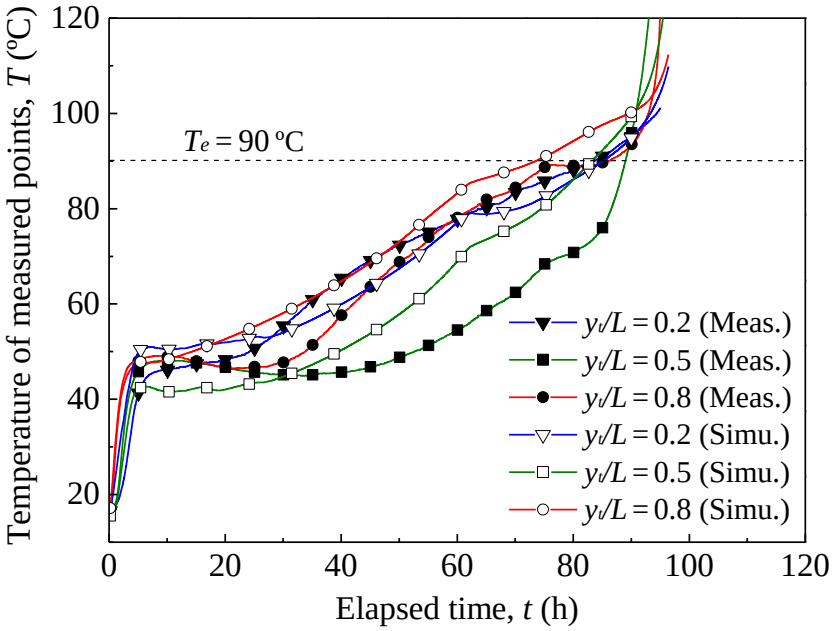

Figure 3- 9. Measured and simulated coal temperatures versus time at T_e = 90 °C and L = 25 cm ($\gamma = 4\times10^{-5}$ s^{-1}).

After the coal temperature increase to the range of 40 to 60 °C, the moisture evaporation rate gradually increases as latent heat is absorbed from the coal particles, which in turn slows the temperature increase rate of the coal. With the temperature increased gradually, The downward airflow decreases versus time at coal temperatures below T_e. It leads to that the O_2 supplied by conventional way decreased and thus the O_2 concentration in the inner part was low. After most of the water in the coal evaporating, the coal temperature is dramatically increased due to the heat adsorption

from oven and heat generation from coal oxidation.

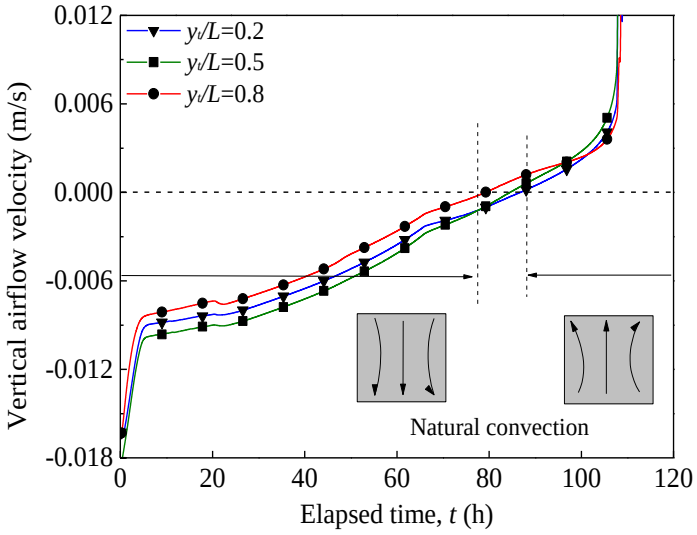

(a) air velocities

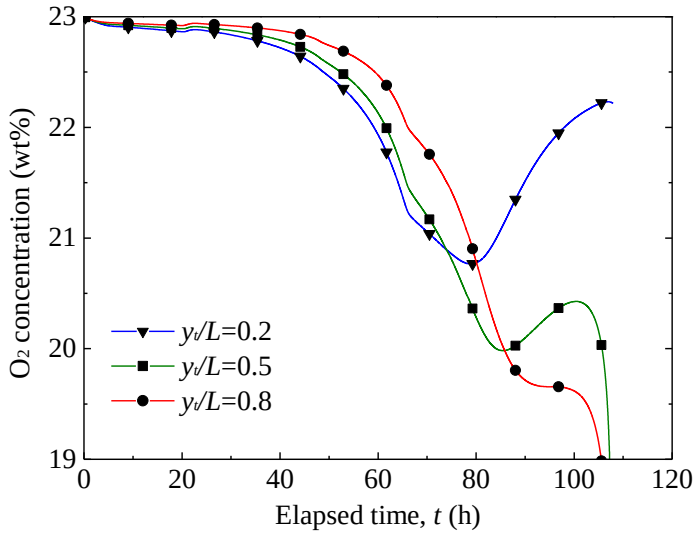

(b) O_2 concentration

Figure 3- 10. Simulated natural convective air velocities and O_2 concentration versus time ($\gamma = 4\times10^{-5}$ s^{-1}, $T_e = 90$ °C, $L = 25$ cm).

When T_c approaches T_e, the flow velocity becomes very low and so the O_2 transfer rate occurs solely owing to molecular diffusion through pores in the pile. Consequently, the O_2 concentration in the coal pile center is lowest when T_c is close to T_e. When T_c is higher than T_e, the naturally downward convective airflow is formed and became stronger due to the increasing temperature. The supplied amount of O_2 is increased,

despite that, the consumption rate of O_2 is high. The self-ignition will take place under the continuous unbalance between heat dissipation and generation.

Figure 3-11 shows the temperature distributions along the vertical plane ($z = L/2$) in the coal piles for which L = 25 and 5 cm, below their supercritical temperatures (T_e = 90 °C for L = 25 cm and T_e = 135 °C for L = 5 cm) at the time at which $T_c = T_e$.

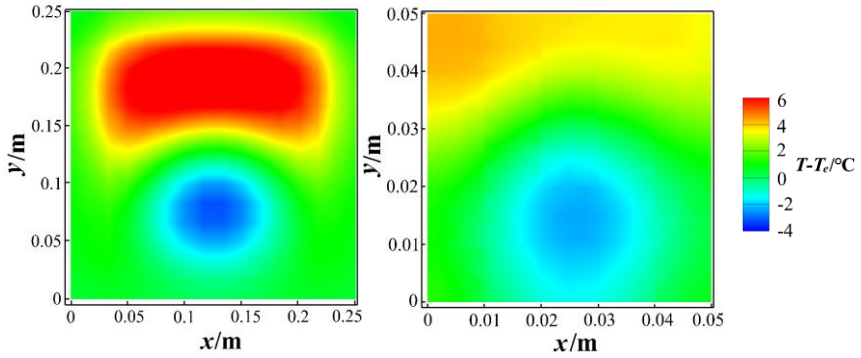

(a) L = 25 cm and T_e = 90 °C (b) L = 5 cm and T_e = 135 °C

Figure 3- 11. Coal temperature distributions in the case that $T_c = T_e$ ($z = L/2$).

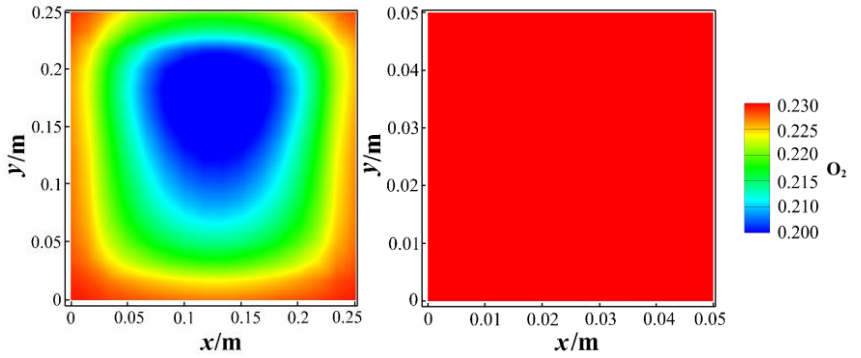

(a) L = 25 cm and T_e = 90 °C (b) L = 5 cm and T_e = 135 °C

Figure 3- 12. O_2 concentration distributions in the case that $T_c = T_e$ ($z = L/2$).

Under the same conditions, Figure 3-12 displays the O_2 distributions for the two coal piles. The temperature distributions of the two coal piles are seen to be similar, in that the temperature in the upper region is higher than that in the lower part. This result is ascribed to the higher O_2 concentration in the upper region in the pile due to downward convection when $T_c < T_e$. The decreased O_2 concentration in the larger pile occurs as

a consequence of the decreased surface area/volume ratio of the coal pile because O_2 molecules must migrate from the surface to the center. However, when $T_c > T_e$, the velocity of air moving through the pile is increased and so the O_2 concentration at the pile center rose with increasing T_c. In the subcritical case ($T_e < T_{CSIT}$), the EOE-time increases as the hotspot temperature decreased toward T_e after reaching a peak temperature, based on heat dissipation from the center of the coal pile. Conversely, under supercritical conditions ($T_e > T_{CSIT}$), EOE-time is continuously reduced as the coal temperature rose and O_2 is provided via natural convective flow.

Under the same conditions, Figure 3-12 displays the O_2 distributions for the two coal piles. The temperature distributions of the two coal piles are seen to be similar, in that the temperature in the upper region is higher than that in the lower part. This result is ascribed to the higher O_2 concentration in the upper region in the pile due to downward convection when $T_c < T_e$. The decreased O_2 concentration in the larger pile occurs as a consequence of the decreased surface area/volume ratio of the coal pile because O_2 molecules must migrate from the surface to the center. However, when $T_c > T_e$, the velocity of air moving through the pile is increased and so the O_2 concentration at the pile center rose with increasing T_c. In the subcritical case ($T_e < T_{CSIT}$), the EOE-time increases as the hotspot temperature decreased toward T_e after reaching a peak temperature, based on heat dissipation from the center of the coal pile. Conversely, under supercritical conditions ($T_e > T_{CSIT}$), EOE-time is continuously reduced as the coal temperature rose and O_2 is provided via natural convective flow.

3.7.4 Difference between wet and dry coal samples

The effect of the moisture content of the coal on numerical simulations compared with that in actual experimental tests is assessed by performing WMB tests using dry and wet coal. Numerical simulations are also conducted using the EOE-time theory in conjunction with $\gamma = 4\times10^{-5}$ s^{-1}. In the case of the dry coal particles, ω in Equation (3-15) is assumed to have a value of 0. The input parameters and the boundary and initial

conditions employed in these simulations are provided in Tables 3-2 and 3-3 respectively.

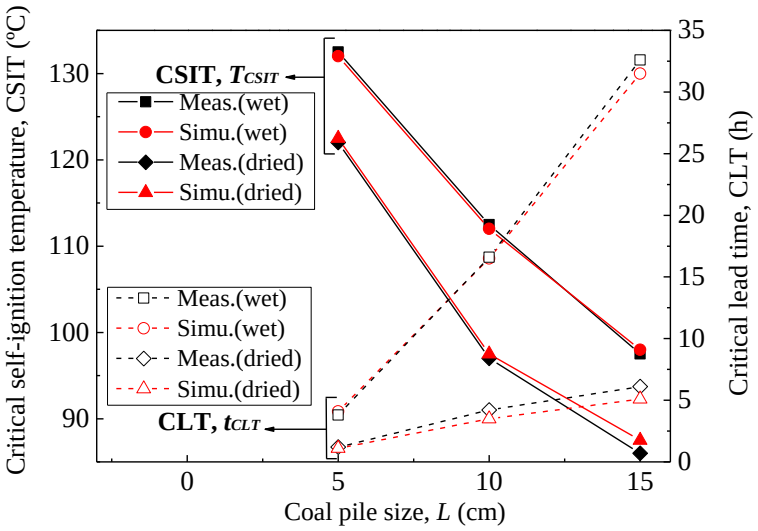

Figure 3- 13. Comparisons between simulated and theoretical CSIT and CLT values for wet and dry coals as functions of pile size ($\gamma = 4\times10^{-5}$ s^{-1}).

Figure 3-13 shows comparisons of the numerically simulated and experimentally determined CSIT and CLT values for different basket sizes of wet and dry coals. The numerical CSIT and CLT results show good agreement with the measured data for both wet and dry samples. the CSIT values for the dry coal are lower than those of the wet material, while moisture evaporation from the wet coal increases the CLT by a factor of three to six. It is therefore evident that the evaporation of water from the coal not only prolongs the spontaneous heating period but also decreases the likelihood of spontaneous combustion. Similar findings were previously reported by Arisoy and Akgün (1994). The close concordance between the WMB test data and the theoretical results demonstrates the applicability of the present model to the analysis of moisture evaporation from coal particles.

3.8 Simulation on the effect of SMN/PVA gel on decay-power factor

The SMN/PVA gel by the reaction of C-WS with CO_2 gases provides a covering function of inlets and inhibits the oxidation reaction of coal. Its function can be evaluated by increasing the decay-power factor, γ, because SMN/PVA gel results in shifting CSIT to a higher temperature and decreasing in the spontaneous combustion tendency of coal. Figure 3-14 shows the simulated and measured CSITs of raw coal versus WMB size (Deformation of Figure 3-7).

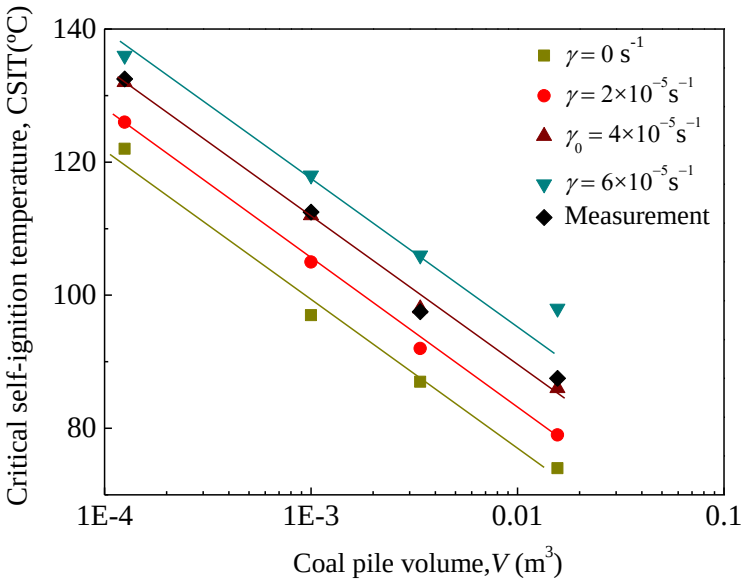

Figure 3- 14. Comparisons between simulated CSITs and measured CSITs versus pile volume (γ = (0-6) $\times 10^{-5}$ s^{-1}).

The simulated CSITs vs. V using EOE-time theory shows a good agreed with the measured CSITs vs. V when setting the decay-power factor as 4 $\times 10^{-5}$ s^{-1}. Therefore, γ_0 = 4 $\times 10^{-5}$ s^{-1} is assumed to be the reference value to predict the CSITs with different values of γ, as follows,

$$CSIT(\gamma) = CSIT(\gamma_0) + 3.25 \times 10^5 \times (\gamma - \gamma_0) \quad (3\text{-}18)$$

where CSIT (γ_0) is estimated to be closed to the measured CSIT. Therefore, the effect of aging effect on the increasing temperature of CSIT, ΔCSIT, shows the relation expressed by,

$$\Delta\text{CSIT} = 3.25\times10^5\times(\gamma-\gamma_0) \tag{3- 19}$$

Figure 3-15 shows the relationship between measured ΔCSIT and SMN concentration at different PVA concentrations in Run#3-4 tests in Section 2.4.2. The ΔCSIT is the difference between CSIT of coal wetted by C-WS (corresponding to changing γ) and CSIT of raw coal (156 ºC, corresponding to γ_0).

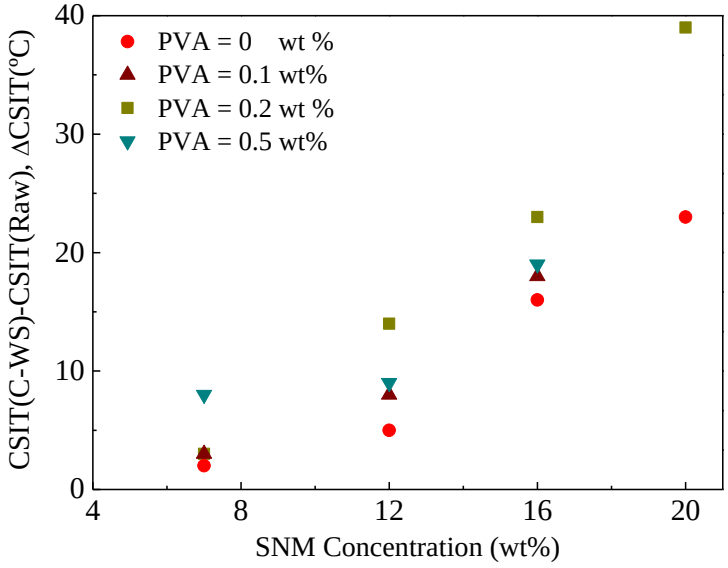

Figure 3- 15. ΔCSIT between raw coal and coal wetted by C-WS.

The SMN/PVA gel increases the CSIT of raw coal around 1.01 to 1.15 times. Therefore, the value of γ of coal wetted by C-WS can be expressed as,

$$\gamma = \gamma_0 + \frac{\Delta\text{CSIT}}{3.25\times10^5} \tag{3- 20}$$

Furthermore, the ΔCSIT in Equation (3-20) could be expressed by the concentrations of SMN and PVA in C-WS by Equation (2-12), as follows,

$$\Delta CSIT = CSIT_{C\text{-}WS} - CSIT_{raw}(V, d) = 0.08\ SMN^2 + 25\ PVA\ ; \quad 0 \le SMN\ (wt\%) \le 20\ wt\%,\ 0 \le PVA(wt\%) \le 0.5\ wt\% \tag{3-21}$$

3.9 Conclusion

(a) Numerical simulations are carried out to determine the optimal value for γ, which is determined to be 4×10^{-5} s^{-1} based on comparisons with measured laboratory WMBs data using basket sizes of L = 5 to 25 cm. Theoretical predictions based on EOE-time theory with higher γ values give higher CSIT values because of a strong aging effect and greater reductions in heat production. Correspondingly, CLT values increase with a decrease in γ.

(b) The distributions of airflow velocity, temperature and O_2 concentration are successfully simulated, as a means of analyzing the self-ignition process. The simulation results also show the effect of pile volume on the internal distributions of temperature and O_2 concentration.

(c) CSIT and CLT values for both wet and dry coal piles in the laboratory WMB tests are successfully predicted by combing the models of EOE-time and moisture evaporation. The effects of moisture on heat generation are investigated to increase CLT values and increase CSIT values, that is, reduce the spontaneous combustion tendency of coal.

(d) The effect of C-WS on preventing coal self-ignition was evaluated to be equal effect by increasing the value of γ based on the comparisons of increased CSIT.

Chapter 4: Field-scale numerical simulation of spontaneous combustion of coal stockpile

4.1 Introduction

The heating process of coal stockpiles in field-scale is induced by the accumulation of unbalance of heat generation from coal oxidation and heat dissipation from the stockpile to the atmosphere. However, monitoring of self-heating behaviors of cumulative coal lumps under different conditions, such as coal stockpiles and underground coal-mine gob, is difficult to detect inside of the stockpile. In this chapter, the exothermic behavior and the influencing factors of field-scale coal stockpile are investigated using the numerical simulations.

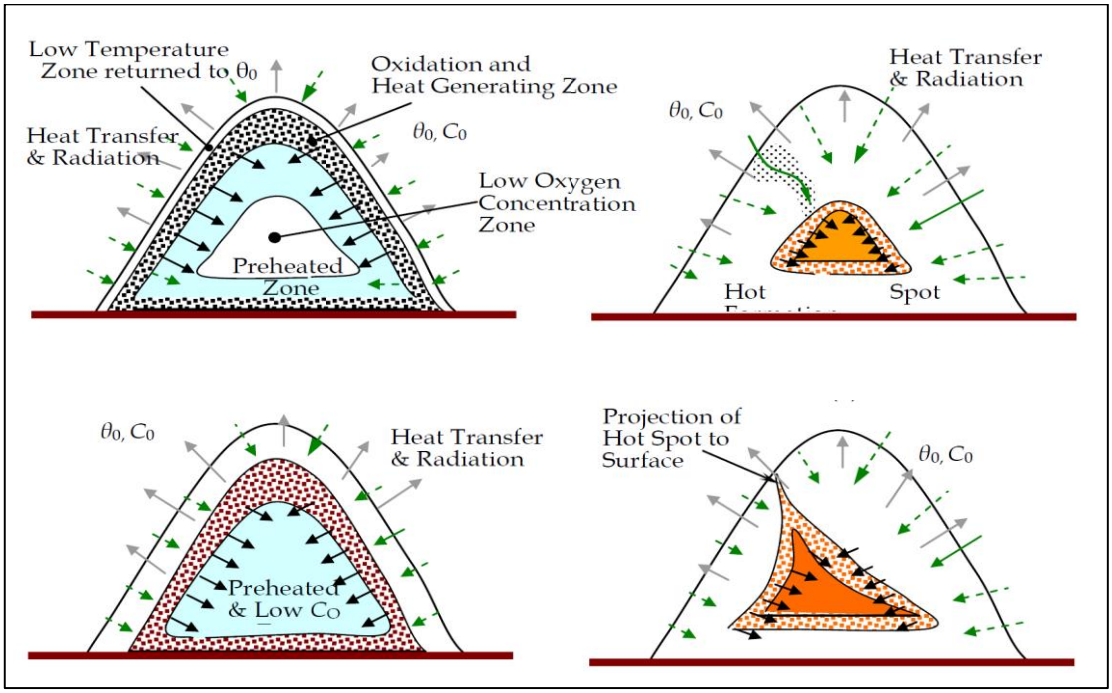

Figure 4- 1. Schematic showing the spontaneous combustion of coal stockpile (Sasaki & Sugai, 2011).

Figure 4-1 shows the typical process of spontaneous combustion of coal stockpile

presented by Sasaki and Sugai (2011). Fresh coal stockpile is exposed to the atmosphere with constant O_2 concentration and air temperature. A preheated zone is formed in the inner part of the coal stockpile due to the excellent heat storage capacity. However, the O_2 molecule from the atmosphere to the preheated zone is limited, which results in the emergent of low O_2 concentration zone. The continuous increase of temperature in the preheated zone induces the EOE-time smaller by receiving heat from outside, and thus, more generated heat transfers to the coal located outside. However, the low O_2 concentration restricts coal oxidation. Therefore, the high-temperature hotspot moves to the stockpile surface where the O_2 concentration is high. That is why smoke due to coal self-ignition is always observed on the coal stockpile surface.

In this chapter, a 2-D model of coal stockpile (longitudinal length >> pile width and height) was used and simulated at low temperatures using the aging effect model. Especially the decay-power factor, γ, was the key parameter to control the spontaneous combustion of coal stockpile. The critical decay-power factor, γ_c was investigated for operating the simulations. Distributions of temperature and O_2 were mainly focused to understand the dynamic-heating process of the stockpile.

4.2 Mathematical model of coal stockpile

As shown in Figure 4-2, a typical model of the trapezoid coal stockpile, which longitudinal length, l, is much larger than the pile height, h, and pile bottom width (hereinafter width), w, is used in this study. The ratio of w to h is 10:3.5. To simplify the model and save computational resources, a 2-D trapezoidal stockpile (xy section) was built as the mathematical model. The computational domain is large enough to eliminate the influence of longitudinal change. Therefore, an air zone of $10w$ in width and $10h$ in height, as well as a soil basement of $10w$ in width and 2 m in height were found to be sufficient for present numerical simulations. Multiphysics software of ANSYS FLUENT, which has been proved to be a powerful finite-element-based simulation tool, was adopted in the simulations. The total domain was divided into

72866 mesh blocks, including 8109 mesh blocks in the coal stockpile zone. The time step was set as 2h, which was around 0.1% to 0.36% of the whole simulation time (around 25-80 days).

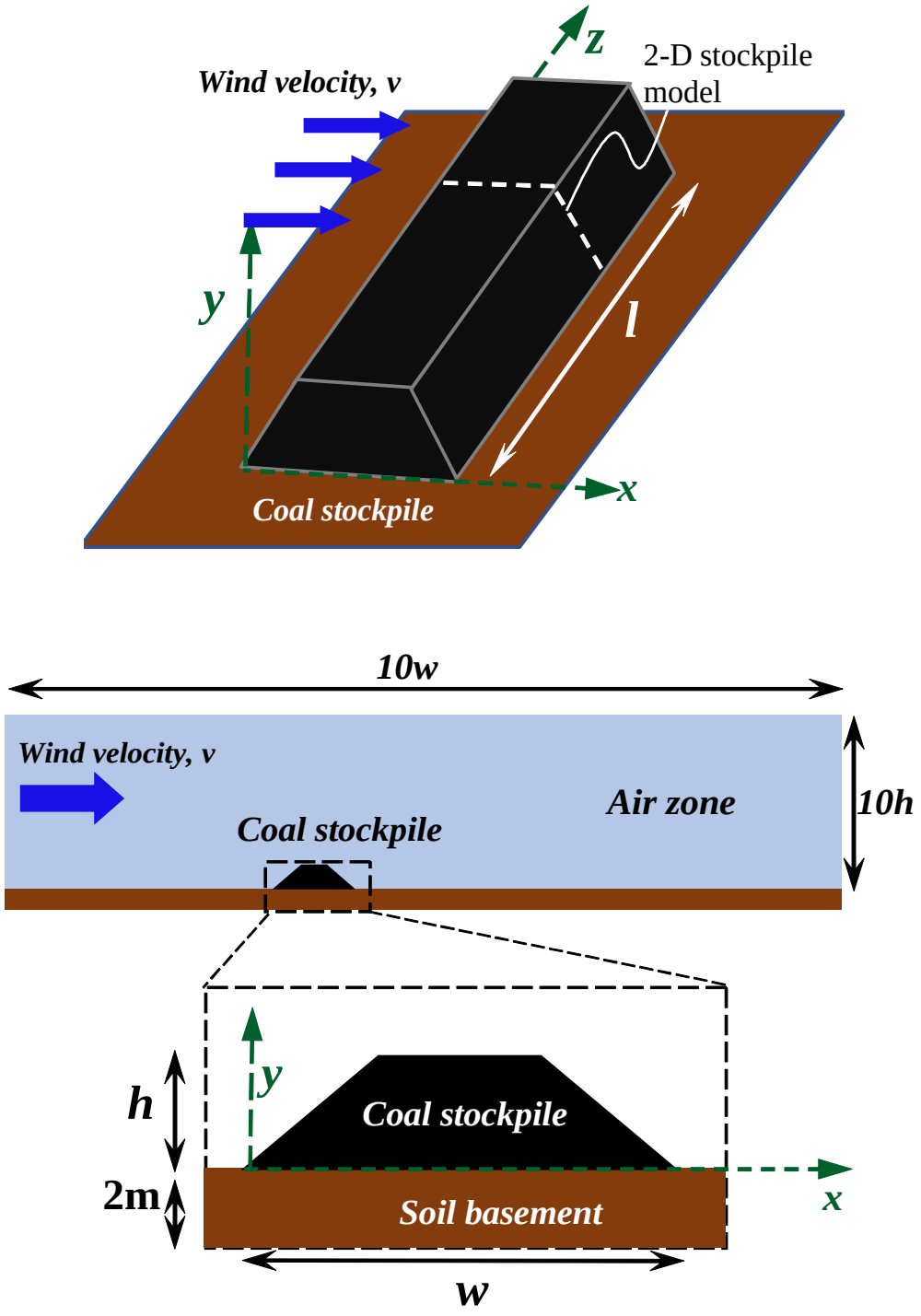

Figure 4- 2. The numerical 2-D model of coal stockpile.

A base case for the 2-D model was built with the boundary and initial conditions are given in Table 4-1. The main parameters used in the simulations are provided in Table 4-2. The governing equations and source terms in the numerical model have been introduced in Section 3.2 and 3.4. Moreover, the effect of moisture evaporation is not considered in the numerical simulation.

Table 4- 1. Boundary and initial conditions in the coal stockpile model.

Boundary conditions	Intake	$x = 0$ $y = 0$ to $10h$	Velocity: v=2 m/s Temperature: 27 °C O_2 fraction: 0.23(mass ratio)
	Exhaust	$x = 10l$ $y = 0$ m to $10h$	Free outflow
		Other boundaries	Heat flux: 0
Initial conditions	Temperature	Entire domain	27 °C
	Velocity	Air zone Coal stockpile zone	0
	O_2 fraction	Air zone Coal stockpile zone	23% (mass ratio)

Table 4- 2. Main parameters considered in the numerical simulation (base case).

Parameters	Items	Value	Unit
γ	Decay-power factor	1×10^{-6}	s^{-1}
n	Porosity	0.33	-
ρ_a	Density of air	1.225	kg/m^3
ρ_c	Density of coal	1300	kg/m^3
ρ_s	Density of soil	1630	kg/m^3
c_a	Specific heat capacity of air	1007	J/(kg·K)
c_c	Specific heat capacity of coal	1210	J/(kg·K)
c_s	Specific heat capacity of soil	1520	J/(kg·K)
λ_a	Thermal conductivity of air	0.04	W/(m·K)
λ_c	Thermal conductivity of coal	0.21	W/(m·K)
λ_s	Thermal conductivity of soil	0.5	W/(m·K)
E	Activation energy	78.9	kJ/mol
A_0	Pre-exponential factor	2.62×10^{11}	W/kg
d	Particle size	3	mm
w	Stockpile width	15	m

4.3 Spontaneous combustion analysis of base case

Figure 4-3 shows the distributions of seepage airflow and temperature in the coal stockpile at t = 27 days. The coal stockpile suffers the forced-convection airflow from its two slopes. This airflow distribution is similar to that reported by Taraba et al. (2014). The seepage velocity in the windward side is larger than that of leeward side. Thus, the hot zone in the windward side due to the larger amount of supplied O_2 from the front surface.

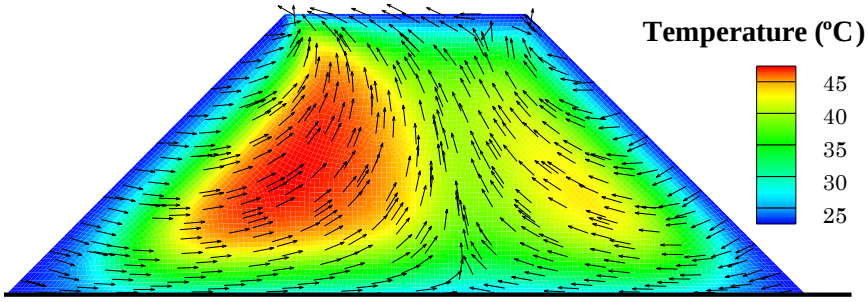

(a) Temperature distribution and seepage velocity direction

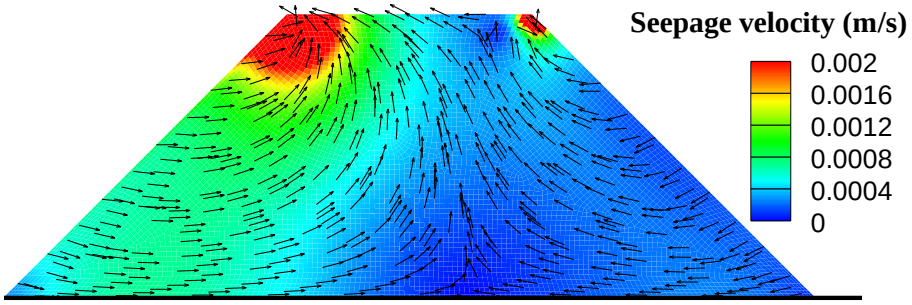

(b) Distributions of seepage velocity

Figure 4- 3. Seepage airflow and temperature distribution in coal stockpile (base case, t = 27 days).

Figure 4-4 shows the maximum temperature, T_{max}, and minimum O_2 concentration, C_{min}, versus time at the base case. T_{max} grows with a low heating rate until reaching 60 °C. The temperature in the coal stockpile is runaway at t = 43 days when the T_{max} arriving around 80 °C. The C_{min} in the stockpile fast decrease to 12 wt% at t = 2 days and then increase to 17.8 wt% at t = 20 days. Then, a large amount of O_2 is consumed

due to the coal-oygen reaction with decreasing C_{min}.

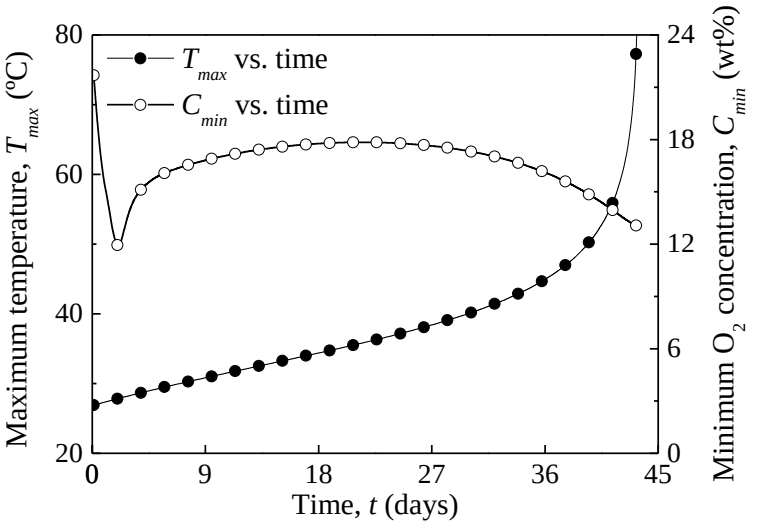

Figure 4- 4. Values of T_{max} and C_{min} in the coal stockpile versus time (base case, $\gamma = 1\times10^{-6}$ s^{-1}).

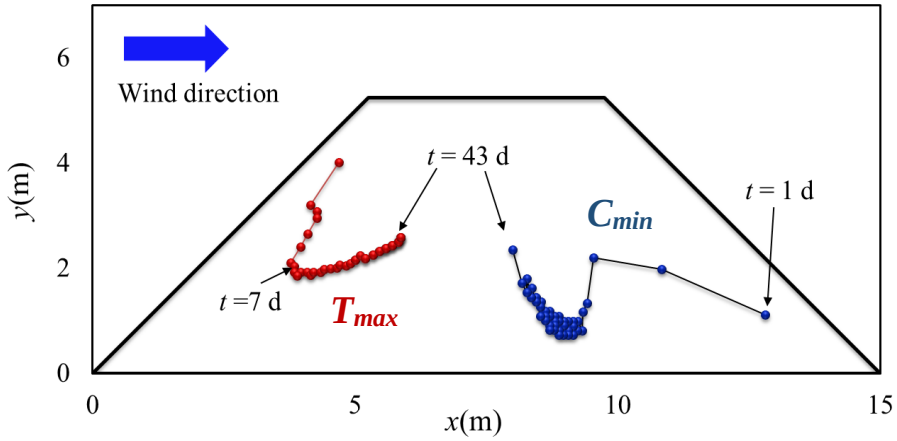

Figure 4- 5. Moving locations of T_{max} and C_{min} in the coal stockpile (base case, $\gamma = 1\times10^{-6}$ s^{-1}).

As shown in Figure 4-5, The hotspot forms in the upper-windward part of the pile and then moves toward the front corner for adsorbing more O_2. In the first 7 days, the T_{max} slowly increases from the ambient temperature of 27 °C to 30 °C. When t = 7 days, the hotspot reaches the limitation of the position that most closed to the front-angle. In the same period, the moving location of C_{min} starts from near the back-angle and then transfers to the inner part. After t = 7 days, the T_{max} point moves toward the upper-leeward direction with a low moving rate. The main reasons for this trend are as

follows: (a) the increase of coal temperature promotes the heated-forced convection, and more cooling and fresh air enter the coal stockpile. Thus, the hotspot migrates toward the zone with superior heat-storage capacity. (b) the effect of the aging effect becomes apparent. An increase of EOE-time in the windward side of coal stockpile weakens the heat-generation. In brief, the hotspot moves toward the leeward side to oxidize the "fresh" coal.

When t = 43 days, the point of T_{max} in the coal stockpile is thermal-runaway in the windward part and near the stockpile centerline. The distance between the hotspot and the surface is around 3 m. The point of C_{min} is always located in the downward side of the hotspot. The distributions of temperature and O_2 concentration in the entire coal stockpile at different times are shown in Figure 4-6(a) and (b). Two hot zones exist in the coal stockpile due to outside air entering the stockpile from both slopes. A meniscus belt with low O_2 concentration locates between the two hot zones. Figures 4-4 and 4-6 show that the O_2 concentration in the coal stockpile exhibits an evolution of decrease-increase-decrease. At t < 3 days, the O_2 in the coal stockpile is consumed by the exothermic reaction. However, the amount of O_2 provided by natural convection is limited due to the low coal temperature. Therefore, the value of C_{min} decreases sharply. With the coal temperature increasing, the buoyancy effect becomes stronger, and more O_2 transfers into the coal stockpile by convection, which leads to the O_2 concentration increasing. However, the rapid coal-oxygen reaction after around t = 25 days results in the O_2 concentration decreasing before the thermal runaway.

As shown in Figures 4-6(c) and (d), an interesting result is the relationship between the distributions of EOE-time vs. elapsed-time and the heat generation rate. Sasaki and Sugai (2011) proposed that the EOE-time of coal is increased with heat dissipation from coal stockpile. An increase in EOE-time reduces the heat generation rate of coal. However, when the coal receiving enough heat from outside, the reduced EOE-time increases the heat generation. Zhang et al. (2018) put forward the negative correlation between EOE-time vs. elapsed-time and heat generation rate. Therefore, the opposite distributions of the two variables are observed in Figure 4-6.

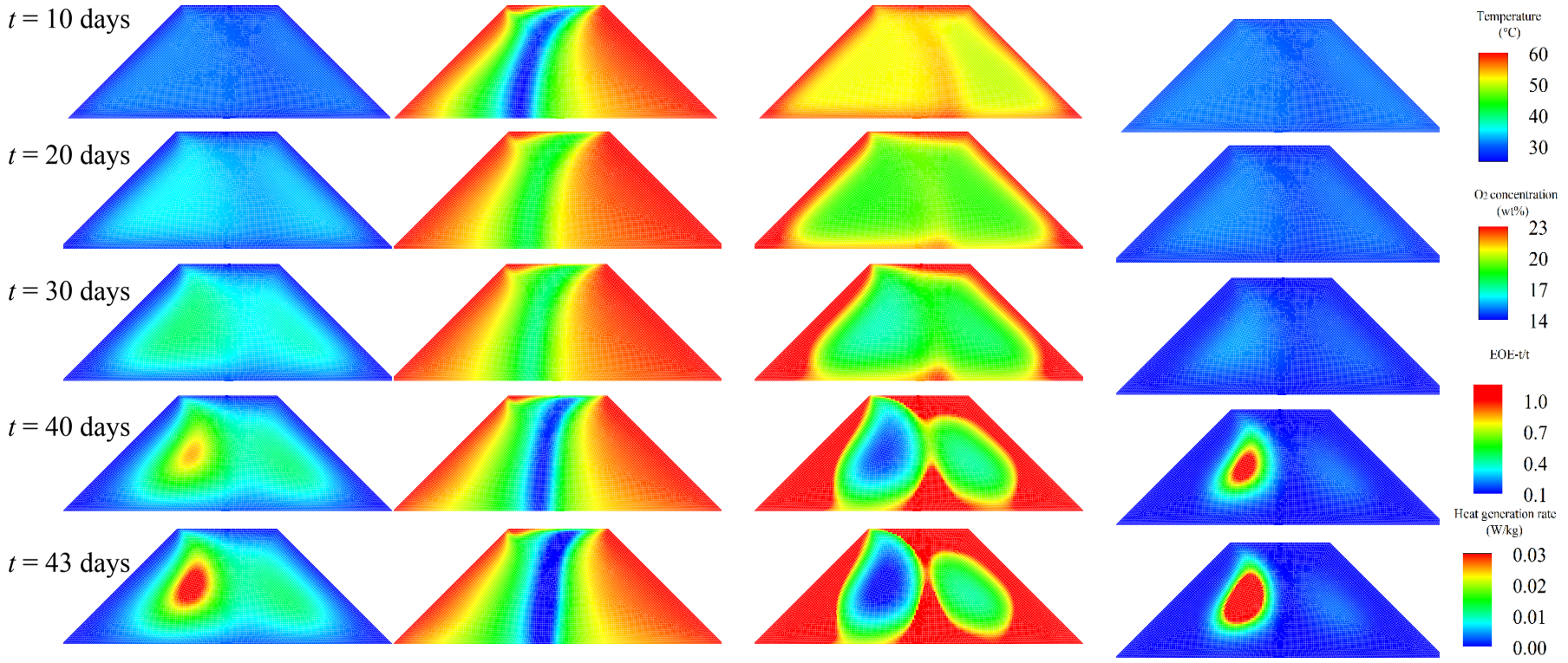

(a) Temperature (b) O_2 concentration (c) EOE-time vs. elapsed-time (d) Heat generation rate

Figure 4- 6. The distributions of the various parameters in the coal stockpile at a different time (base case, $\gamma = 1\times10^{-6}$ s^{-1}).

4.4 Effect of decay-power factor on spontaneous combustion of coal stockpile

4.4.1 Critical decay-power factor

The numerical simulations were carried out by for $\gamma = 0$ (Arrhenius equation), 1×10^{-7}, 1×10^{-6}, 1.2×10^{-6}, 1.3×10^{-6}, 1.5×10^{-6} and 4×10^{-5} s^{-1} to investigate the effect of decay-power factor on coal spontaneous combustion. The values of T_{max} in the coal stockpile for various γ are shown in Figure 4-7. Here, the safe storage time coal stockpile, t_{80}, is defined as the period changing from 27 ºC (Initial temperature) to 80 ºC (fast heating). Moreover, the critical decay-power factor, γ_c, is assumed as the middle value of the super-critical and sub-critical γ. It is similar to the definition of CSIT in Section 2.1.2, Therefore, γ_c is 1.25×10^{-6} s^{-1} for present coal stockpile, as illustrated in Figure 4-7. When $\gamma > \gamma_c$, the field coal stockpile is thermal safe due to the large aging effect on heat generation at low temperatures.

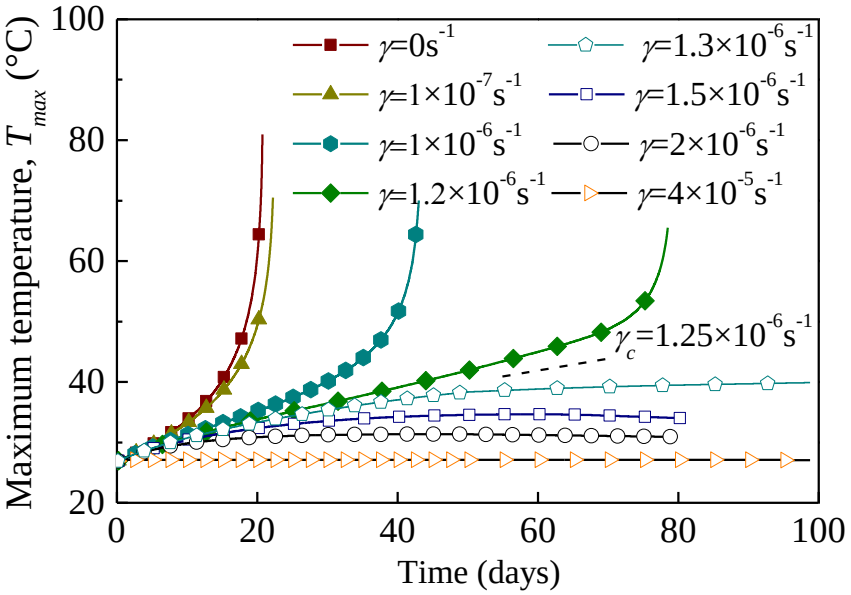

Figure 4- 7. Definition of critical decay-power factor, γ_c (w = 15 m, v = 2 m/s, d = 3 mm, n = 0.33).

The result by setting $\gamma = 0$ (Arrhenius model) shows the shortest t_{80} to spontaneous combustion (t_{80} = 20 days). While the result by setting $\gamma = 1.2 \times 10^{-6}$ shows the longest t_{80} of 79 days. Therefore, with increasing γ, the value of t_{80} is dramatically increased. For the case of higher γ, the coal suffers a larger decay rate of heat generation and lower potential of spontaneous combustion. The simulation results show that the coal stockpile does not ignite at $\gamma \geq 1.3 \times 10^{-6}$ s^{-1}. Thus, $\gamma = 1.25 \times 10^{-6}$ s^{-1} is estimated to be the critical decay-power factor in the present 2-D stockpile model. Therefore,

(a) $\gamma < 1.25 \times 10^{-6}$ s^{-1}: the coal is active in heat generation. The accumulative heat from the exothermic reaction leads to the self-ignition of the coal stockpile. the lower the value of γ, the shorter t_{80} and the lower the CSIT is expected.

(b) $\gamma > 1.25 \times 10^{-6}$ s^{-1}: the heat-generation potential of the coal stockpile is decreased with increasing γ without the self-ignition of coal. The maximum value of T_{max} in coal stockpile is declined with increasing γ.

As shown in Figure 4-7, the value of $\gamma = 4 \times 10^{-5}$ s^{-1} described in Chapter 3 is much higher than the critical value $\gamma_c = 1.25 \times 10^{-6}$ s^{-1} for 2-D coal stockpile under conditions listed in Tables 4-1 and 4-2. It means that the coal stockpile is safe when the value of γ_c is estimated to be less than the value of 4×10^{-5} s^{-1} measured by WMB tests.

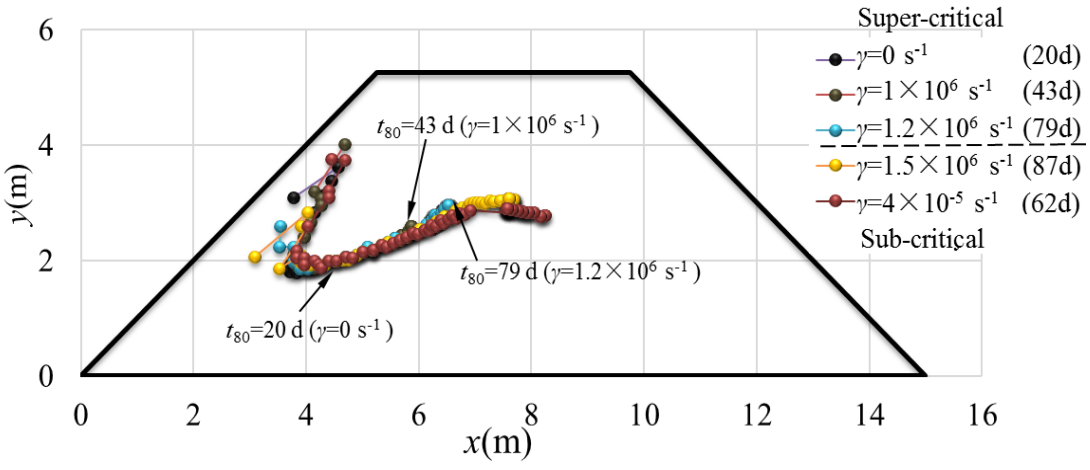

Figure 4- 8. Moving locations of T_{max} in the coal stockpile versus time for different decay-power factor, γ (l = 15 m, v = 2 m/s, d = 3 mm, n = 0.33).

The moving positions at T_{max} in the coal stockpile are shown in Figure 4-8. The moving locations for various γ are almost coincident. It demonstrates that the moving locations exhibit independence on the coal activity. As γ increasing, the depth of the thermal-burst point is larger. This distance around 2 m between the thermal-burst point and the stockpile surface ($\gamma = 0$ s^{-1}) is agreed with other studies (Akgün & Essenhigh, 2001; Arisoy & Akgün, 2000; Ejlali et al., 2009; Taraba et al., 2014). However, the distance when $\gamma > 0$ s^{-1} is around 3-4 m. It is due to the coal with high γ is inclined to be "old".

4.4.2 Critical decay-power factors versus stockpile width

The value of γ_c in the coal stockpile with different width, w (= 3, 4, 5, 7, 10, 15, 30 and 50 m) is estimated by conducting the simulations using EOE-model. Figure 4-9 shows the relationship between coal stockpile size, S (stockpile area in xy section, = $0.2275w^2$) and the critical decay-power factor, γ_c. There is no γ_c in the coal stockpile for w = 3 m because the coal stockpile does not to self-ignite even though $\gamma = 0$ s^{-1} (Arrhenius model). The generated heat from coal oxidation is difficult to be accumulated in the stockpile of w = 3 m.

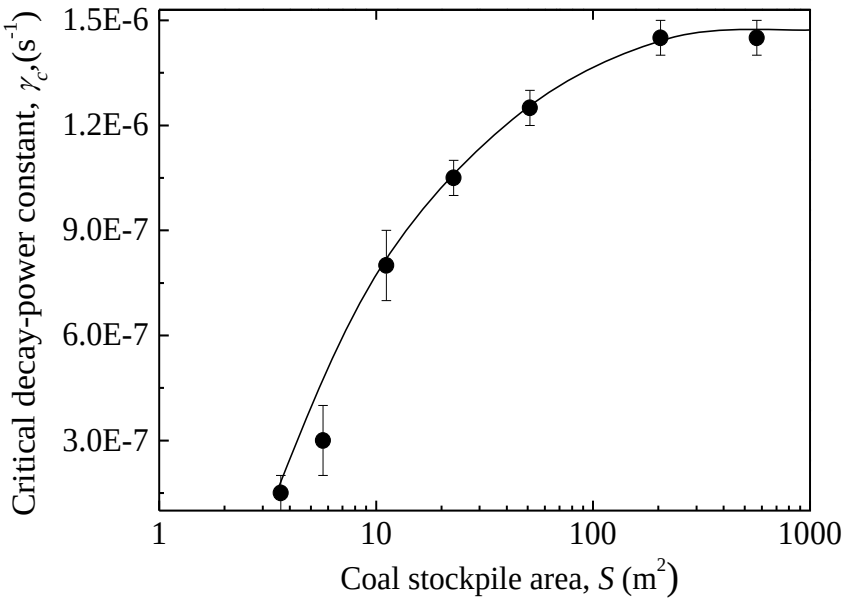

Figure 4- 9. Relationship between coal stockpile size, S, and critical decay-power factor, γ_c, ($S = 0.2275\ w^2$)

The value of γ_c is very sensitive to the coal stockpile size at S < 100 m^2, and then approaches to around 1.4×10^{-6} s^{-1}. Therefore, the coal consisting of the stockpile having the $\gamma < \gamma_c$ will be self-ignition. Therefore, it is necessary to decrease the coal stockpile size to prevent self-ignition.

4.4.3 Spontaneous combustion of coal stockpile wetted by optimal C-WS

To investigate the effect of C-WS on the spontaneous combustion of coal stockpile, the coal in the stockpile are wetted by the optimal C-WS (SMN-16 wt%, PVA-0.2 wt%). Based on Equation (3-20) and (3-21), the reference value of decay-power factor is supposed to be $\gamma = 1.4\times10^{-6}$ s^{-1} (base case), and the increased value of γ is estimated to be 7.9×10^{-5} s^{-1}. Figure 4-10 shows the comparison of T_{max} of raw coal ($\gamma = 1\times10^{-6}$ s^{-1}) and coal wetted by optimal C-WS ($\gamma = 7.9\times10^{-5}$ s^{-1}). The coal stockpile wetted by C-WS does not self-ignite due to the strong aging effect on the heat generation of coal. Therefore, the coal stockpile wetted by optimal C-WS is thermally safe and the C-WS is an effective inhibitor to prevent coal fire.

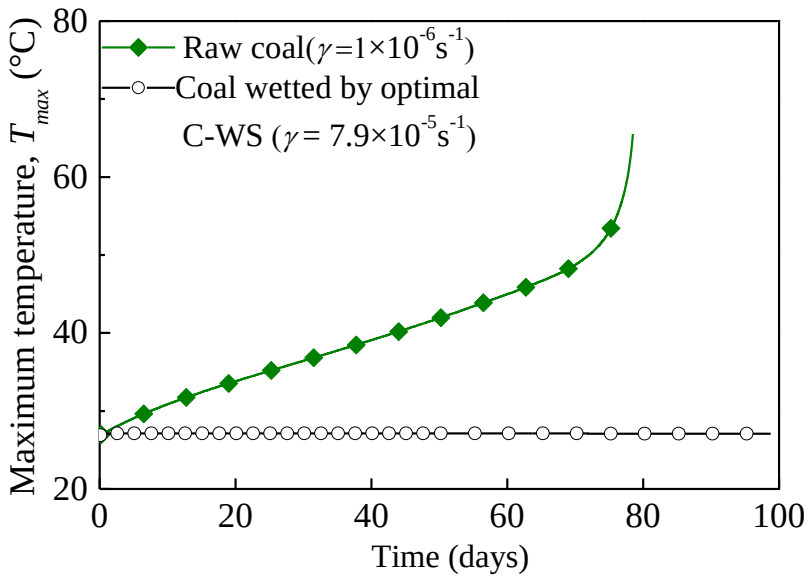

Figure 4- 10. Values of T_{max} of raw coal and coal wetted by optimal C-WS (SMN-16 wt%, PVA-0.2 wt%)

4.5 Sensitivity study on the base case

As listed in Table 4-3, the sensitivity study was done for stockpile width, wind velocity, porosity and particle size, on the coal spontaneous combustion.

Table 4- 3. Controlled variables in the numerical simulations ($\gamma = 1\times10^{-6}$ s^{-1}).

Items	Base case	Controlled variable
Wind velocity, v (m/s)	2	0, 1, 2, 4, 6, 8, 9, 10, 14
Coal stockpile width, w (m)	15	5, 8,10, 15, 20, 30
Particle size, d (mm)	3	0.3, 1, 3, 6, 8, 10
Porosity, n (-)	0.33	0.1, 0.17, 0.2, 0.33, 0.4, 0.55,0.6

4.5.1 Effect of wind velocity

Seepage airflow in the coal stockpile is mainly affected by the wind velocity approaching to the stockpile. The convective seepage airflow is a dominant power to transporting heat and O_2. The values of T_{max} and C_{min}, as well as their moving locations versus elapsed time at different wind velocity, v, are plotted in Figures 4-11 and 4-12. Airflow provides the fresh air for the exothermic coal-oxygen reaction. Therefore, with the wind velocity increasing, the value of t_{80} is reduced from 56 days (v = 0 m/s) to 41.5 days (v = 6 m/s). The initial hotspot (t = 1 day) is distributed in the windward side (4-11(a)). But, the larger v, the longer the distance from the stockpile surface to the hotspot is observed. It is because the stronger wind takes the outside air into the coal stockpile and forces the hotpot forming in the deeper position from the stockpile surface.

For v = 0 m/s, the seepage velocity field in the coal stockpile becomes symmetric. Therefore, there are two hotspots in the coal stockpile (only the upstream hotspot is plotted in Figure 4-12(a)) and the point at C_{min} appears near the centerline of coal stockpile. With increasing the wind velocity, more O_2 is provided to promote the heat generation. However, more internal heat in the stockpile is dissipated by natural and forced convection with increasing v. Therefore, the value of t_{80} is extended from 41.5

days for v = 6 m/s to 44.5 days for v = 8 m/s.

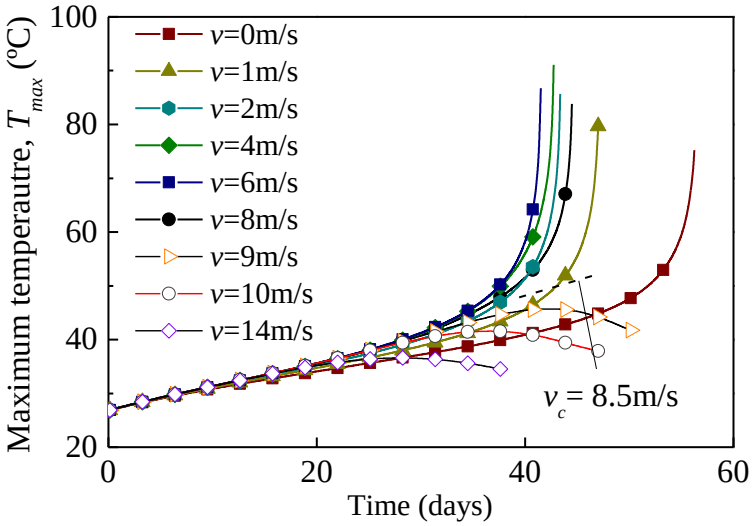

(a) Values of T_{max} versus time

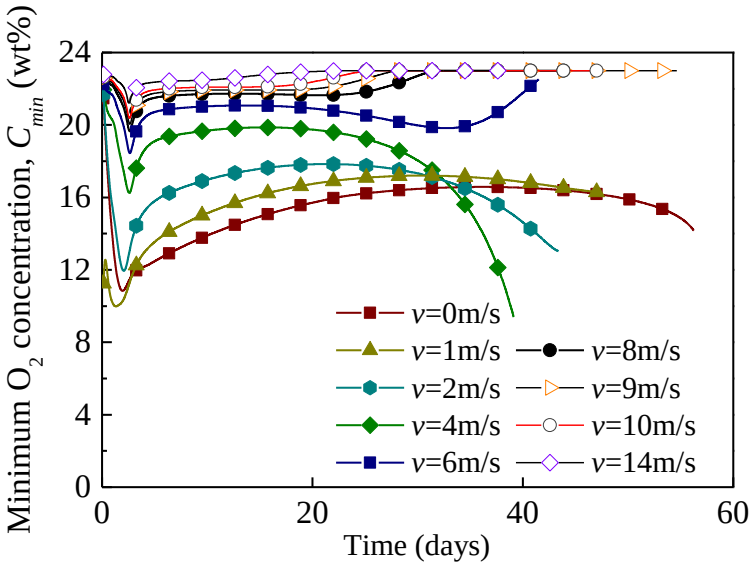

(b) Values of C_{min} versus time

Figure 4- 11. Values of T_{max} and C_{min} in the coal stockpile versus time for different wind velocity, v (w = 15 m, d = 3 mm, n = 0.33, $\gamma = 1\times10^{-6}$ s^{-1}).

The coal stockpile does not ignite when the value of v exceeds the critical value, v_c = 8.5 m/s, in present model. Moreover, the hotspot location is moving to a deep position from the surface with increasing v due to heat convection. This result is agreed with that proposed by Zhu et al. (2013). Accordingly, the zone of low concentration O_2 follows the hotspot and moves toward the downstream area in the stockpile (Figure 4-

12(b)). The value of C_{min} versus time shows the typical trend of fast decrease-gently increase (Figure 4-11(b)). However, when t > 32 days, the value of C_{min} for v = 2 and 4 m/s dropped more rapidly than that of v = 0 m/s due to the remarkable coal-oxygen reaction (Figure 4-11(a)), although larger airflow takes more O_2 into the stockpile.

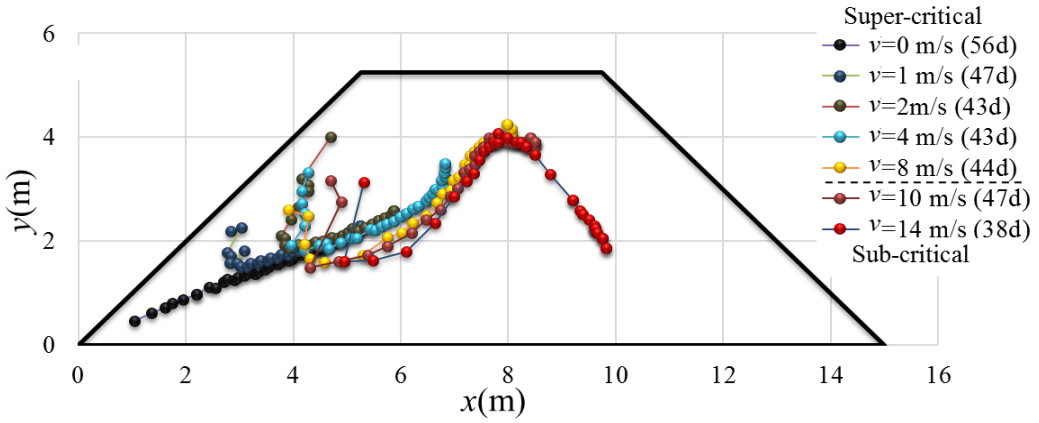

(a) Moving locations of T_{max}

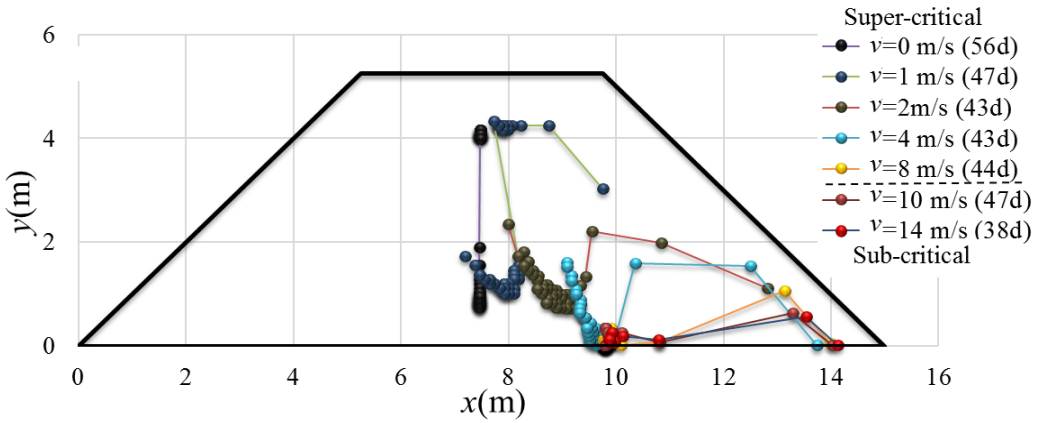

(b) Moving locations of C_{min}

Figure 4- 12. Moving locations of T_{max} and C_{min} in the stockpile versus time for different wind velocity, v (w = 15 m, d = 3 mm, n = 0.33, $\gamma = 1\times10^{-6}$ s^{-1}).

4.5.2 Effect of stockpile width

Figure 4-13 describes the effect of stockpile width, w, on the values and moving locations of T_{max} and C_{min} in the coal stockpile. By decreasing from 30 m to 15 m in w the value of t_{80} is increased by 3 days. However, 5 m decrease from w = 15 m to 10 m

leads to an extension of 25 days in t_{80}. When w smaller than a critical value of w = 9 m, the coal stockpile shows no self-ignite due to larger heat dissipation. The heat generated from the exothermic reaction is easily dissipated to the surroundings by convection flow. Akgün and Essenhigh (2001) also found the coal stockpile shows no self-ignite if the stockpile size lower than the critical value.

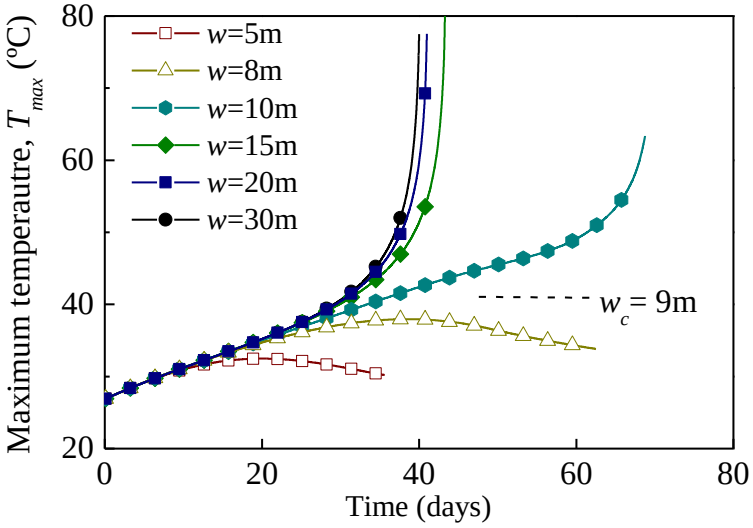

(a) Values of T_{max} versus time

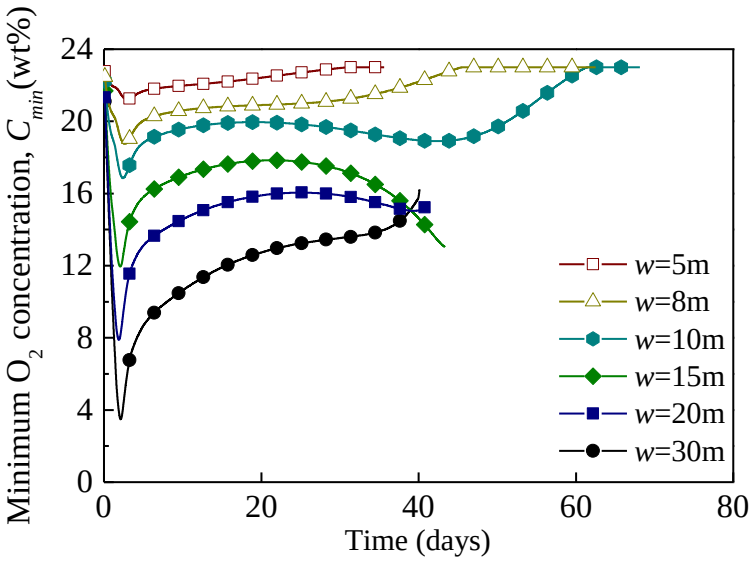

(b) Values of C_{min} versus time

Figure 4- 13. Values of T_{max} and C_{min} in the coal stockpile versus time for different stockpile width, w (v = 2 m/s, d = 3 mm, n = 0.33, $\gamma = 1\times10^{-6}$ s^{-1}).

Figure 4-14 shows the initial hotspot locates in the upper and upstream side and then moves toward the lower and downstream side. Although the trajectories of the hotspot are different for various w, the sites showing thermal runaway are located at the position which is distance around 3-4 m from the pile surface. The moving locations of C_{min} point for various w show a similar path. Thus, the stockpile width larger than w = 9 m shows the high potential of spontaneous combustion in present simulations.

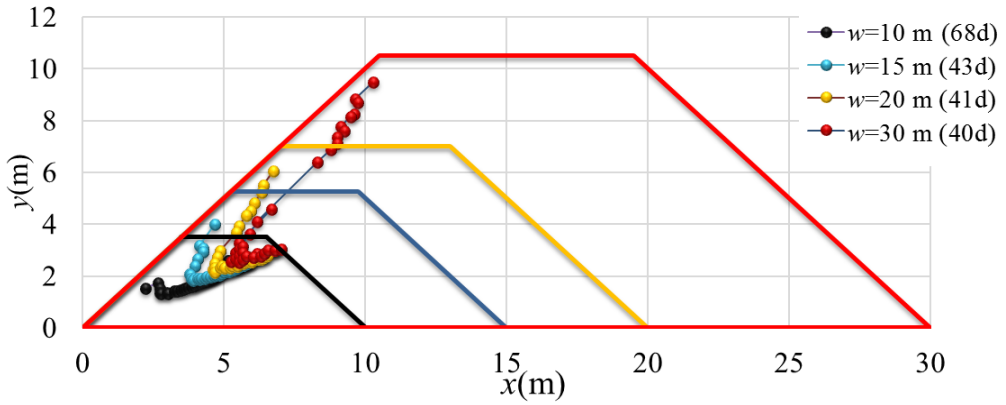

(a) Moving locations of T_{max}

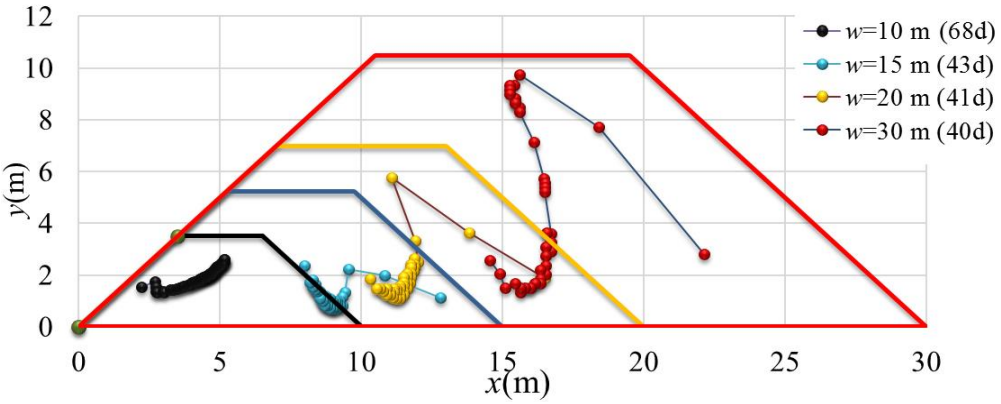

(b) Moving locations of C_{min}

Figure 4- 14. Moving locations of T_{max} and C_{min} in the coal stockpile versus time for different stockpile width, w (v = 2 m/s, d = 3 mm, n = 0.33, $\gamma = 1\times10^{-6}$ s^{-1}).

4.5.3 Effect of particle size

Permeability of coal stockpile is one of the key roles to control the seepage intensity.

Lower porosity or smaller particle size reduces the permeability (See Equation (3-6)) and restricts the seepage velocity in the porous stockpile. Coal particles with small size have a high reactivity because of the relatively larger internal surface exposed to air.

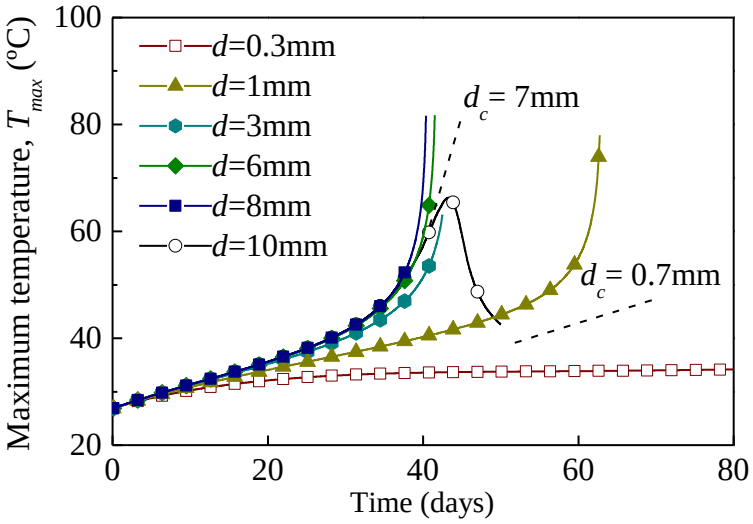

(a) Values of T_{max} versus time

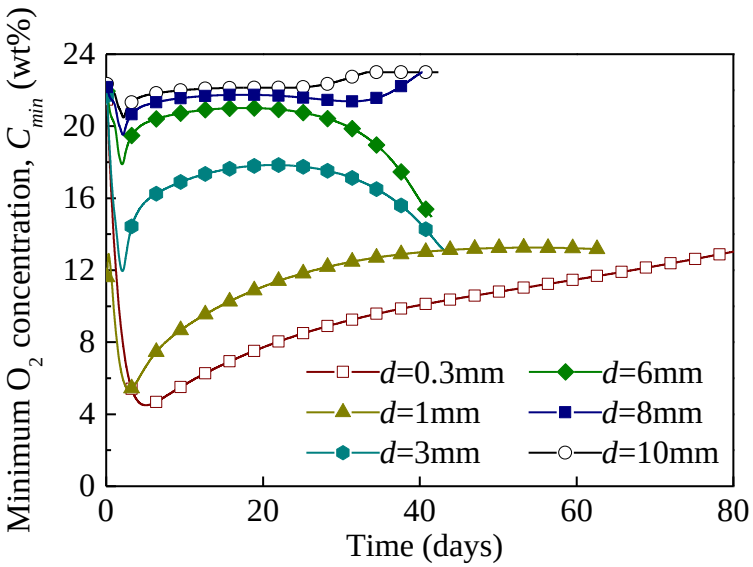

(b) Values of C_{min} versus time

Figure 4- 15. Values of T_{max} and C_{min} in the coal stockpile versus time for different particle sizes, d (w = 15 m, v = 2 m/s, n = 0.33, $\gamma = 1\times10^{-6}$ s^{-1}).

However, Krishnaswamy et al. (1996) proposed that the effect of particle size on permeability is deemed more critical than that of reaction rate. Some researchers have presented that a reduction in coal particle size leads to the hotspot moving toward the

pile surface due to the low permeability (Akgün & Essenhigh, 2001; Arisoy & Akgün, 1994; Krishnaswamy et al., 1996; Zhang et al., 2016). Similar results are found in this study, as shown in Figure 4-15(a), the smaller the particle size results in decreasing C_{min}. Therefore, Fine particles of coal have been applied to cover the coarse coal stockpile for preventing spontaneous combustion (Yang et al., 2014).

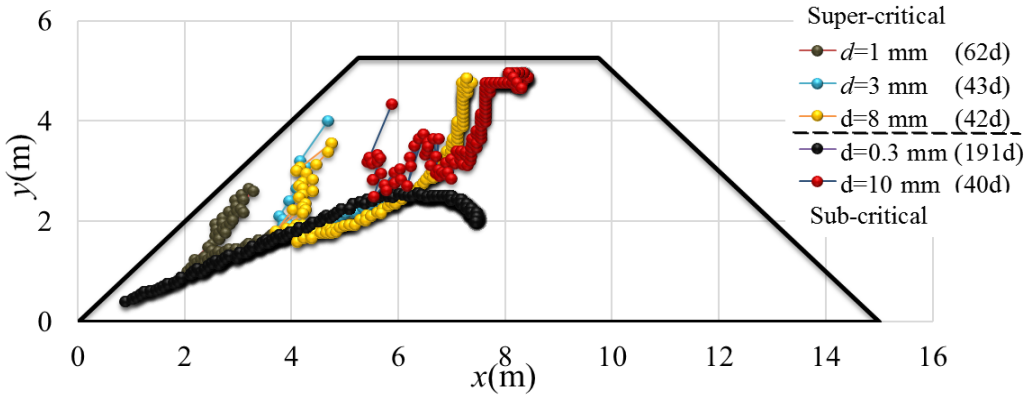

(a) Moving locations of T_{max}

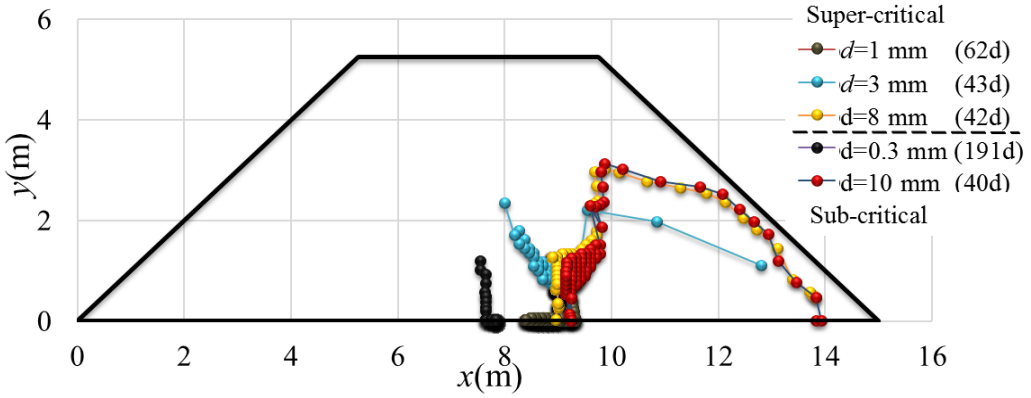

(b) Moving locations of T_{max}

Figure 4- 16. Moving locations of T_{max} and C_{min} in the coal stockpile versus time for different particle sizes, d (w = 15 m, v = 2 m/s, n = 0.33, $\gamma = 1\times10^{-6}$ s^{-1}).

However, when the particle size, d, exceeding 9 mm, the coal stockpile cannot combust spontaneously due to increasing heat dissipation to surroundings by intensive forced convention. Therefore, there are two critical particle size: the upper critical value of 7 mm and the lower critical value of 0.7 mm. The location of C_{min} at d = 0.3 mm is always located near the bottom-centerline of coal stockpile (Figure 4-16(b)). The T_{max}

takes more than 150 days to arrive the similar positions where the self-ignition occurs in the coal stockpile with $d > 1$ mm (t_{80} = 42-62 days).

4.5.4 Effect of porosity

Figure 4-17 and 4-18 show the values and moving locations of T_{max} and C_{min}, as well as their moving locations versus elapsed time for different porosity, n. The porosity is related to the degree of compaction of coal stockpile.

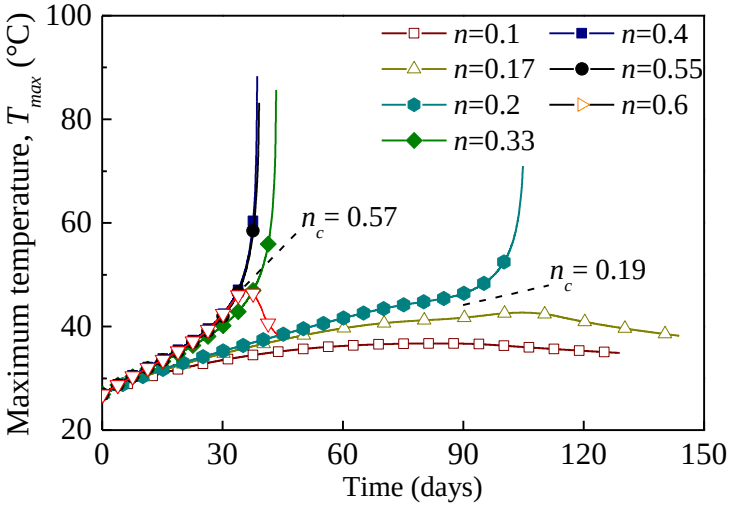

(a) Values of T_{max} versus time

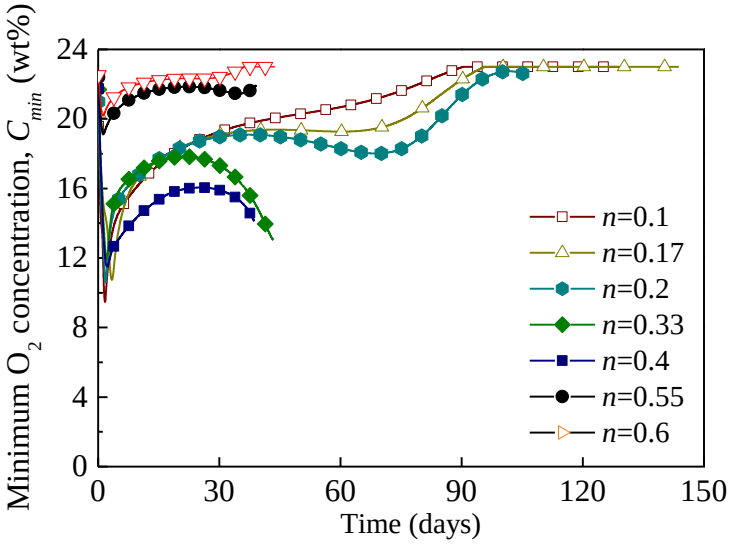

(b) Values of C_{min} versus time

Figure 4- 17. Values of T_{max} and C_{min} in the coal stockpile versus time for different porosity, n (w = 15 m, v = 2 m/s, d = 3 mm, $\gamma = 1\times10^{-6}$ s^{-1}).

An increase in coal porosity affects the self-ignition behavior of coal stockpile in four aspects: (i) more O_2 enters the coal stockpile due to the higher permeability; (ii) the heat from coal oxidation is difficult to transfer to outside by thermal diffusion; (iii) stronger seepage airflow contributes to the heat dissipation in the coal stockpile; (iv) higher n involves less coal mass and less heat generation.

As shown in Figure 4-17(a), there are two critical values observed in the present simulation: the lower critical porosity of 0.19 and the upper critical porosity of 0.57.

(i) $n < 0.19$: the coal stockpile does not combust due to the limitation of the O_2 supply. Therefore, the maximum value of T_{max} is increased with increasing n. the hotspot moves through the pile centerline, as shown in Figure 4-18(a).

(ii) $0.19 < n < 0.57$: the coal stockpiles get self-ignition. With the n increasing, the value of t_{80} expresses a decreased trend first because more O_2 is provided to the coal pile and reacts with coal, as shown in Figure 4-17(b). However, the increasing n leads to less coal mass per unit coal volume and reduces exothermic heat in unit coal volume.

(iii) $0.57 < n$: with the n increasing, more O_2 enters to the pile by forced convection airflow. Therefore, the C_{min} of higher n is larger than that of the low one, as shown in Figure 4-17(b). The coal stockpile does not combust due to the low reacted heat at large n. The hotspot at the last period locates in the top position of the pile due to the strong convention induced by large n.

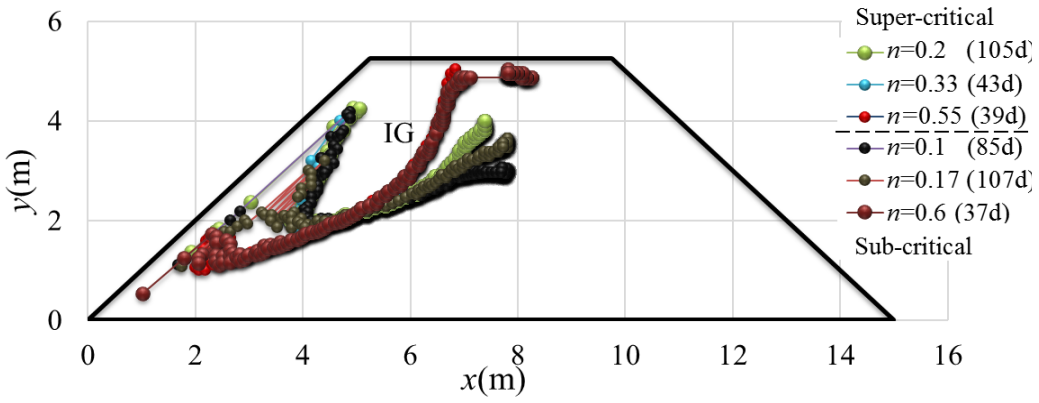

(a) Moving locations of T_{max}

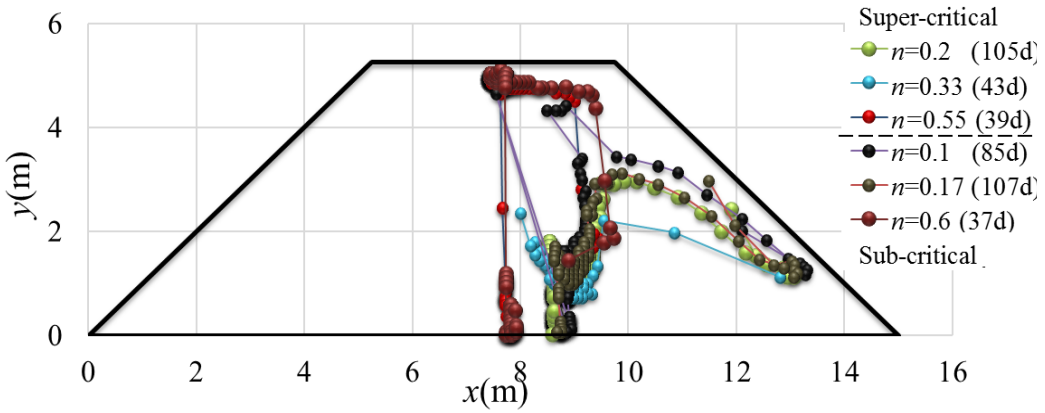

(b) Moving locations of T_{max}

Figure 4- 18. Moving locations of T_{max} and C_{min} in the coal stockpile versus time for different porosity, n (w = 15 m, v = 2 m/s, d = 3 mm, $\gamma = 1\times10^{-6}$ s^{-1}).

4.5.5 Comprehensive analysis

The single-controlled variable affecting the spontaneous combustion of the coal stockpile characterizes the critical values at super-critical decay-power factor, $\gamma = 1\times10^{-6}$ s^{-1}. as listed in Table 4-4.

Table 4- 4. Critical values of the four parameters of the coal stockpile ($\gamma = 1\times10^{-6}$ s^{-1})

Items	Lower critical value	Upper critical value
Wind velocity, v (m/s)	Null	8.5
Coal stockpile width, w (m)	9	Null
Particle size, d (mm)	0.7	7
Porosity n (-)	0.19	0.57

There is no critical value for the parameter of wind velocity, v, and pile width, w. It indicates that in this model with $\gamma = 1\times10^{-6}$ s^{-1}, the self-ignition of coal stockpile is inevitable when $v < 8.5$ m/s and $w > 9$ m.

Based on the above analysis, the following practical measures should be carried out to prevent the self-ignition in coal stockpile:

(i) Cover the stockpile using fine coal particles to decrease providing O_2 into the

stockpile;

(ii) Compact the coal stockpile to decrease the porosity;

(iii) Install the wind barrier around coal stockpile to reduce the pressure difference and seepage velocity in the stockpile;

(iv) Spray the inhibitory material on the coal stockpile to change the decay-power constant, γ, to a large value.

(v) Compact the coal stockpile in smaller volume to prevent heat accumulation.

4.6 Conclusions

In this chapter, the spontaneous combustion of coal stockpile considering the aging effect is investigated with forecasting the critical decay-power factor, γ_c. The results in this chapter are summarized as follows,

(a) A 2-D mathematical model (base case, coal stockpile width w = 15 m, particle size d = 3 mm, wind velocity v = 2 m/s, porosity n = 0.33 and decay-power factor γ = 1×10^{-6} s^{-1}) is built to study the spontaneous combustion process of coal stockpile at low temperatures. ANSYS FLUENT software is used for solving the governing equations. The maximum temperature, T_{max}, and minimum O_2 concentration, C_{min}, as well as their moving locations are analyzed.

(b) The critical decay-power factor, γ_c, is increased with increasing stockpile volume. It can be concluded that satisfying $\gamma > \gamma_c$ is needed for coal stockpile safety by predicting spontaneous combustion. The value of γ_c for a typical coal stockpile (w = 15 m, d= 3 mm, v = 2 m/s and n = 0.33) is estimated to be $\gamma_c = 1.25\times10^{-6}$ s^{-1}. It means that the coal stockpile is safe when the value of γ_c for the stockpile conditions is less than the value of γ estimated by the history matching with the results of WMB tests in Chapter 3.

(c) Effects of different parameters, w = 5 to 30 m, v = 0 to 14 m/s, d = 0.3 to 10 mm and n = 0.1 to 0.6, on the coal self-ignition were studied based on the base case.

Chapter 5: Conclusions and outlook

5.1 Summary of the present research

5.1.1 Wire mesh basket (WMB) tests

Lignite excavated from the Baiyinhua coalfield in Inner Mongolia, China, was used in the WMB test. The WMB tests using four basket sizes (L = 5, 10, 15, 25 cm) and particle size of d = 10 mm were carried out to investigate the self-ignition behavior and the characteristic parameters, such as critical self-ignition temperature (CSIT) and critical lead time (CLT). The larger volume of the coal pile expressed a lower CSIT and longer CLT. CSIT of dried coal at certain basket size showed a lower temperature at least 10 °C than that of wet coal. The coal pile with larger particle size always has a higher CSIT and shorter CLT.

5.1.2 Cross-linked gel to prevent coal spontaneous combustion

The complex water solution (C-WS) of SMN and PVA forms the cross-linked gel (SMN/PVA gel) with CO_2 gases was examined as an inhibitor to prevent coal spontaneous combustion by carrying out the WMB tests. The C-WS expressed a better effect on inhibiting self-ignition than conventional silicate gel. The effects of SMN and PVA concentrations on the fire-prevention of lignite were investigated and the optimal concentrations of SMN and PVA were suggested to be 16 wt% and 0.2 wt% respectively. The empirical equation to estimate the CSIT was presented by adding the effects of SMN and PVA concentrations to the previous equation between CSIT and pile volume as well as particle size for the raw coal.

5.1.3 Numerical simulation on WMB tests considering aging effect

the equivalent oxidation exposure time (EOE-time) theory incorporates the aging effect and is applied in the numerical simulation on the WMB tests. The optimal value for the decay-power factor, γ, is determined to be 4×10^{-5} s^{-1} based on the history matching of simulation to the measured CSIT in WMB tests of L = 5 to 25 cm. Theoretical predictions based on EOE-time theory with larger γ give higher CSIT values and lower CLT values because of a stronger aging effect on the heat generation rate. CSIT and CLT values for both wet and dry coal piles are successfully predicted using the EOE-time theory by considering the aging effect. The effects of moisture on heat generation are investigated to increase CSIT and CLT values, that is, reduce the spontaneous combustion tendency of coal. Besides, the effect of C-WS on preventing coal self-ignition was evaluated to be equal effect by increasing the value of γ based on the comparisons of increased CSIT.

5.1.4 Numerical simulations on spontaneous combustion of coal stockpile

the spontaneous combustion process of surface coal pile is evaluated by applying the EOE-time theory. A 2-D mathematical model for coal stockpiles was constructed using ANSYS FLUENT. Firstly, the spontaneous combustion process of coal stockpile of base case was analysed (stockpile width w = 15 m, particle size d= 3 mm, wind velocity v = 2 m/s, porosity n = 0.33 and $\gamma = 1\times10^{-6}$ s^{-1}). Then, the numerical simulation on the spontaneous combustion process of coal pile with different γ is conducted and the critical value of γ is estimated to be 1.25×10^{-6} s^{-1}, which is much lower than that estimated from the history matching with the WMB tests. Last, the sensitivity of base case for different variables, such as wind velocity, pile width, particle size and porosity on the coal self-ignition is studied.

5.2 Outlook

Based on the present research, there are some challenges and difficulties which should be considered in future works, as follows,

(a) The decay-power factor, γ, is a key parameter to estimate the heat generation rate of coal. The measurement of the heat generation rate of Baiyinhua lignite should be carried out to verify the value of γ obtained in this study.

(b) The present model of water evaporation has been applied in the WMB tests, as described in Chapter 3. However, the application of water evaporation model combined with EOE-time theory in field-scale coal was not conducted in this study. We deduce that the decay-power factor has a closed relationship with the water content of coal mass at the low-temperature range. Therefore, the water evaporation model should be improved for satisfying the simulations for field models.

(c) This work did not investigate the relationship between particle size and coal reactivity. Particle size is an important parameter on coal self-ignition. Thus, the coupling effects of particle size on the decay-power factor, permeability, porosity and water evaporation rate will be explored in the next step.

(d) The lignite from Baiyinhua coalfield was used in WMB tests and numerical simulations in this study. More coal samples with different ranks should be tested and simulated to investigate the relationship between coal rank and decay-power factor.

Reference

Adam V. (2019). *Smoke Blankets Borneo*. NAsa Earth Obervatory. https://earthobservatory.nasa.gov/images/145614/smoke-blankets-borneo?src=eoa-iotd

Adamus A. (1998). Laboratorní metody ověřování náchylnosti uhlí k samovznícení v OKR. *Listovka „Záchranář*, *2*, 6–7.

Adewunmi, A. A., Ismail, S., Sultan, A. S. (2015). Study on strength and gelation time of polyacrylamide/polyethyleneimine composite gels reinforced with coal fly ash for water shut-off treatment. *Journal of Applied Polymer Science*, *132*(5), 1–8. https://doi.org/10.1002/app.41392

Akgün, F., Essenhigh, R. H. (2001). Self-ignition characteristics of coal stockpiles: theoretical prediction from a two-dimensional unsteady-state model. *Fuel*, *80*(3), 409–415.

Akgün, F., Arisoy, A. (1994). Effect of particle size on the spontaneous heating of a coal stockpile. *Combustion and Flame*, *99*(1), 137–146. https://doi.org/10.1016/0010-2180(94)90085-X

Allardice, D. J. (1966). The adsorption of oxygen on brown coal char. *Carbon*, *4*(2), 255–262. https://doi.org/10.1016/0008-6223(66)90087-X

Anderson, K. B., Johns, R. B. (1986). Oxidation studies of Australian coals-I. Aliphatic and aromatic hydrocarbon centres of oxidative attack. *Organic Geochemistry*, *9*(5), 219–224. https://doi.org/10.1016/0146-6380(86)90093-8

Ansys Fluent Inc. (2012). Fluent 15.0, Help-User's guide. In *Fluent Inc*.

Arisoy, A., Akgün, F. (1994). Modelling of spontaneous combustion of coal with moisture content included. *Fuel*, *73*(2), 281–286. https://doi.org/10.1016/0016-2361(94)90126-0

Arisoy, A., Akgün, F. (2000). Effect of pile height on spontaneous heating of coal stockpiles. *Combustion Science and Technology*, *153*(1), 157–168.

Arisoy, A., Beamish, B. (2015). Reaction kinetics of coal oxidation at low temperatures. *Fuel*, *159*, 412–417.

Arisoy, A., Beamish, B. B., Çetegen, E. (2006). Modelling spontaneous combustion of coal. *Turkish Journal of Engineering and Environmental Sciences*, *30*(3), 193–201. https://doi.org/10.3906/sag-1204-97

Arisoy, A., Beamish, B., Yoruk, B. (2017). Moisture moderation during coal self-heating. *Fuel*, *210*(April), 352–358. https://doi.org/10.1016/j.fuel.2017.08.075

Astm, E. (2001). Standard test method for hot-surface ignition of dust layers. *ASTM E2021*.

Austin, K. G., Harris, N. L., Wijaya, A., Murdiyarso, D., Harvey, T., Stolle, F., Kasibhatla, P. S. (2018). A review of land-based greenhouse gas flux estimates in Indonesia. *Environmental Research Letters*, *13*(5). https://doi.org/10.1088/1748-9326/aab531

Avila, C., Wu, T., Lester, E. (2014). Estimating the spontaneous combustion potential of coals using thermogravimetric analysis. *Energy and Fuels*, *28*(3), 1765–1773. https://doi.org/10.1021/ef402119f

Banerjee, S. C., Chakravorty, R. N. (1967). Use of DTA in the study of spontaneous combustion of coal. *Journal of Mines, Metals & Fuels*, *15*(1), 1–5.

Beamish, B. B., Arisoy, A. (2008). Effect of mineral matter on coal self-heating rate. *Fuel*, *87*(1), 125–130.

Beamish, B. B., Barakat, M. A., St. George, J. D. (2000). Adiabatic testing procedures for determining the self-heating propensity of coal and sample ageing effects. *Thermochimica Acta*, *362*(1–2), 79–87. https://doi.org/10.1016/S0040-6031(00)00588-8

Beamish, B. B., Lau, A. G., Moodie, A. L., Vallance, T. A. (2002). Assessing the self-heating behaviour of Callide coal using a 2-metre column. *Journal of Loss Prevention in the Process Industries*, *15*(5), 385–390. https://doi.org/10.1016/S0950-4230(02)00020-7

Bell, F. G., Bullock, S. E. T., Hälbich, T. F. J., Lindsay, P. (2001). Environmental

impacts associated with an abandoned mine in the Withbank Coalfield, South Africa. *International Journal of Coal Geology*, *45*(2–3), 195–216. https://doi.org/10.1016/S0166-5162(00)00033-1

Bowes, P. C. (1984). Self-heating: Evaluating and controlling the hazards. *Elsevier, Amsterdam*, 373.

Bowes, P. C., Cameron, A. (2007). Self-heating and ignition of chemically activated carbon. *Journal of Applied Chemistry and Biotechnology*, *21*(9), 244–250. https://doi.org/10.1002/jctb.5020210902

British Petroleum Company. (2019). BP Statistical Review of World Energy Statistical Review of World. In *The Editor BP Statistical Review of World Energy*. https://www.bp.com/content/dam/bp/business-sites/en/global/corporate/pdfs/energy-economics/statistical-review/bp-stats-review-2019-full-report.pdf

Brooks, K., Glasser, D. (1986). A simplified model of spontaneous combustion in coal stockpiles. *Fuel*, *65*(8), 1035–1041. https://doi.org/10.1016/0016-2361(86)90163-8

Calderone, J., Insider, T. (2016). *This small town might burn for 250 years*. Business Insider; Business Insider. https://www.businessinsider.com/centralia-town-on-fire-since-1962-2016-4

Carras, J. N., Day, S. J., Saghafi, A., Williams, D. J. (2009). Greenhouse gas emissions from low-temperature oxidation and spontaneous combustion at open-cut coal mines in Australia. *International Journal of Coal Geology*, *78*(2), 161–168.

Chakravorty, R. N., Kar, K. L. (1986). *Characterization of western Canadian coals with respect to their susceptibility to spontaneous combustion*. Canada Centre for Mineral and Energy Technology.

Chandralal, N., Mahapatra, D., Shome, D., Dasgupta, P. (2014). Behaviour of low rank high moisture coal in large stockpile under ambient conditions. *American International Hournal of Reserach in Formal, Applied & Natural Sciences*,

6(1), 19–26.

Chanuvin, R., Lodel, R., Philippe, J. (1985). Spontaneous combustion of Coal. *Proceedings of the 21 St Safety In Mines Testing and Research Institutes*, 465–473.

Chen, H., Qi, H., Long, R., Zhang, M. (2012). Research on 10-year tendency of China coal mine accidents and the characteristics of human factors. *Safety Science*, *50*(4), 745–750. https://doi.org/10.1016/j.ssci.2011.08.040

Chen, X. D. (1999). On basket heating methods for obtaining exothermic reactivity of solid materials: The extent and impact of the departure of the crossing-point temperature from the oven temperature. *Process Safety and Environmental Protection*, *77*(4), 187–192. https://doi.org/10.1205/095758299530053

Chen, X. D., Chong, L. V. (1998). Several important issues related to the crossing-point temperature (CPT) method for measuring self-ignition kinetics of combustible solids. *Process Safety and Environmental Protection*, *76*(2), 90–93. https://doi.org/10.1205/095758298529380

Choi, H., Jo, W., Kim, S., Yoo, J., Chun, D., Rhim, Y., Lim, J., Lee, S. (2014). Comparison of spontaneous combustion susceptibility of coal dried by different processes from low-rank coal. *Korean Journal of Chemical Engineering*, *31*(12), 2151–2156. https://doi.org/10.1007/s11814-014-0174-4

Choi, H., Thiruppathiraja, C., Kim, S., Rhim, Y., Lim, J., Lee, S. (2011). Moisture readsorption and low temperature oxidation characteristics of upgraded low rank coal. *Fuel Processing Technology*, *92*(10), 2005–2010.

Chu, T., Yu, M., Jiang, D. (2017). Experimental investigation on the permeability evolution of compacted broken coal. *Transport in Porous Media*, *116*(2), 847–868.

Clemens, A. H., Matheson, T. W., Rogers, D. E. (1991). Low temperature oxidation studies of dried New Zealand coals. *Fuel*, *70*(2), 215–221.

Cliff, D., Davis, R., Bennett, T., Galvin, G., Clarksosn, F. (1998). *large scale laboratory testing of the spontaneous combustibility of wustralian coals.pdf*.

Coates, D. A., Heffern, E. L., Naeser, C. W., Reiners, P. (2005). Coal bed fires—a long history of burning and change in the Northern Great Plains. *Proceedings of the International Conference on Coal Fire Research*, *29*(01.12), 2005.

Colaizzi, G. J. (2004). Prevention, control and/or extinguishment of coal seam fires using cellular grout. *International Journal of Coal Geology*, *59*(1–2), 75–81.

Committee of Experts on the Transport of Dangerous, United Nations, Recommendations on the transport of dangerous goods: manual of tests and criteria 361 (2009). https://doi.org/10.1177/019263653301704705

Cook, A. P., Lloyd, P. J. D. (2012). The estimation of greenhouse gas emissions from South African surface and abandoned coal mines. *Journal of the Southern African Institute of Mining and Metallurgy*, *112*(12), 1087–1090.

Davis, J. D., Byrne, J. F. (1924). An Adiabatic Method for Studying Spontaneous Heating of Coal. *Journal of the American Ceramic Society*, *7*(11), 809–816.

Day, S. J., Carras, J. N., Fry, R., Williams, D. J. (2010). Greenhouse gas emissions from Australian open-cut coal mines: contribution from spontaneous combustion and low-temperature oxidation. *Environmental Monitoring and Assessment*, *166*(1–4), 529–541.

Deng, J., Ma, X., Zhang, Y., Li, Y., Zhu, W. (2015). Effects of pyrite on the spontaneous combustion of coal. *International Journal of Coal Science & Technology*, *2*(4), 306–311.

Deng, J., Xiao, Y., Li, Q., Lu, J., Wen, H. (2015). Experimental studies of spontaneous combustion and anaerobic cooling of coal. *Fuel*, *157*, 261–269. https://doi.org/10.1016/j.fuel.2015.04.063

Deng, J., Yang, Y., Zhang, Y.-N., Liu, B., Shu, C.-M. (2018). Inhibiting effects of three commercial inhibitors in spontaneous coal combustion. *Energy*, *160*, 1174–1185.

Department of the Environment and Energy, A. G. (2019). *National Inventory Report 2017 Table of Contents* (Vol. 3).

Ejlali, A., Aminossadati, S. M., Hooman, K., Beamish, B. B. (2009). A new criterion

to design reactive coal stockpiles. *International Communications in Heat and Mass Transfer*, *36*(7), 669–673. https://doi.org/10.1016/j.icheatmasstransfer.2009.04.005

Ejlali, A., Mee, D. J., Hooman, K., Beamish, B. B. (2011). Numerical modelling of the self-heating process of a wet porous medium. *International Journal of Heat and Mass Transfer*, *54*(25–26), 5200–5206. https://doi.org/10.1016/j.ijheatmasstransfer.2011.08.025

Ellyett, C. D., Fleming, A. W. (1974). Thermal infrared imagery of The Burning Mountain coal fire. *Remote Sensing of Environment*, *3*(1), 79–86. https://doi.org/10.1016/0034-4257(74)90040-6

Engle, M. A., Radke, L. F., Heffern, E. L., O'Keefe, J. M. K., Hower, J. C., Smeltzer, C. D., Hower, J. M., Olea, R. A., Eatwell, R. J., Blake, D. R., Emsbo-Mattingly, S. D., Stout, S. A., Queen, G., Aggen, K. L., Kolker, A., Prakash, A., Henke, K. R., Stracher, G. B., Schroeder, P. A., … ter Schure, A. (2012). Gas emissions, minerals, and tars associated with three coal fires, Powder River Basin, USA. *Science of the Total Environment*, *420*, 146–159. https://doi.org/10.1016/j.scitotenv.2012.01.037

Engle, M. A., Radke, L. F., Heffern, E. L., O'Keefe, J. M. K., Smeltzer, C. D., Hower, J. C., Hower, J. M., Prakash, A., Kolker, A., Eatwell, R. J., ter Schure, A., Queen, G., Aggen, K. L., Stracher, G. B., Henke, K. R., Olea, R. A., Román-Colón, Y. (2011). Quantifying greenhouse gas emissions from coal fires using airborne and ground-based methods. *International Journal of Coal Geology*, *88*(2–3), 147–151. https://doi.org/10.1016/j.coal.2011.09.003

European committee for standardization. (2007). *Determination of the spontaneous ignition behaviour of dust accumulations* (Vol. 3).

Fan, Y. J., Zhao, Y. Y., Hu, X. M., Wu, M. Y., Xue, D. (2020). A novel fire prevention and control plastogel to inhibit spontaneous combustion of coal: Its characteristics and engineering applications. *Fuel*, *263*, 116693.

Fierro, V., Miranda, J. L., Romero, C., Andres, J. M., Arriaga, A., Schmal, D.

(2001). Model predictions and experimental results on self-heating prevention of stockpiled coals. *Fuel*, *80*(1), 125–134.

Fierro, V., Miranda, J. L., Romero, C., Andrés, J. M., Arriaga, A., Schmal, D., Visser, G. H. (1999). Prevention of spontaneous combustion in coal stockpiles. Experimental results in coal storage yard. *Fuel Processing Technology*, *59*(1), 23–34. https://doi.org/10.1016/S0378-3820(99)00005-3

Frank-Kamenetskii, D. A. (2015). *Diffusion and heat exchange in chemical kinetics*. Princeton University Press.

García-Torrent, J., Ramírez-Gómez, Á., Querol-Aragón, E., Grima-Olmedo, C., Medic-Pejic, L. (2012). Determination of the risk of self-ignition of coals and biomass materials. *Journal of Hazardous Materials*, *213*, 230–235.

Gaveau, D. L. A., Salim, M. A., Hergoualc'H, K., Locatelli, B., Sloan, S., Wooster, M., Marlier, M. E., Molidena, E., Yaen, H., DeFries, R., Verchot, L., Murdiyarso, D., Nasi, R., Holmgren, P., Sheil, D. (2014). Major atmospheric emissions from peat fires in Southeast Asia during non-drought years: Evidence from the 2013 Sumatran fires. *Scientific Reports*, *4*, 1–7. https://doi.org/10.1038/srep06112

Gervet, B. (2007). Coal Fire Emission Contributes to Global Warming. *Renewable Energy Research Group, Division of Architecture and Infrastructure, Luleå University of Technology*, *March*.

Ghani, M. J., Rajoka, M. I., Akhtar, K. (2015). Investigations in fungal solubilization of coal: Mechanisms and significance. *Biotechnology and Bioprocess Engineering*, *20*(4), 634–642. https://doi.org/10.1007/s12257-015-0162-5

Ghosh, A. K., Banerjee, B. D. (1967). Use of the Carbon-Hydrogen Ratio as an Index in the Investigation of Explosions and Underground Fires. *Journal of Mines, Metals & Fuels*, *15*(11), 334–340.

Gielisch, H., Kropp, C. (2018). Coal Fires a major Source of Greenhouse Gases- a forgotten problem. *Environmental Risk Assessment and Remediation*, *02*(01), 1–4. https://doi.org/10.4066/2529-8046.100030

Graham, J. I. (1920). The normal production of carbon monoxide in coal-mines. *Transaction Institution of Mining Engineers*, *60*, 1920–1921.

Guideline, V. D. I. (1992). VDI 2263: Dust fires and dust explosions; hazards, assessment, protective measures;inerting. *Beuth, Berlin Und Köln*.

Hamilton, M. S., Miller, R. O., Whitehouse, A. (2000). Continuing fire threat in Southeast Asia. *Environmental Science and Technology*, *34*(3), 1–4. https://doi.org/10.1021/es0031366

Hausfather, Z. (2019). *Analysis: Global fossil-fuel emissions up 0.6% in 2019 due to China*. Carbon Brief; Carbon Brief. https://www.carbonbrief.org/analysis-global-fossil-fuel-emissions-up-zero-point-six-per-cent-in-2019-due-to-china

Hayward, D., Trapnell, B. (1964). Chemisorption. In *Butterworths, London* (Vol. 1).

Heffern, E. L., Coates, D. A. (2004). Geologic history of natural coal-bed fires, Powder River basin, USA. *International Journal of Coal Geology*, *59*(1–2), 25–47. https://doi.org/10.1016/j.coal.2003.07.002

Henao, M., Antonio, J., Carreño, P., María, A., Quintero, D., Alexander, J., Candela, H., Angel, S., Ríos, R., Alberto, C. (2010). Petrography and application of the Rietveld method to the quantitative analysis of phases of natural clinker generated by coal spontaneous combustion. *Earth Sciences Research Journal*, *14*(1), 17–30.

Hill, C. R. (1986). *Particle size and moisture effects o the low-temperature oxidation of coal*. http://wiredspace.wits.ac.za/bitstream/handle/10539/16784/Hill Cavan Raymond 1986-001.pdf?sequence=1

Hongqing, Z., Xingkui, L. (2012). Theoretical investigation on the relationship between tail roadway methane drainage and distribution of easily spontaneous combustible region in gob. *Safety Science*, *50*(4), 618–623. https://doi.org/10.1016/j.ssci.2011.09.002

Hooman, K., Maas, U. (2014). Theoretical analysis of coal stockpile self-heating. *Fire Safety Journal*, *67*, 107–112.

Huang, Z., Sun, C., Gao, Y., Ji, Y., Wang, H., Zhang, Y., Yang, R. (2018). R&D of

colloid components of composite material for fire prevention and extinguishing and an investigation of its performance. *Process Safety and Environmental Protection*, *113*, 357–368.

Hull, A. S., Lanthier, J. L., Chen, Z., Agarwal, P. K. (1997). The role of the diffusion of oxygen and radiation on the spontaneous combustibility of a coal pile in confined storage. *Combustion and Flame*, *110*(4), 479–493.

Humphreys, D. R. (1979). *A study of the propensity of Queensland coals to spontaneous combustion.*

Ide, S. T., Orr, F. M. (2011). Comparison of methods to estimate the rate of CO2 emissions and coal consumption from a coal fire near Durango, CO. *International Journal of Coal Geology*, *86*(1), 95–107. https://doi.org/10.1016/j.coal.2010.12.005

International Energy Agency. (2019). *World Energy Outlook 2019*. https://webstore.iea.org/download/summary/2467?fileName=Japanese-Summary-WEO2019.pdf

Janès, A., Vignes, A., Dufaud, O. (2019). Ignition temperatures of dust layers and bulk storages in hot environments. *Journal of Loss Prevention in the Process Industries*, *59*, 106–117. https://doi.org/10.1016/j.jlp.2018.12.005

Jingcai, X., Lingmei, G., Dunliang, H. (1989). Study on the spontaneous combustion process of coal at low temperature. *Mining Safety & Environmental Protection*, *5*, 17–21.

Jo, W., Choi, H., Kim, S., Yoo, J., Chun, D., Rhim, Y., Lim, J., Lee, S. (2013). A comparison of spontaneous combustion susceptibility of coal according to its rank. *Korean Journal of Chemical Engineering*, *30*(5), 1034–1038.

Jones, J. C. (1999). Calculation of the Frank-Kamenetskii critical parameter for a cubic reactant shape from experimental results on bituminous coals. *Fuel*, *78*(1), 89–91. https://doi.org/10.1016/S0016-2361(98)00116-1

Jones, J. C. (2000). A new and more reliable test for the propensity of coals and carbons to spontaneous heating. *Journal of Loss Prevention in the Process*

Industries, *13*(1), 69–71. https://doi.org/10.1016/S0950-4230(99)00055-8

Jones, J. C. (2006). A new test for spontaneous combustion propensity utilising microcalorimetry. *Applications Note*, *22026*.

Jones, J. C., Chiz, P. S., Koh, R., Matthew, J. (1996). Kinetic parameters of oxidation of bituminous coals from heat-release rate measurements. *Fuel*, *75*(15), 1755–1757.

Jones, J. C., Cook, B. (2000). Towards an alternative criterion for the shipping safety of activated carbons : Part 5. Reproducibility checks. *Journal of Loss Prevention in the Process Industries*, *13*(2), 175–176. https://doi.org/10.1016/S0950-4230(99)00078-9

Jones, J. C., Vais, M. (1991). Factors influencing the spontaneous heating of low-rank coals. *Journal of Hazardous Materials*, *26*(2), 203–212. https://doi.org/10.1016/0304-3894(91)80005-9

Josh G. (2020). *Coal mines emit more methane than oil-and-gas sector, study finds*. Carbon Brief; Carbon Brief. https://www.carbonbrief.org/coal-mines-emit-more-methane-than-oil-and-gas-sector-study-finds

Junice, D. U., Masek, O., Abass, O. (2014). Determination of Spontaneous Ignition Behaviour of Biochar Accumulations. *International Journal of Science and Research*, *3*(8), 656–661.

Kaji, R., Hishinuma, Y., Nakamura, Y. (1987). Low temperature oxidation of coals—a calorimetric study. *Fuel*, *66*(2), 154–157.

Kaji, R., Muranaka, Y., Otsuka, K., Hishinuma, Y. (1986). Water absorption by coals: effects of pore structure and surface oxygen. *Fuel*, *65*(2), 288–291. https://doi.org/10.1016/0016-2361(86)90023-2

Kane, S. N., Mishra, A., Dutta, A. K. (2016). Greenhouse gas and air pollutant emissions from land and forest fire in Indonesia during 2015 based on satellite data. *Journal of Physics: Conference Series*, *755*(1). https://doi.org/10.1088/1742-6596/755/1/011001

Karsner, G. G., Perlmutter, D. D. (1982). Model for coal oxidation kinetics. 1.

Reaction under chemical control. *Fuel*, *61*(1), 29–34. https://doi.org/10.1016/0016-2361(82)90289-7

Kholod, N., Evans, M., Pilcher, R. C., Roshchanka, V., Ruiz, F., Coté, M., Collings, R. (2020). Global methane emissions from coal mining to continue growing even with declining coal production. *Journal of Cleaner Production*, *256*(February), 120489. https://doi.org/10.1016/j.jclepro.2020.120489

Kim, C. J., Sohn, C. H. (2016). Effects of wind barrier design and closed coal storage on spontaneous ignition of coal stockpiles. *Journal of Loss Prevention in the Process Industries*, *40*, 529–536.

Kök, M. V. (2008). Recent developments in the application of thermal analysis techniques in fossil fuels. *Journal of Thermal Analysis and Calorimetry*, *91*(3), 763–773.

Kong, B., Li, Z., Wang, E., Lu, W., Chen, L., Qi, G. (2018). An experimental study for characterization the process of coal oxidation and spontaneous combustion by electromagnetic radiation technique. *Process Safety and Environmental Protection*, *119*, 285–294. https://doi.org/10.1016/j.psep.2018.08.002

Krajčiová, M., Jelemenský, L., Kiša, M., Markoš, J. (2004). Model predictions on self-heating and prevention of stockpiled coals. *Journal of Loss Prevention in the Process Industries*, *17*(3), 205–216. https://doi.org/10.1016/j.jlp.2004.02.002

Krishnaswamy, S., Agarwal, P. K., Gunn, R. D. (1996). Low-temperature oxidation of coal. 3. Modelling spontaneous combustion in coal stockpiles. *Fuel*, *75*(3), 353–362.

Krishnaswamy, S., Gunn, R. D., Agarwal, P. K. (1996). Low-temperature oxidation of coal. 2. An experimental and modelling investigation using a fixed-bed isothermal flow reactor. *Fuel*, *75*(3), 344–352.

Kuchta, J. M., Furno, A. L., Dalverny, L. E., Sapko, M. J., Litton, C. D. (1982). *Diagnostics of sealed coal mine fires. Report of investigations*. Bureau of Mines, Pittsburgh, PA (USA). Pittsburgh Research Center.

Kuchta, J. M., Rowe, V. R., Burgess, D. S. (1980). *Spontaneous combustion susceptibility of US coals* (Vol. 8474). US Dept. of the Interior, Bureau of Mines.

Küçük, A., Kadioğlu, Y., Gülaboğlu, M. Ş. (2003). A study of spontaneous combustion characteristics of a Turkish lignite: Particle size, moisture of coal, humidity of air. *Combustion and Flame*, *133*(3), 255–261. https://doi.org/10.1016/S0010-2180(02)00553-9

Kuenzer, C., Stracher, G. B. (2012). Geomorphology of coal seam fires. *Geomorphology*, *138*(1), 209–222. https://doi.org/10.1016/j.geomorph.2011.09.004

Kuenzer, C., Wessling, S., Zhang, J., Litschke, T., Schmidt, M., Schulz, J., Gielisch, H., Wagner, W. (2007). Concepts for green house gas emission estimating of underground coal seam fires. *Geophysical Research Abstracts*, *9*, 11716.

Kuenzer, C., Zhang, J., Li, J., Voigt, S., Mehl, H., Wagner, W. (2007). Detecting unknown coal fires: Synergy of automated coal fire risk area delineation and improved thermal anomaly extraction. *International Journal of Remote Sensing*, *28*(20), 4561–4585. https://doi.org/10.1080/01431160701250432

Kuenzer, C., Zhang, J., Tetzlaff, A., van Dijk, P., Voigt, S., Mehl, H., Wagner, W. (2007). Uncontrolled coal fires and their environmental impacts: Investigating two arid mining regions in north-central China. *Applied Geography*, *27*(1), 42–62. https://doi.org/10.1016/j.apgeog.2006.09.007

Kus, J. (2017). Impact of underground coal fire on coal petrographic properties of high volatile bituminous coals: A case study from coal fire zone No. 3.2 in the Wuda Coalfield, Inner Mongolia Autonomous Region, North China. *International Journal of Coal Geology*, *171*, 185–211. https://doi.org/10.1016/j.coal.2016.12.002

Lacey, A. A., Wake, G. C. (1983). Exothermic systems with diminishing reaction rates: Mathematical analysis. *Combustion and Flame*, *50*(C), 19–27. https://doi.org/10.1016/0010-2180(83)90045-7

Le, T. T. (2018). *Study on Susceptibility to Spontaneous Combustion of Anthracite in Vietnamese Coal Mine*.

Li, B., Chen, G., Zhang, H., Sheng, C. (2014). Development of non-isothermal TGA-DSC for kinetics analysis of low temperature coal oxidation prior to ignition. *Fuel*, *118*, 385–391. https://doi.org/10.1016/j.fuel.2013.11.011

Li, B., Li, M., Gao, W., Bi, M., Ma, L., Qin, Q., Shu, C. M. (2020). Effects of particle size on the self-ignition behaviour of a coal dust layer on a hot plate. *Fuel*, *260*(September 2019). https://doi.org/10.1016/j.fuel.2019.116269

Li, J., Li, Z., Yang, Y., Zhang, X. (2019). Study on the generation of active sites during low-temperature pyrolysis of coal and its influence on coal spontaneous combustion. *Fuel*, *241*(December 2018), 283–296. https://doi.org/10.1016/j.fuel.2018.12.034

Li, X. R., Lim, W. S., Iwata, Y., Koseki, H. (2009). Thermal characteristics and their relevance to spontaneous ignition of refuse plastics/paper fuel. *Journal of Loss Prevention in the Process Industries*, *22*(1), 1–6.

Li, Z. H., Wang, Y. L., Song, N., Yang, Y. L., Yang, Y. J. (2009). Experiment study of model compound oxidation on spontaneous combustion of coal. *Procedia Earth and Planetary Science*, *1*(1), 123–129. https://doi.org/10.1016/j.proeps.2009.09.021

Li, Z., Zhang, Y., Jing, X., Zhang, Y., Chang, L. (2016). Insight into the intrinsic reaction of brown coal oxidation at low temperature: Differential scanning calorimetry study. *Fuel Processing Technology*, *147*, 64–70. https://doi.org/10.1016/j.fuproc.2015.07.030

Liang, Y., Liang, H., Zhu, S. (2014). Mercury emission from coal seam fire at Wuda, Inner Mongolia, China. *Atmospheric Environment*, *83*, 176–184.

Lienhard, J. H. (2011). *A heat transfer textbook*. Courier Corporation.

Liu, J., Chen, W. S., Qi, Q. J. (2005). Study on the spontaneous combustion tendency of coal based on activation energy index. *Journal of the China Coal Society*, *30*(1), 67–70.

Liu, L., Zhou, F. B. (2010). A comprehensive hazard evaluation system for spontaneous combustion of coal in underground mining. *International Journal of Coal Geology*, *82*(1–2), 27–36. https://doi.org/10.1016/j.coal.2010.01.014

Liu, W., Qin, Y. (2017). Multi-physics coupling model of coal spontaneous combustion in longwall gob area based on moving coordinates. *Fuel*, *188*, 553–566.

Liu, Y., Zhang, L., Li, W., Sang, C., Wang, E. (2017). Air-flowing field and gas-concentration field of the coal left in goaf based on the moving coordinate. *Journal of Liaoning Technical University*, *36*(3), 243–248. https://doi.org/10.11956/j.issn.1008-0562.2017.03.004

Liu, Z., Zhang, Z., Choi, S. K., Lu, Y. (2018). Surface properties and pore structure of anthracite, bituminous coal and lignite. *Energies*, *11*(6), 1502.

Long, W., Hanxu, L. (2016). New Method for Judging Tendency of Coal Spontaneous Combustion Based on Pyrolysis Activation Energy. *Coal Technology*, *35*(4), 174–176. https://doi.org/10.13301/j.cnki.ct.2016.04.071

Lu, P., Liao, G. X., Sun, J. H., Li, P. D. (2004). Experimental research on index gas of the coal spontaneous at low-temperature stage. *Journal of Loss Prevention in the Process Industries*, *17*(3), 243–247.

Lu, W., Wang, D. M., Zhong, X. X., Zhou, F. B. (2006). Tendency of spontaneous combustion of coal based on activation energy. *Journal of China University of Mining and Technology*, *35*(2), 201–205.

Lu, X., Liao, J., Mo, Q., Wen, Y., Bao, W., Chang, L. (2019). Evolution of Pore Structure during Pressurized Dewatering and Effects on Moisture Readsorption of Lignite. *ACS Omega*, *4*(4), 7113–7121.

Luo, Y., Wang, X. Y. (2012). *A mathematical model of R 70 self-heating test for the propensity of coal spontaneous combustion*. *March*, 407–414.

Marfin, Y. S., Vashurin, A. S., Rumyantsev, E. V, Puhovskaya, S. G. (2013). Sol–gel synthesis of highly effective catalyst based on cobalt tetrasulfophthalocyanine complex and silicon oxide. *Journal of Sol-Gel Science and Technology*, *66*(2),

306–311.

Mason, T., Tideswell, F. (1939). The detection of gob fires. *Transactions of the Institution of Mining Engeneers*, *98*, 1–19.

McManus, J. D., Brown, S. D., Hall, P. J. (1999). The influence of mineral matter on the self heating of coals. *Science and Technology Press*, *1*, 307–310.

Melody, S. M., Johnston, F. H. (2015). Coal mine fires and human health: What do we know? *International Journal of Coal Geology*, *152*, 1–14. https://doi.org/10.1016/J.COAL.2015.11.001

Meng, X., Chu, R., Wu, G., Xu, H., Zhu, J., Wang, Z. (2010). Thermogravimetric study of the effect of a PVA oxygen-insulating barrier on the spontaneous combustion of coal. *Mining Science and Technology*, *20*(6), 882–885. https://doi.org/10.1016/S1674-5264(09)60300-8

Michael, S., Sawyer, D. (2014). *The infrared characterization and mechanism of oxygen adsorption in coal*. Environmental Justice Atlas; Environmental Justice Atlas. https://ejatlas.org/conflict/2014-hazelwood-open-cut-coal-mine-fire

Ministry of Emergency and Management. (n.d.). *Cause analysis and prevention of coal mine gas explosion*. https://www.mem.gov.cn/

Mishra, R. K., Pandey, J. K., Pandey, J., Kumar, S., Roy, P. N. S. (2020). Detection and Analysis of Coal Fire in Jharia Coalfield (JCF) Using Landsat Remote Sensing Data. *Journal of the Indian Society of Remote Sensing*, *48*(2), 181–195.

Mitsumata, T., Kawada, H., Takimoto, J. ichi. (2007). Thermosensitive solutions and gels consisting of poly(vinyl alcohol) and sodium silicate. *Materials Letters*, *61*(18), 3878–3881. https://doi.org/10.1016/j.matlet.2006.12.051

Miura, K. (2016). Adsorption of Water Vapor from Ambient Atmosphere onto Coal Fines Leading to Spontaneous Heating of Coal Stockpile. *Energy and Fuels*, *30*(1), 219–229. https://doi.org/10.1021/acs.energyfuels.5b02324

Miura, K., Ohgaki, H., Sato, N., Matsumoto, M. (2017). Formulation of the Heat Generation Rate of Low-Temperature Oxidation of Coal by Measuring Heat Flow and Weight Change at Constant Temperatures Using Thermogravimetry–

Differential Scanning Calorimetry. *Energy & Fuels*, *31*(11), 11669–11680.

Mohalik, N. K., Lester, E., Lowndes, I. S. (2017). Review of experimental methods to determine spontaneous combustion susceptibility of coal–Indian context. *International Journal of Mining, Reclamation and Environment*, *31*(5), 301–332. https://doi.org/10.1080/17480930.2016.1232334

Mohalik, N. K., Lester, E., Lowndes, I. S., Singh, V. K. (2016). Estimation of greenhouse gas emissions from spontaneous combustion/fire of coal in opencast mines–Indian context. *Carbon Management*, *7*(5–6), 317–332. https://doi.org/10.1080/17583004.2016.1249216

Muangthong-On, T., Wannapeera, J., Ohgaki, H., Miura, K. (2017). TG-DSC Study to Measure Heat of Desorption of Water during the Thermal Drying of Coal and to Examine the Role of Adsorption of Water Vapor for Examining Spontaneous Heating of Coal over 100 °C. *Energy and Fuels*, *31*(10), 10691–10698. https://doi.org/10.1021/acs.energyfuels.7b01836

Namah, M. (2016). *jharia-fire-nh*. Indian Travel & Toursm. http://www.musafirnamah.com/jharia-fire-zone-tourist-site/jharia-fire-nh/#.XogXwkgzYdU

Nelson, M. I., Chen, X. D. (2007). Survey of experimental work on the self-heating and spontaneous combustion of coal. *GSA Reviews in Engineering Geology*, *18*(December), 31–83. https://doi.org/10.1130/2007.4118(04)

Nimaje, D. S., Tripathy, D. P. (2016). Characterization of some Indian coals to assess their liability to spontaneous combustion. *Fuel*, *163*, 139–147. https://doi.org/10.1016/j.fuel.2015.09.041

Niu, H. Y., Zhang, X. H. (2007). Research on the coal self-ignition and prevention techniques classification. *Industrial Safety and Dust Control*, *33*(1), 45–48.

Nolter, M. A., Vice, D. H. (2004). Looking back at the Centralia coal fire: A synopsis of its present status. *International Journal of Coal Geology*, *59*(1–2), 99–106. https://doi.org/10.1016/j.coal.2003.12.008

Nordon, P. (1979). A model for the self-heating reaction of coal and char. *Fuel*,

58(6), 456–464.

Nordon, P., Young, B. C., Bainbridge, N. W. (1979). The rate of oxidation of char and coal in relation to their tendency to self-heat. *Fuel*, *58*(6), 443–449.

O'Keefe, J. M. K., Henke, K. R., Hower, J. C., Engle, M. A., Stracher, G. B., Stucker, J. D., Drew, J. W., Staggs, W. D., Murray, T. M., Hammond, M. L., Adkins, K. D., Mullins, B. J., Lemley, E. W. (2010). CO2, CO, and Hg emissions from the Truman Shepherd and Ruth Mullins coal fires, eastern Kentucky, USA. *Science of the Total Environment*, *408*(7), 1628–1633. https://doi.org/10.1016/j.scitotenv.2009.12.005

O'Keefe, J. M. K., Neace, E. R., Lemley, E. W., Hower, J. C., Henke, K. R., Copley, G., Hatch, R. S., Satterwhite, A. B., Blake, D. R. (2011). Old Smokey coal fire, Floyd County, Kentucky: estimates of gaseous emission rates. *International Journal of Coal Geology*, *87*(2), 150–156.

OCDE. (2019). *Coal Information 2019*.

Office of Surface Ming Reclamation and enforcement. (2017). *Mine Fires and Burning Refuse*. Office of Sueface Ming Reclamation and enforcement. https://www.osmre.gov/programs/tdt/mineFires.shtm

Ogunsola, O. I., Mikula, R. J. (1991). A study of spontaneous combustion characteristics of Nigerian coals. *Fuel*, *70*(2), 258–261. https://doi.org/10.1016/0016-2361(91)90162-4

Onifade, M., Genc, B. (2019). A review of spontaneous combustion studies–South African context. *International Journal of Mining, Reclamation and Environment*, *33*(8), 527–547. https://doi.org/10.1080/17480930.2018.1466402

Onifade, M., Genc, B., Carpede, A. (2018). A new apparatus to establish the spontaneous combustion propensity of coals and coal-shales. *International Journal of Mining Science and Technology*, *28*(4), 649–655. https://doi.org/10.1016/j.ijmst.2018.05.012

Oyj, V. (2013). humidity conversion formulas-Calculation formulas for humidity. *Humidity Conversion Formulas*.

Ozdeniz, A. H. (2010). Determination of spontaneous combustion in industrial-scale coal stockpiles. *Energy Sources, Part A: Recovery, Utilization and Environmental Effects*, *32*(7), 665–673. https://doi.org/10.1080/15567030802606129

Page, S. E., Siegert, F., Rieley, J. O., Boehm, H. D. V., Jaya, A., Limin, S. (2002). The amount of carbon released from peat and forest fires in Indonesia during 1997. *Nature*, *420*(6911), 61–65. https://doi.org/10.1038/nature01131

Pan, R., Yu, M., Lu, L. (2009). Experimental study on explosive mechanism of spontaneous combustion gangue dump. *Journal of Coal Science and Engineering (China)*, *15*(4), 394.

Pandey, B., Agrawal, M., Singh, S. (2014). Assessment of air pollution around coal mining area: Emphasizing on spatial distributions, seasonal variations and heavy metals, using cluster and principal component analysis. *Atmospheric Pollution Research*, *5*(1), 79–86. https://doi.org/10.5094/APR.2014.010

Pandey, J., Kumar, D., Mishra, R. K., Mohalik, N. K., Khalkho, A., Singh, V. K. (2013). Application of Thermography Technique for Assessment and Monitoring of Coal Mine Fire: A Special Reference to Jharia Coal Field, Jharkhand, India. *International Journal of Advanced Remote Sensing and GIS*, *1*(1), 138–147.

Panigrahi, D. C., Ojha, A., Saxena, N. C., Kejriwal, B. K. (1997). A study of coal oxygen interaction by using russian U-index and its correlation with basic constituents of coal with particular reference to Jharia Coalfield. *New Delhi, India*, *1*, 493–499.

Panigrahi, D. C., Sahu, H. B. (2004). Classification of coal seams with respect to their spontaneous heating susceptibility - A neural network approach. *Geotechnical and Geological Engineering*, *22*(4), 457–476. https://doi.org/10.1023/B:GEGE.0000047040.70764.90

Parsa, M. R., Tsukasaki, Y., Perkins, E. L., Chaffee, A. L. (2017). The effect of densification on brown coal physical properties and its spontaneous combustion

propensity. *Fuel*, *193*, 54–64. https://doi.org/10.1016/j.fuel.2016.12.016

Pennsylvania Department of Environmental Protection. (2019). *the Centralia Mine Fire Frequently Asked Questions/Answers*. http://files.dep.state.pa.us/Mining/Abandoned Mine Reclamation/AbandonedMinePortalFiles/Centralia/CentraliaFrequentlyAskedQuestions.pdf#nameddest=C

Pingan, H., Mengjun, J., Yanyan, Z., Ling, H. (2017). A silica/PVA adhesive hybrid material with high transparency, thermostability and mechanical strength. *RSC Advances*, *7*(5), 2450–2459.

Pone, D. N., Hein, K. A., Stracher, G. B., Finkelman, R. B., Annegarn, H. J. (2008). Potential environmental and health impacts of burning coal in Witbank Coalfield, South Africa. In *Spontaneous Coal Seam Fires: Mitigating a Global Disaster* (Vol. 4, pp. 94–102). UNESCO Beijing.

Praveen, B., Gupta, D. (2017). *Multispectral-TIR Data Analysis by Split Window Algorithm for Coal Fire Detection and Monitoring*. *6*(4), 33–37. www.ijhssi.org

Protection, P. D. of E. (2008). *Pennsylvania Mine Fire Locations*. http://files.dep.state.pa.us/Mining/Abandoned Mine Reclamation/AbandonedMinePortalFiles/Centralia/PAFireLocationMap.pdf

Qi, Y. M., Qian, G. Y. (1996). Method for identifying tendency of coal to spontaneous combustion by oxygen absorption with chromatograph. *Coal*, *2*, 5–9.

Qin, B., Dou, G., Wang, Y., Xin, H., Ma, L., Wang, D. (2017). A superabsorbent hydrogel–ascorbic acid composite inhibitor for the suppression of coal oxidation. *Fuel*, *190*, 129–135.

Qin, B., Li, L., Ma, D., Lu, Y., Zhong, X., Jia, Y. (2016). Control technology for the avoidance of the simultaneous occurrence of a methane explosion and spontaneous coal combustion in a coal mine: a case study. *Process Safety and Environmental Protection*, *103*, 203–211.

Rahi, A. (2019). *Photos: Indian coal mines still burning after a century*. Safety

Science; Wtop news. https://wtop.com/asia/2019/11/ap-photos-indian-coal-mines-still-burning-after-a-century/

Ray, S. K., Panigrahi, D. C., Udayabhanu, G., Saxena, V. K. (2016). Assessment of spontaneous heating susceptibility of Indian coals—A new approach. *Energy Sources, Part a: Recovery, Utilization, and Environmental Effects*, *38*(1), 59–68.

Ren, X., Hu, X., Xue, D., Li, Y., Shao, Z., Dong, H., Cheng, W., Zhao, Y., Xin, L., Lu, W. (2019). Novel sodium silicate/polymer composite gels for the prevention of spontaneous combustion of coal. *Journal of Hazardous Materials*, *371*, 643–654.

Ren, X. W., Wang, F. Z., Guo, Q., Zuo, Z. B., Fang, Q. S. (2015). Application of foam-gel technique to control CO exposure generated during spontaneous combustion of coal in coal mines. *Journal of Occupational and Environmental Hygiene*, *12*(11), D239–D245.

Resilience Australian Disaster. (2014). *Bushfire-Hazelwood open cut mine fire, Morwell*. https://doi.org/10.1016/S0031-0182(00)00194-2

Restuccia, F., Ptak, N., Rein, G. (2017). Self-heating behavior and ignition of shale rock. *Combustion and Flame*, *176*, 213–219.

Russian Technical Standard Association. (1997). *Method for evaluation of coal susceptibility to spontaneous combustion*.

Saffari, A., Sereshki, F., Ataei, M. (2019). A comprehensive study of effect of maceral content on tendency of spontaneous coal combustion occurrence. *Journal of the Institution of Engineers (India): Series D*, *100*(1), 1–13.

Saffari, A., Sereshki, F., Ataei, M., Ghanbari, K. (2017). Presenting an engineering classification system for coal spontaneous combustion potential. *International Journal of Coal Science and Technology*, *4*(2), 110–128. https://doi.org/10.1007/s40789-017-0160-7

Saleh, M., Muharram, Y., Nugroho, Y. S. (2017). Modeling of the Crossing Point Temperature Phenomenon in the Low-temperature Oxidation of Coal.

International Journal of Technology, *8*(1), 102–111.

Salinger, A. G., Aris, R., Derby, J. J. (1994). Modeling the spontaneous ignition of coal stockpiles. *AIChE Journal*, *40*(6), 991–1004. https://doi.org/10.1002/aic.690400610

Sáowik, S. (2008). Classification of coal with respect to its spontaneous ignition susceptibility(KLASYFIKACJA WĉGLA POD KĄTEM SKàONNOĝCI DO SAMOZAPALENIA). *Prace Naukowe GIG. Górnictwo*, *1*, 87–94.

Sasaki, K., Miyakoshi, H., Otsuka, K. (1987). Spontaneous combustion of coal in the low temperature range-application of exposure equivalent-time to numerical analysis. *Journal of the Mining and Metallurgical Institute of Japan*, *103*(11), 771–775.

Sasaki, K., Miyakoshi, H., Saitoh, A., Chiba, T. (1992). Water Vapor Adsorption of Coal and Numerical Simulation Related to Its Effect on Spontaneous Combustion in a Low Temperature Range. *Journal of Mining and Materials Processing Institute of Japan*, *108*(6), 479–486.

Sasaki, K., Sugai, Y. (2011). Equivalent oxidation exposure-time for low temperature spontaneous combustion of coal. In *Heat Analysis and Thermodynamic Effects*. InTech.

Schmal, D. (1987). *A model for the spontaneous heating of stored coal* [Technische Universiteit Delft]. https://repository.tudelft.nl/islandora/object/uuid%3A680f83d3-be29-45d1-9e27-a33644f2d9c3

Schmal, D., Duyzer, J. H., van Heuven, J. W. (1985). A model for the spontaneous heating of coal. *Fuel*, *64*(7), 963–972. https://doi.org/10.1016/0016-2361(85)90152-8

Sevenster, P. G. (1961). Studies on the interaction of oxygen with coal in the temperature range 0 ºC to 90 ºC. *Fuel*, *40*(1), 18–32.

Singh, A. K., Singh, R. V. K., Singh, M. P., Chandra, H., Shukla, N. K. (2007). Mine fire gas indices and their application to Indian underground coal mine fires.

International Journal of Coal Geology, *69*(3), 192–204. https://doi.org/10.1016/j.coal.2006.04.004

Skoogfors, L. (2013). *Pictures: Centralia Mine Fire, at 50, Still Burns With Meaning*. National Geographic; National geographic. https://www.nationalgeographic.com/news/energy/2013/01/pictures/130108-centralia-mine-fire/

Sloss, L.L. (2015). Assessing and managing spontaneous combustion of coal. In *IEA Clean Coal Centre* (Issue October). https://www.usea.org/sites/default/files/media/Assessing and managing spontaneous combustion of coal - ccc259_new.pdf

Sloss, Lesley L. (2013). *Quantifying emissions reductions from spontaneous combustion* (Issue September). https://doi.org/10.13140/RG.2.2.16694.24644

Smith, A. C., Miron, Y., Lazzara, C. P. (1988). *Inhibition of spontaneous combustion of coal*.

Smith, A. C., Miron, Y., Lazzara, C. P. (1991). *Large-Scale Studies of Spontaneous Combustion of Coal*. RI 9346.

Sondreal, E. A., Ellman, R. C. (1974). *Laboratory determination of factors affecting storage of North Dakota lignite*. Bureau of Mines, Grand Forks, N. Dak.(USA). Grand Forks Energy Research Lab.

Song, Z. Y., Kuenzer, C. (2014). Coal fires in China over the last decade: A comprehensive review. *International Journal of Coal Geology*, *133*, 72–99. https://doi.org/10.1016/j.coal.2014.09.004

Song, Z. Y., Kuenzer, C., Zhu, H. Q., Zhang, Z., Jia, Y. R., Sun, Y. L., Zhang, J. Z. (2015). Analysis of coal fire dynamics in the Wuda syncline impacted by fire-fighting activities based on in-situ observations and Landsat-8 remote sensing data. *International Journal of Coal Geology*, *141–142*, 91–102. https://doi.org/10.1016/j.coal.2015.03.008

Song, Z. Y., Zhu, H. Q., Tan, B., Wang, H. Y., Qin, X. F. (2014). Numerical study on effects of air leakages from abandoned galleries on hill-side coal fires. *Fire*

Safety Journal, *69*, 99–110.

Springenschmid, R. (1997). TCE1: Adiabatic and semi-adiabatic calorimetry to determine the temperature increase in concrete due to hydration heat of the cement. *Materials and Structures*, *30*(8), 451–464. https://doi.org/10.1007/bf02524773

Stott, J. B. (1980). *The spontaneous heating of coal and the role of moisture transfer*. Department of Chemical Engineering, University of Canterbury.

Stott, J. B., Dong, C. X. (1992). Measuring the tendency of coal to fire spontaneously. *Colliery Guardian*, *240*(1), 9–16.

Stracher, G. B., Nolter, M. A., Schroeder, P., McCormack, J., Blake, D. R., Vice, D. H. (2006). The great Centralia mine fire: A natural laboratory for the study of coal fires. *Excursions in Geology and History: Field Trips in the Middle Atlantic States*, *8*, 33.

Stracher, G. B., Prakash, A., Sokol, E. V. (2014). *Coal and peat fires: a global perspective: volume 3: case studies–coal fires*. Elsevier.

Stracher, G. B., Taylor, T. P. (2004). Coal fires burning out of control around the world: Thermodynamic recipe for environmental catastrophe. *International Journal of Coal Geology*, *59*(1–2), 7–17. https://doi.org/10.1016/j.coal.2003.03.002

Tang, Y., Zhong, X., Li, G., Yang, Z., Shi, G. (2019). Simulation of dynamic temperature evolution in an underground coal fire area based on an optimised Thermal–Hydraulic–Chemical model. *Combustion Theory and Modelling*, *23*(1), 127–146. https://doi.org/10.1080/13647830.2018.1492742

Taraba, B., Michalec, Z. (2011). Effect of longwall face advance rate on spontaneous heating process in the gob area - CFD modelling. *Fuel*, *90*(8), 2790–2797. https://doi.org/10.1016/j.fuel.2011.03.033

Taraba, B., Michalec, Z., Michalcová, V., Blejchař, T., Bojko, M., Kozubková, M. (2014). CFD simulations of the effect of wind on the spontaneous heating of coal stockpiles. *Fuel*, *118*, 107–112. https://doi.org/10.1016/j.fuel.2013.10.064

Taraba, B., Peter, R., Slovák, V. (2011). Calorimetric investigation of chemical additives affecting oxidation of coal at low temperatures. *Fuel Processing Technology*, *92*(3), 712–715.

Tarafdar, M. N., Guha, D. (1989). Application of wet oxidation processes for the assessment of the spontaneous heating of coal. *Fuel*, *68*(3), 315–317. https://doi.org/10.1016/0016-2361(89)90094-X

van Dijk, P., Zhang, J., Jun, W., Kuenzer, C., Wolf, K. H. (2011). Assessment of the contribution of in-situ combustion of coal to greenhouse gas emission; based on a comparison of Chinese mining information to previous remote sensing estimates. *International Journal of Coal Geology*, *86*(1), 108–119. https://doi.org/10.1016/j.coal.2011.01.009

van Genderen, J. L., Haiyan, G. (1997). *Environmental monitoring of spontaneous combustion in the North China coalfields : final report to European Commission*. International Institute for Geo-Information Science and Earth Observation.

Vinogradov, A. V, Kuprin, D. S., Abduragimov, I. M., Kuprin, G. N., Serebriyakov, E., Vinogradov, V. V. (2016). Silica foams for fire prevention and firefighting. *ACS Applied Materials & Interfaces*, *8*(1), 294–301.

Voigt, S., Tetzlaff, A., Zhang, J., Künzer, C., Zhukov, B., Strunz, G., Oertel, D., Roth, A., van Dijk, P., Mehl, H. (2004). Integrating satellite remote sensing techniques for detection and analysis of uncontrolled coal seam fires in North China. *International Journal of Coal Geology*, *59*(1–2), 121–136. https://doi.org/10.1016/j.coal.2003.12.013

Wang, C., Yang, S., Li, J., Li, X., Jiang, C. (2018). Influence of coal moisture on initial gas desorption and gas-release energy characteristics. *Fuel*, *232*(March), 351–361. https://doi.org/10.1016/j.fuel.2018.06.006

Wang, D., Xu-yao, Q., Xiao-xing, Z., Jun-jie, G. (2009). Test method for the propensity of coal to spontaneous combustion. *Procedia Earth and Planetary Science*, *1*(1), 20–26.

Wang, H., Dlugogorski, B. Z., Kennedy, E. M. (2003). Coal oxidation at low temperatures: oxygen consumption, oxidation products, reaction mechanism and kinetic modelling. *Progress in Energy and Combustion Science*, *29*(6), 487–513.

Wang, H. H., Dlugogorski, B. Z., Kennedy, E. M. (2003). Coal oxidation at low temperatures: oxygen consumption, oxidation products, reaction mechanism and kinetic modelling. *Progress in Energy and Combustion Science*, *29*(6), 487–513.

Wang, H. Y., Chen, C. (2015). Experimental Study on Greenhouse Gas Emissions Caused by Spontaneous Coal Combustion. *Energy and Fuels*, *29*(8), 5213–5221. https://doi.org/10.1021/acs.energyfuels.5b00327

Wang, J. R., Deng, C. B., Shan, Y. F., Hong, L., Lu, W. D. (2008). New classifying method of the spontaneous combustion tendency. *Journal of the China Coal Society*, *33*(1), 47–50.

Wang, J. R., Sun, Y. Q., Zhao, Q. F., Deng, C. B., Deng, H. Z. (2008). Basic theory research of coal spontaneous combustion. *Journal of Coal Science and Engineering*, *14*(2), 239–243. https://doi.org/10.1007/s12404-008-0050-0

Wang, J., Zhang, Y., Xue, S., Wu, J., Tang, Y., Chang, L. (2018). Assessment of spontaneous combustion status of coal based on relationships between oxygen consumption and gaseous product emissions. *Fuel Processing Technology*, *179*(March), 60–71. https://doi.org/10.1016/j.fuproc.2018.06.015

Wang, S., Luo, K., Wang, X., Sun, Y. (2016). Estimate of sulfur, arsenic, mercury, fluorine emissions due to spontaneous combustion of coal gangue: An important part of Chinese emission inventories. *Environmental Pollution*, *209*, 107–113. https://doi.org/10.1016/j.envpol.2015.11.026

Wang, X., Luo, Y., Vieira, B. (2018). Experimental technique and modeling for evaluating heat of rewetting effect on coals' propensity of spontaneous combustion based on adiabatic oxidation method. *International Journal of Coal Geology*, *187*(January), 1–10. https://doi.org/10.1016/j.coal.2018.01.002

Wang, Y., Zhang, X., Sugai, Y., Sasaki, K. (2015). A Study on Preventing Spontaneous Combustion of Residual Coal in a Coal Mine Goaf. *Journal of Geological Research, 2015,* 1–8. https://doi.org/10.1155/2015/712349

Wang, Y., Zhang, X., Sugai, Y., Sasaki, K. (2017). Determination of critical self-ignition temperature of low-rank coal using a 1 m wire-mesh basket and extrapolation to industrial coal piles. *Energy & Fuels*, *31*(7), 6700–6710.

Wang, Y., Zhang, X., Zhang, H., Sasaki, K. (2019). Effects of temperature gradient and particle size on self-ignition temperature of low-rank coal excavated from inner Mongolia, China. *Royal Society Open Science*, *6*(9), 190374.

Wen, H., Yu, Z., Deng, J., Zhai, X. (2017). Spontaneous ignition characteristics of coal in a large-scale furnace: An experimental and numerical investigation. *Applied Thermal Engineering*, *114,* 583–592. https://doi.org/10.1016/j.applthermaleng.2016.12.022

Wessling, S., Kuenzer, C., Kessels, W., Wuttke, M. W. (2008). Numerical modeling for analyzing thermal surface anomalies induced by underground coal fires. *International Journal of Coal Geology*, *74*(3–4), 175–184. https://doi.org/10.1016/j.coal.2007.12.005

Wessling, S., Litschke, T., Wiegand, J., Schloemer, S., Kessels, W. (2006). Simulating Dynamic Subsurface Coal Fires and its Applications. *Accepted in: ERSEC Ecological Book Series - 4 on Coal Fire Research, December 2017*, 1–31.

Whitehouse, A. E., Mulyana, A. A. S. (2004). Coal fires in Indonesia. *International Journal of Coal Geology*, *59*(1–2), 91–97. https://doi.org/10.1016/j.coal.2003.08.010

Willet, H. L. (1952). The interpretation of samples from behind stoppings with a view to re-opening. *Transaction of the Institution of Mining Engineers (111),* 629–651.

Williams, D. J., Carras, J. N., Mallett, C., Mark, M., Cooke, D., Randall, C. (1998). Scoping study on the management and abatement of greenhouse gas emissions.

ACARP Project C7050 Final Report.

Wu, D., Norman, F., Schmidt, M., Vanierschot, M., Verplaetsen, F., Berghmans, J., Van den Bulck, E. (2017). Numerical investigation on the self-ignition behaviour of coal dust accumulations: The roles of oxygen, diluent gas and dust volume. *Fuel*, *188*, 500–510.

Wu, D., Vanierschot, M., Verplaetsen, F., Berghmans, J., Van den Bulck, E. (2016). Numerical study on the ignition behavior of coal dust layers in air and O2/CO2 atmospheres. *Applied Thermal Engineering*, *109*, 709–717.

Xi, Z., Wang, X., Wang, X., Wang, L., Li, D., Guo, X., Jin, L. (2019). Self-hardening thermoplastic foam for the inhibition of coal oxidation at low temperatures. *Combustion Science and Technology*, *191*(11), 1942–1959.

Xia, T., Wang, X., Zhou, F., Kang, J., Liu, J., Gao, F. (2015). Evolution of coal self-heating processes in longwall gob areas. *International Journal of Heat and Mass Transfer*, *86*, 861–868. https://doi.org/10.1016/j.ijheatmasstransfer.2015.03.072

Xia, T., Zhou, F., Gao, F., Kang, J., Liu, J., Wang, J. (2015). Simulation of coal self-heating processes in underground methane-rich coal seams. *International Journal of Coal Geology*, *141–142*, 1–12. https://doi.org/10.1016/j.coal.2015.02.007

Xia, T., Zhou, F., Liu, J., Kang, J., Gao, F. (2014). A fully coupled hydro-thermo-mechanical model for the spontaneous combustion of underground coal seams. *Fuel*, *125*, 106–115. https://doi.org/10.1016/j.fuel.2014.02.023

Xia, T., Zhou, F., Wang, X., Kang, J., Pan, Z. (2017). Safety evaluation of combustion-prone longwall mining gobs induced by gas extraction: A simulation study. *Process Safety and Environmental Protection*, *109*, 677–687.

Xia, T., Zhou, F., Wang, X., Zhang, Y., Li, Y., Kang, J., Liu, J. (2016). Controlling factors of symbiotic disaster between coal gas and spontaneous combustion in longwall mining gobs. *Fuel*, *182*, 886–896. https://doi.org/10.1016/j.fuel.2016.05.090

Xiaodong, P. (2014). Measuringanalysisand studyon concomitant disaster of gas and coal spontaneous combustion in goaf. *Coal Technolo- Gy*, *33*(9), 57–59.

Xin, H., Wang, D., Qi, X., Qi, G., Dou, G. (2014). Structural characteristics of coal functional groups using quantum chemistry for quantification of infrared spectra. *Fuel Processing Technology*, *118*, 287–295.

Xu, Q., Yang, S., Cai, J., Zhou, B., Xin, Y. (2018). Risk forecasting for spontaneous combustion of coals at different ranks due to free radicals and functional groups reaction. *Process Safety and Environmental Protection*, *118*, 195–202. https://doi.org/10.1016/j.psep.2018.06.040

Xu, Y., Wang, L., Tian, N., Zhang, J., Yu, M., Delichatsios, M. A. (2017). Spontaneous combustion coal parameters for the crossing-point temperature (CPT) method in a temperature–programmed system (TPS). *Fire Safety Journal*, *91*, 147–154.

Xuyao, Q., Wang, D., Milke, J. A., Zhong, X. (2011). Crossing point temperature of coal. *Mining Science and Technology*, *21*(2), 255–260. https://doi.org/10.1016/j.mstc.2011.02.024

Yang, S., Xu, Q., Huang, J., Chu, T. (2009). The Three Zones Microcirculation Theory of Goaf Spont aneous Combust ion and a Numer ical Simulat ion of the Air Leakage Flow Field. *Journal of China University of Mning & Technology*, *38*(6), 769–788.

Yang, Y., Li, Z., Tang, Y., Liu, Z., Ji, H. (2014). Fine coal covering for preventing spontaneous combustion of coal pile. *Natural Hazards*, *74*(2), 603–622. https://doi.org/10.1007/s11069-014-1203-7

Yokono, T., Miyazawa, K., Sanada, Y., Marsh, H. (1981). Nuclear magnetic proton relaxation studies of oxidized coals. *Fuel*, *60*(7), 598–602.

Yongchen, Y., Fuming, L., Xiujiang, L., Yingli, L. (2016). Cause Analysis of an Extraordinarily Big Gas Explosion Accident Occurred in Chenjiashan Mine of Tongchuan Coal Mining Administration. *Mining Safety & Environmental Protection*, *034*(005), 85–87.

Yu, S., Jia, B. (2012). Preparation and Coagulating Characteristics of New-type Ammonia-free Gel. *Journal of Shandong University of Science and Technology. Natural Science*, *31*(2), 42–47.

Yuan, H., Restuccia, F., Richter, F., Rein, G. (2019). A computational model to simulate self-heating ignition across scales, configurations, and coal origins. *Fuel*, *236*(September 2018), 1100–1109. https://doi.org/10.1016/j.fuel.2018.09.065

Yuan, L., Smith, A. C. (2008). Numerical study on effects of coal properties on spontaneous heating in longwall gob areas. *Fuel*, *87*(15–16), 3409–3419. https://doi.org/10.1016/j.fuel.2008.05.015

Yuan, L., Smith, A. C. (2009). CFD modeling of spontaneous heating in a large-scale coal chamber. *Journal of Loss Prevention in the Process Industries*, *22*(4), 426–433. https://doi.org/10.1016/j.jlp.2009.02.016

Zambra, C. E., Moraga, N. O., Rosales, C., Lictevout, E. (2012). Unsteady 3D heat and mass transfer diffusion coupled with turbulent forced convection for compost piles with chemical and biological reactions. *International Journal of Heat and Mass Transfer*, *55*(23–24), 6695–6704. https://doi.org/10.1016/j.ijheatmasstransfer.2012.06.078

Zarrouk, S. J., O'sullivan, M. J., St George, J. D. (2006). Modelling the spontaneous combustion of coal: the adiabatic testing procedure. *Combustion Theory and Modelling*, *10*(6), 907–926.

Zhang, D., Yang, S., Wang, Q., Wang, L., Luo, H., Liu, G. (2006). Numerical simulation on the spontaneous combustion of loose coal in the top-coal caving region of coal drift. *China University of Mining and Technology-Chinese Edition*, *35*(6), 757.

Zhang, H., Sasaki, K., Zhang, X., Sugai, Y., Wang, Y. (2019). Numerical simulations on the self-heating behaviours of coal piles considering aging effect. *Combustion Theory and Modelling*, *23*(6), 1169–1190. https://doi.org/10.1080/13647830.2019.1644378

Zhang, H., Zhang, X., Wang, Y., Wang, J., Sasaki, K. (2018). Study on spontaneous combustion of lignite based on the theory of equivalent oxidation exposure time. *Journal of China Coal Society*, *43*(5), 1358–1364.

Zhang, J., Choi, W., Ito, T., Takahashi, K., Fujita, M. (2016). Modelling and parametric investigations on spontaneous heating in coal pile. *Fuel*, *176*, 181–189. https://doi.org/10.1016/j.fuel.2016.02.059

Zhang, J. M., Guan, H. Y., Cao, D. Y. (2008). Underground coal fires in China: origin, detection, fire-fighting, and prevention. *China Coal Industry Publishing House: Beijing, China*, 3.

Zhang, J., Ren, T., Liang, Y., Wang, Z. (2016). A review on numerical solutions to self-heating of coal stockpile: Mechanism, theoretical basis, and variable study. *Fuel*, *182*, 80–109.

Zhang, L., Qin, B., Shi, B., Wen, K. (2016). Formation mechanism of foamed gel for controlling the coal spontaneous combustion. *Combustion Science and Technology*, *188*(1), 132–143.

Zhang, T., Xu, J., Zeng, J., Lou, K. (2013). Diversity of prokaryotes associated with soils around coal-fire gas vents in MaNasi county of Xinjiang, China. *Antonie van Leeuwenhoek*, *103*(1), 23–36.

Zhang, W., Jiang, S., Wang, K., Wang, L., Xu, Y., Wu, Z., Shao, H., Wang, Y., Miao, M. (2015). Thermogravimetric dynamics and FTIR analysis on oxidation properties of low-rank coal at low and moderate temperatures. *International Journal of Coal Preparation and Utilization*, *35*(1), 39–50.

Zhang, Y., Wu, J., Chang, L., Wang, J., Li, Z. (2013). Changes in the reaction regime during low-temperature oxidation of coal in confined spaces. *Journal of Loss Prevention in the Process Industries*, *26*(6), 1221–1229. https://doi.org/10.1016/j.jlp.2013.05.008

Zhang, Y., Ye, L., Cui, M., Yang, B., Li, J., Sun, H., Yao, F. (2015). Physically crosslinked poly(vinyl alcohol)-carrageenan composite hydrogels: Pore structure stability and cell adhesive ability. *RSC Advances*, *5*(95), 78180–78191.

https://doi.org/10.1039/c5ra11331h

Zhao, Y., Zhang, J., Chou, C.-L., Li, Y., Wang, Z., Ge, Y., Zheng, C. (2008). Trace element emissions from spontaneous combustion of gob piles in coal mines, Shanxi, China. *International Journal of Coal Geology*, *73*(1), 52–62.

Zhong, X., Wang, D., Yin, X. (2010). Test method of critical temperature of coal spontaneous combustion based on the temperature programmed experiment. *Meitan Xuebao/Journal of the China Coal Society*, *35*(SUPPL. 1), 128–131. https://doi.org/10.13225/j.cnki.jccs.2010.s1.036

Zhong, X., Wang, D., Zhou, F., Lu, W. (2006). Critical Accumulative Thickness Prediction of Coal Spontaneous Combustion with a Wire-mesh Bakset Crossing Piont Mehod. *Journal of China University of Mining & Technology*, *35*(6), 718–721.

Zhou, F. B., Shi, B. B., Cheng, J. W., Ma, L. J. (2015). A new approach to control a serious mine fire with using liquid nitrogen as extinguishing media. *Fire Technology*, *51*(2), 325–334.

Zhou, L., Zhang, D., Wang, J., Huang, Z., Pan, D. (2013). Mapping land subsidence related to underground coal fires in the Wuda Coalfield (Northern China) using a small stack of ALOS PALSAR differential interferograms. *Remote Sensing*, *5*(3), 1152–1176.

Zhu, H., Li, F., Jiang, Y., Pan, F., Hao, J. (2012). Design on automatic pressure balanced fire prevention and control system in mine. *Coal Science and Technology*, *40*(4), 95–99.

Zhu, H., Song, Z., Tan, B., Hao, Y. (2013). Numerical investigation and theoretical prediction of self-ignition characteristics of coarse coal stockpiles. *Journal of Loss Prevention in the Process Industries*, *26*(1), 236–244.

Zong, L. I., Qiang, W. U., Ya, X. (2008). Numerical Simulation of Coupling Mechanism of Coal Spo nt aneous Combustion and Gas Effusion in Goaf. *Journal of China University of Mning & Technology*, *37*(1), 38–42.

Zubíček, V. (2008). *Assessment of Susceptibility of Coal To Spontaneous Combustion in Okr*. *LIV*(4), 1–9.